www.reanimatology.com
ISSN 2411-7110 (online)

GENERAL REANIMATOLOGY

ОБЩАЯ РЕАНИМАТОЛОГИЯ

SCIENTIFIC-AND-PRACTICAL JOURNAL

научно-практический журнал

Volume 19 **Том 19**

№ 3

Moscow
Москва
2023

22 31 десятилетие науки и технологий

ФНКЦ РР

ФЕДЕРАЦИЯ АНЕСТЕЗИОЛОГОВ И РЕАНИМАТОЛОГОВ

Сеченовский Университет
НАУК О ЖИЗНИ

XXV Юбилейная всероссийская конференция с международным участием

ЖИЗНЕОБЕСПЕЧЕНИЕ ПРИ КРИТИЧЕСКИХ СОСТОЯНИЯХ

10-11 ноября 2023 | Москва

ТЕМАТИКИ КОНФЕРЕНЦИИ

- острая дыхательная недостаточность. ИВЛ, экстракорпоральная оксигенация;
- травма, кровопотеря, шок;
- инфекционные осложнения критических состояний. Сепсис;
- неотложные состояния в кардиологии;
- ведение пациентов в хроническом критическом состоянии;
- ранняя реабилитация в нейрореаниматологии;
- экстракорпоральные методы детоксикации;
- проблема гемостаза в анестезиологии-реаниматологии;
- нутритивная поддержка при критических состояниях;
- анестезиология-реаниматология в специализированных областях (педиатрия, акушерство-гинекология, сердечно-сосудистая хирургия, нейрохирургия и др.);
- механизмы развития критических состояний;
- экспериментальные исследования в анестезиологии-реаниматологии;
- образовательные технологии в анестезиологии-реаниматологии.

ФОРМАТ И МЕСТО ПРОВЕДЕНИЯ

Очно — Конгресс-центр Сеченовского Университета,
г. Москва, ул. Трубецкая, 8

CRITICALCONF.RU

Тел.: +7 (499) 390 34 38
E-mail: criticalconf@confreg.org

Научно-исследовательский институт общей реаниматологии имени В.А. Неговского ФНКЦ РР

Ассоциация акушерских анестезиологов-реаниматологов

Кафедра анестезиологии и реаниматологии с курсом медицинской реабилитации Российского университета дружбы народов

Кафедра анестезиологии и реаниматологии Московского государственного медико-стоматологического университета имени А.И. Евдокимова

Общество по изучению шока (Россия)

Национальный совет по реанимации

Ассоциация анестезиологов и реаниматологов Узбекистана

Фонд «Медицина критических состояний»

ISSN 1813-9779 (print) ISSN 2411-7110 (online)

GENERAL REANIMATOLOGY

OBSHCHAYA REANIMATOLOGIYA

Scientific-and-Practical Peer-Reviewed Journal
Since 2005

• Covers issues of critical care medicine
• Manuscripts in Russian and English are published free-of-charge
• Included in SCOPUS (since 2015), RINTs, RSCI, DOAJ, and other databases, as well as in the Official list of editions recommended for publication of dissertations (PhD, DSci) by the Russian Higher Attestation Commission

Registration certificate of the Journal «Obshchaya reanimatologiya» (General Reanimatology): ПИ № ФС77-18690, November 2, 2004, Federal Service for Supervision of Compliance with Legislation in the Sphere of Mass Communications and Protection of Cultural Heritage
Publication Frequency: 6 numbers per year.
Founder:

ОБЩАЯ РЕАНИМАТОЛОГИЯ

OBŜAÂ REANIMATOLOGIÂ

научно-практический рецензируемый журнал
Выходит с 2005 г.

• охватывает вопросы медицины критических состояний
• публикует рукописи на русском и английском языках бесплатно
• включен в базы данных SCOPUS (с 2015 г.), РИНЦ, RSCI, DOAJ и др. базы данных; Перечень изданий, рекомендованных ВАК для публикации результатов диссертационных работ

Свидетельство о регистрации: ПИ № ФС77-18690 от 02 ноября 2004 г. Печатное издание журнал «Общая реаниматология» зарегистрирован Федеральной службой по надзору за соблюдением законодательства в сфере массовых коммуникаций и охране культурного наследия.
Периодичность: 6 раз в год
Учредитель:

Publisher:
Federal Research and Clinical Center of Intensive Care Medicine and Rehabilitology, Moscow, Russia
Издатель:
Федеральный научно-клинический центр реаниматологии и реабилитологии (ФНКЦ РР), Москва, Россия

Supported by Russian Federation of Anesthesiologists and Reanimatologists
При поддержке Общероссийской общественной организации «Федерация анестезиологов и реаниматологов»

Artwork: Natalia V. Golubeva
Page-proof: Sergey V. Shishkov
Printing House:
Printed at LLC «Advanced Solutions». 19, Leninsky prospekt, build. 1, Moscow, 119071. www.aov.ru
Contacts:
25 Petrovka Str., Bldg. 2, 107031 Moscow, Russia.
Tel. +7-495-694-17-73.
E-mail: **journal_or@mail.ru;**
Web: **www.reanimatology.com**

Subscription:
Index 46338, refer to catalog of «Книга-Сервис»
Signed for printing: 03.07.2023

Оригинал-макет: Н. В. Голубева
Верстка: С. В. Шишков
Типография: отпечатано в ООО «Адвансед солюшнз». 119071, г. Москва, Ленинский пр-т, д. 19, стр. 1. www.aov.ru
Контакты с редакцией:
Россия, 107031, г. Москва, ул. Петровка, д. 25, стр. 2.
Тел.: +7-495-694-17-73.
E-mail: **journal_or@mail.ru;**
сайт: **www.reanimatology.com**

Подписка и распространение: индекс издания по каталогу «Книга-Сервис» — 46338.
Цена свободная
Подписано в печать: 03.07.2023

CONTENTS **СОДЕРЖАНИЕ**

CLINICAL STUDIES **КЛИНИЧЕСКИЕ ИССЛЕДОВАНИЯ**

Prognostic Value of Cystatin C as a Predictor of Adverse Outcome in Severe Pneumonia Associated with COVID-19
Daniil I. Korabelnikov, Magomedali O. Magomedaliev, Sergey E. Khoroshilov
4 Прогностическое значение цистатина С как предиктора неблагоприятного исхода при пневмонии тяжелого течения, ассоциированной с COVID-19
Корабельников Д. И., Магомедалиев М. О., Хорошилов С. Е.

Meglumine Sodium Succinate in Diabetic Ketoacidosis
Mikhail I. Neimark, Evgenij A. Kloster, Andrej A. Bulganin, Andrej V. Ioshhenko
12 Применение меглюмина натрия сукцината при диабетическом кетоацидозе
Неймарк М. И., Клостер Е. А., Булганин А. А., Иощенко А. В.

Risk Factors for COVID-19 Adverse Outcomes in ICU Settings of Various Types Repurposed Hospitals
Alexander A. Avramov, Evgeny V. Ivanov, Alexander V. Melekhov, Ruslan S. Menzulin, Andrey I. Nikiforchin
20 Факторы риска неблагоприятного исхода COVID-19 в ОРИТ перепрофилированных стационаров разного типа
Аврамов А. А., Иванов Е. В., Мелехов А. В., Мензулин Р. С., Никифорчин А. И.

FOR PRACTITIONER **В ПОМОЩЬ ПРАКТИЧЕСКОМУ ВРАЧУ**

Modified Supraclavicular and Pectoral Nerves Blocks for Implantation of Intravenous Port System in Cancer Patients
Maxim P. Yakovenko, Eduard E. Antipin, Nadezhda A. Bochkareva, Natalia I. Koroleva, Ekaterina F. Drobotova, Eduard V. Nedashkovsky
28 Модифицированные блокады надключичного и грудных нервов при имплантации внутривенной порт-системы у онкологических пациентов
Яковенко М. П., Антипин Э. Э., Бочкарева Н. А., Королева Н. И., Дроботова Е. Ф., Недашковский Э. В.

The Analgesic Efficacy of Prolonged Erector Spinae Fascial Plane Block in Patients with Multiple Rib Fractures
Visolat H. Sharipova, Ivan V. Fokin
39 Эффективность продленной блокады фасциальной плоскости мышцы, выпрямляющей спину, при множественных переломах ребер
Шарипова В. Х., Фокин И. В.

EXPERIMENTAL STUDIES **ЭКСПЕРИМЕНТАЛЬНЫЕ ИССЛЕДОВАНИЯ**

Experimental Study of Neuroprotective Properties of Inhaled Argon-Oxygen Mixture in a Photoinduced Ischemic Stroke Model
Ekatherine A. Boeva, Denis N. Silachev, Elmira I. Yakupova, Marina A. Milovanova, Lydia A. Varnakova, Sergey N. Kalabushev, Sergey O. Denisov, Victoria V. Antonova, Ivan A. Ryzhkov, Konstantin N. Lapin, Alexandra A. Grebenchikova
46 Изучение нейропротективного эффекта ингаляции аргон-кислородной смеси после фотоиндуцированного ишемического инсульта
Боева Е. А., Силачев Д. Н., Якупова Э. И., Милованова М. А., Варнакова Л. А., Калабушев С. Н., Денисов С. О., Антонова В. В., Рыжков И. А., Лапин К. Н., Гребенчикова А. А.

REVIEWS **ОБЗОРЫ**

Photochemicallly Induced Thrombosis as a Model of Ischemic Stroke
Irina V. Ostrova, Anastasia S. Babkina, Maxim A. Lyubomudrov, Andrey V. Grechko, Arkady M. Golubev
54 Применение метода фотохимического тромбоза для моделирования ишемического инсульта
Острова И. В., Бабкина А. С., Любомудров М. А., Гречко А. В., Голубев А. М.

https://doi.org/10.15360/1813-9779-2023-3-4-11

Prognostic Value of Cystatin C as a Predictor of Adverse Outcome in Severe Pneumonia Associated with COVID-19

Daniil I. Korabelnikov[1,2], Magomedali O. Magomedaliev[1,2]*, Sergey E. Khoroshilov[3]

[1] Haass Moscow Medical and Social Institute,
5 Brestskaya 2nd Str., 123056 Moscow, Russia
[2] Military Clinical Hospital 1586, Ministry of Defense of Russia
[3] Academician N. N. Burdenko Main Military Clinical Hospital, Ministry of Defense of Russia

For citation: *Daniil I. Korabelnikov1, Magomedali O. Magomedaliev, Sergey E. Khoroshilov.* Prognostic Value of Cystatin C as a Predictor of Adverse Outcome in Severe Pneumonia Associated with COVID-19. *Obshchaya Reanimatologiya = General Reanimatology.* 2023; 19 (3): 4–11. https://doi.org/10.15360/1813-9779-2023-3-4-11 [In Russ. and Engl.]

***Correspondence to:** Magomedali O. Magomedaliev, magomedalim@mail.ru

Summary

Objective. To assess the cystatin C (CysC) prognostic value for probability of death in patients with severe and extremely severe pneumonia associated with COVID-19.

Material and methods. A single-center prospective study included 72 patients with severe and extremely severe pneumonia associated with COVID-19 undergoing treatment in the ICU of multifunctional medical center from September 2020 to October 2021. Recovered survivors (*N*=55) were analyzed as a Group 1, non-survivors (*N*=17) were considered as a Group 2.

Results. The serum (s-CysC) and urine (u-CysC) CysC concentrations were significantly lower in Group 1 patients vs Group 2, averaging 1.31 mg/l vs 1.695 mg/l (*P*=0.013550), and 0.25 mg/l vs 0.94 mg/l (*P*=0.026308), respectively. Significant differences were also revealed in the subgroups differed by age (*P*=0.0094), platelet count (*P*=0.001), serum fibrinogen concentration (*P*=0.016), as well as CURB (*P*=0.02334), CRB-65 (*P*=0.032564), and SOFA (*P*=0.042042) scores. Therefore, s-CysC and u-CysC were statistically significant predictors of death in patients with pneumonia associated with severe and extremely severe COVID-19: 16.273 (95% CI: 2.503–105,814), *P*=0.003 and 1.281 (95% CI: 1.011–1.622), *P*=0.040, respectively. Urine and serum CysC were established as predictors of death in pneumonia associated with severe and extremely severe COVID-19, where u-CysC was defined as highly informative (ROC AUC 0.938 (95% CI: 0.867–1.000; *P*=0.000), with 90% sensitivity and specificity), and s-CysC — as informative (ROC AUC 0.863 (95%CI: 0.738–0.988; *P*=0.000) with 80% sensitivity and 72% specificity) predictive markers.

Conclusion. Levels of S-CysC and u-CysC are of high prognostic significance and may contribute to identifying patients at a high risk of unfavorable outcome (death) due to pneumonia associated with severe and extremely severe COVID-19. Both S-CysC and u-CysC concentrations increasing up to ⩾1.44 mg/l and ⩾0.86 mg/l, respectively, were associated with high probability of death.

Keywords: cystatin C, predictor; pneumonia; coronavirus infection; COVID-19; death; fatal outcome

Conflict of interest. The authors declare no conflict of interest.

COVID-19 is an infectious disease caused by severe acute respiratory syndrome coronavirus (SARS-CoV-2). The first outbreak of COVID-19 occurred in late 2019, originating from Wuhan City, Hubei Province, People's Republic of China [1]. According to the World Health Organization (WHO), as of April 3, 2022, there have been more than 489 million cases and more than 6 million deaths from COVID-19 worldwide [2]. According to the Russian Federal State Agency for Health and Consumer Rights, as of April 8, 2022, there were 17,955,120 cases of COVID-19 in the Russian Federation [3].

SARS-CoV-2 virus enters the human body through the epithelium of the upper respiratory and gastrointestinal tracts, with the lungs being the target organ in most cases. Eighty-one percent of patients have mild COVID-19, 14% have severe COVID-19, and 5% have extremely severe (critical) COVID-19 [4].

Due to the severity of the disease, approximately 10.2% of those infected with SARS-CoV-2 coronavirus require intensive care unit (ICU) treatment [5]. Mortality in COVID-19 depends on disease severity, comorbidities, and treatment, and is approximately 49% in ICU patients [6].

The main reason for ICU admission is acute respiratory failure, which develops in 60–70% of ICU patients. The need for mechanical ventilation in different countries ranges from 29.3% (China) to 59% (UK) and up to 89.9% (USA) [4].

The systemic inflammatory response contributes significantly to the patient's deterioration. The SARS-CoV-2 enhanced immune response appears to play an important role in the pathogenesis and progression of COVID-19. The antiviral immune response is often exaggerated and characterized by massive release of pro- and anti-inflammatory cytokines [7], followed by lymphopenia and granulocyte and monocyte abnormalities [8]. Thus, the major pathogenetic events of the disease include infection, sepsis, and septic shock, leading to multiple organ failure.

The systemic inflammatory response is a universal component of critical illness, involving a cascade of interactions between pro- and anti-inflammatory cytokines and their imbalance [9]. As the disease progresses, hypercytokinemia eventually leads to multiple organ failure and can be fatal [10].

Currently, when assessing the severity of the patient's condition and immune status, including the decision on further treatment, both Russian and international protocols recommend measuring the traditional well-established markers of systemic inflammatory response, such as procalcitonin, C-reactive protein, fibrinogen, ferritin, leukocyte count, neutrophil percentage, appearance of immature leukocytes (left shift in the differential) and lymphocytes [11, 12].

Cystatin-C is a well-established marker of acute kidney injury (AKI) [13]. Meanwhile, AKI in COVID-19 is one of the earliest manifestations of multiple organ failure [4], which determined our interest in assessing cystatin as a criterion for multiple organ failure. We did not find any publications on u-CysC in COVID-19 in the available literature.

The intensity of the immune response is known to directly correlate with the severity of COVID-19 [11]. Therefore, it would be useful to have a readily available and reliable laboratory biomarker to objectively determine the prognosis of COVID-19 in a timely manner and to differentiate and/or predict clinical variants of the disease at an early stage, before the development of clinical manifestations and organ damage, thus enabling the administration of the optimal treatment regimen.

Real clinical practice shows that the organization of medical care in COVID-19 pandemic, with the shortage of medical staff and beds, especially in the ICU, requires objective markers [1] that allow timely prediction of the need for ICU admission for intensive care and monitoring of vital functions.

In this context, the level of CysC deserves attention as a potential predictor of COVID-19 severity and as an indicator of the intensity of the immune response to coronavirus.

The current literature shows that CysC is a reliable diagnostic and prognostic biomarker for acute kidney injury (AKI), and its level directly correlates with the severity of renal damage. The more severe the kidney damage and the worse the nephron function, the higher the concentration of cystatin-C in blood (s-CysC) and urine (u-CysC) [14]. Currently, there is considerable evidence that s-CysC levels are elevated in kidney disease and that s-CysC not only increases earlier than serum creatinine (SCr) in AKI, but also decreases earlier than SCr ($P<0.001$) [15]. An international expert group (International Survey on the Management of Acute Kidney Injury and Continuous Renal Replacement Therapies) concluded in 2018 that novel biomarkers should be used to detect AKI in routine clinical practice. The most common new-generation routine diagnostic laboratory marker for AKI (19% of cases) was CysC [16].

The CysC polypeptide is produced at the same rate by all nucleated cells and 99% of it is metabolized by the kidneys, while the remaining CysC is excreted unchanged in the urine. Due to its low molecular weight, CysC is freely filtered through the renal glomerular filter with subsequent reabsorption and catabolism in the proximal convoluted tubule of the nephron without entering the systemic bloodstream. Such kinetics allow CysC to be considered an almost ideal noninvasive biomarker for the assessment of renal function [17].

Although the exact mechanisms are still unknown, a considerable body of clinical and experimental evidence has accumulated indicating the direct involvement of CysC in many immunological processes, including COVID-19. An increase in serum and urine CysC levels in the midst of complete renal «normality» has been observed [18, 19].

The production of CysC is regulated by different inflammatory processes in response to various endogenous and exogenous antigens, while CysC affects the systemic inflammatory process by inducing immune response [20].

We suggest that CysC is not only a reliable diagnostic and prognostic biomarker of AKI, but may also serve as a marker of the intensity of the immune response in COVID-19 and predict severe disease, allowing early adjustments in therapy, including early initiation of biologic therapy and steroid pulse treatment.

In 1991, Collins A. R. et al. evaluated the inhibitory effect of recombinant human CysC on human OC43 and 229e coronaviruses in a laboratory experiment [21]. Both viruses were found to be 99% inhibited at a CysC concentration of 0.1 mM. The beneficial effects of CysC were attributed to its ability to inhibit papain-like proteases, which are part of the coronavirus polymerase complex. Human coronaviruses OC43 and 229e were also inhibited at moderate CysC concentrations of 1–2 μM (physiological CysC levels in biological media are much lower, e.g. 0.5 μM in cerebrospinal fluid and 0.1 μM in blood serum).

Similar results were shown by Collins A.R. et al. (1998), who investigated the effect of cystatin D (a salivary cysteine protease inhibitor) on the replication of human OC43 and 229e coronaviruses. After incubation of human OC43 and 229e coronaviruses and subsequent addition of recombinant cystatin D, a significant reduction in virus replication to IC50 of 0.8 pM (its reference range in human saliva is 0.12–1.9 pM) was observed for both virus strains. The authors concluded that cystatin D is a potent inhibitor of coronavirus replication [22].

There are also published studies showing antiviral activity of CysC against other viruses [23], such as herpes simplex virus type 1 [24], human immunodeficiency virus [25], rotavirus [26].

CysC has also been investigated as a promising antiviral drug to inhibit picornavirus replication [27].

Thus, CysC is a proven biochemical marker of AKI, but given the pathophysiological mechanisms of its elevation, it can be considered as a broader diagnostic and prognostic marker, especially in critical illness.

Aim: To study the prognostic value of cystatin-C in assessing the probability of death in patients with severe and extremely severe pneumonia associated with novel coronavirus infection (COVID-19).

Materials and Methods

Patients with severe and extremely severe pneumonia associated with COVID-19, treated in the ICU of the Multidisciplinary Medical Center of the 1586 Military Clinical Hospital of the Ministry of Defense of Russia from September 2020 to October 2021, were included in this single-center prospective study.

Inclusion criteria:

— age 18 to 80 years;

— diagnosis of COVID-19 confirmed by detection of specific nucleic acids in nasopharyngeal swabs by polymerase chain reaction and/or antibodies in blood by enzyme-linked immunosorbent assay; as well as typical clinical and laboratory manifestations, lung damage confirmed by computed tomography;

— severe pneumonia evidenced by at least one of the following: dyspnea (respiratory rate >30/min), $SpO_2 \leqslant 93\%$, oxygenation index ⩽300 mm Hg, agitation, decreased consciousness, hemodynamic instability (systolic blood pressure less than 90 mm Hg and/or diastolic blood pressure less than 60 mm Hg), oligo- or anuria, computed tomography pattern typical of severe lung injury (CT grade 3–4, i.e, >50% lung volume involvement according to the semiquantitative scale used in Russia), arterial lactate >2 mmol/l, 2 or more points on the qSOFA scale, acute respiratory distress syndrome, respiratory failure requiring respiratory support, including high-flow oxygen therapy and noninvasive ventilation, septic shock, multiple organ failure.

Exclusion criteria:

— underlying renal and urinary tract diseases, other acute infectious and internal diseases, malignant neoplasms, including multiple myeloma, hyper- or hypothyroidism;

— history of cardiac, aortic, or great vessel surgery.

All patients received standard comprehensive intensive care according to the current provisional guidelines for the prevention, diagnosis and treatment of novel coronavirus infections (COVID-19).

Patients were divided into two groups based on clinical outcome:

— group 1 (survivors), 55 patients;

— group 2 (non-survivors), 17 patients.

The clinical, laboratory, and instrumental characteristics of the patients are shown in Table 1.

The study was approved by the local ethics committee of the Haas Moscow Medical and Social Institute and was conducted in accordance with the current legislation of the Russian Federation and the ethical principles adopted by the World Medical Association (Declaration of Helsinki).

Laboratory tests. All instrumental and laboratory tests were performed at the 1586 Military Hospital according to existing standards and protocols, and the results were documented and evaluated retrospectively from the time of patient admission to the ICU until transfer to the infectious disease unit. Venous blood and urine samples were collected simultaneously on the first day of ICU admission and sent to the laboratory within 10–20 minutes.

The concentration of s-CysC and u-CysC was determined by the immunoturbidimetric method on an automated biochemical analyzer AU 480 from Beckman Coulter, Inc., USA, using reagents from DiaSys Diagnostic Systems GmbH, Germany.

In planning the study, a sample size corresponding to a power of 90% with an error of less than 0.05 was considered optimal [28]. The minimum power for a significance level of <0.05 was 44 subjects [29]. The calculation was performed to one of the endpoints, death/recovery. The sample size was 72 patients (17 died, 55 recovered), which, according to the results of the analysis using XLSTAT software, was characterized by a multivariate Cox regression power of 1.0 with an acceptable first-level error of less than 0.05. The size of the effect was calculated using Cohen's formula $d=(X1-X2)/\sqrt{(SD1^2-SD2^2)/2}$ [30]. The magnitude of effect for s-CysC was 0.589 (mean effect size) and for u-CysC was 0.761 (mean effect size).

Statistical analysis of the material was performed using Excel 2013 of Microsoft Office 2013 (Microsoft, USA) and SPSS Statistics (IBM, USA) package. Statistical significance of differences between groups was determined using the nonparametric Mann–Whitney *U* test. Multivariate Cox regression was used to determine the association between s-CysC, u-CysC and adverse outcome (death). The optimal threshold for predicting death with sensitivity and specificity was determined using the ROC curve. Quantitative data were presented as median (*Me*) and interquartile range (25%; 75%). Differences were considered significant at $P<0.05$.

Results

SARS-CoV-2 virus was identified by polymerase chain reaction in 47 patients. The pattern of antibodies to SARS-CoV-2 virus in blood serum was as follows: IgM positive in 34 patients, negative in 11 patients; IgG positive in 23 patients, negative in 19 patients. The mean time of admission after the onset of illness was 7.6±4.45 days, and the ICU stay was 9.46±4.2 days. Mortality was 23.6% (*N*=17), the main causes of death were acute respiratory failure (10), multiple organ failure (3), heart failure (1).

A significant difference in CysC concentrations was observed between survivors and non-survivors.

The s-CysC level was 1.31 (1.04;1.61) mg/mL in group 1 and 1.695 (1.3;2.02) mg/mL in group 2 (*P*=0.013550). The u-CysC level was 0.25 (0.17; 0.46) mg/L in group 1 and 0.94 (0.35; 7.21) mg/L in group 2 (*P*=0.026308).

The mean age of the surviving patients was lower than that of the non-surviving patients (*P*=0.0094). Platelet count (*P*=0.001) and fibrinogen level (*P*=0.016) were also significantly different.

There were intergroup differences in CURB (*P*=0.02334), CRB-65 (*P*=0.032564), and SOFA (*P*=0.042042) scores.

According to the results of multivariate Cox regression analysis (Table 2), s-CysC 16.273 (95% CI, 2.503–105.814, *P*=0.003) and u-CysC 1.281 (95% CI, 1.011–1.622, *P*=0.040) were significant predictors of fatal outcome.

Table 1. Clinical, laboratory and instrumental characteristics of patients.

№	Parameter	Values of parameters in groups (*Me* (*Q1*; *Q3*))			Mann–Whitney	*P*
		Total, *N*=72	Group 1, *N*=55	Group 2, *N*=17	*U*-test	
1	Age, years	48 (43; 55)	47.5 (42; 51)	55 (52; 80)	*U*=90; *Z*=–2.59232595	**0.009466**
2	Men/women, *N*	72	46/14	6/6	—	—
3	Time of admission to the hospital from the onset of the disease, days	7 (5; 10)	7 (5; 11)	7 (5; 8)	*U*=130; *Z*=1.60968	0.107470
4	Time of admission to the ICU from the onset of the disease, days	10 (7; 12)	9 (7; 11)	10 (8; 12)	*U*=192; *Z*=–0.06242	0.95022
5	Duration of treatment in the ICU, days	6 (4; 10)	6 (4; 10)	8 (6; 13)	*U*=159; *Z*=–0.88422	0.37658
6–14	**Severity of disease according to scales, points**					
6	NEWS	7 (7; 8)	7 (7; 8)	7 (7; 8)	*U*=165; *Z*=–0.77392	0.43898
7	CRB-65	1 (0; 1)	0 (0; 1)	1 (1; 1)	*U*=116; *Z*=–2.13742	**0.032564**
8	CURB	1 (0; 1)	1 (0; 1)	1 (1; 2)	*U*=110.5; *Z*=–2.26781	**0.023340**
9	SMRT-CO	4 (3; 4)	4 (3; 4)	4 (4; 4)	*U*=155; *Z*=–1.18055	0.23778
10	SMSRT-COP	4 (3; 4)	4 (3; 4)	4 (4; 4)	*U*=151; *Z*=–1.27735	0.20147
11	PORT(PSI)	15 (0; 30)	15 (0; 30)	0 (0; 40)	*U*=89.5; *Z*=–0.35807	0.720280
12	SOFA	2 (2; 3)	2 (1.5; 3)	3 (2; 3)	*U*=117; *Z*=–2.03311	**0.042042**
13	qSOFA	1 (1; 1)	1 (1; 1)	1 (1; 1)	*U*=171.5; *Z*=1.20176	0.22946
14	APACHE II	5 (4; 7)	5 (4; 7)	5 (4; 6)	*U*=194.5; *Z*=0.012567	0.98997
15	CT score of lung involvement (semi-quantitative assessment) on admission to the ICU	4 (3; 4)	4 (3; 4)	4 (3; 4)	*U*=142.5; *Z*=0.625257	0.531803
16	Hemoglobin, g/l	140 (133; 149)	140 (133; 149)	140 (128; 154)	*U*=162.5; *Z*=–0.794389	0.426969
17	Red blood cells, 10^{12}/L	4.81 (4.54; 5.05)	4.81 (4.50; 5.05)	4.6 (4.56; 5.05)	*U*=184; *Z*=–0.26050	0.794473
18	White blood cells, 10^9/L	9.1 (7.4; 13.6)	9.2 (7.8; 13.8)	8 (6; 10.15)	*U*=129.5; *Z*=1.61261	0.10683
19	Lymphocytes, %	9 (5; 15)	11 (4; 16)	6 (5; 9)	*U*=145; *Z*=1.23033	0.21857
20	Platelets, 10^9/L	226 (196; 296)	268 (207.8; 303)	181 (138; 202)	*U*=65.5; *Z*=3.20042	**0.00137**
21	Total protein, g/L	65 (62; 71)	66 (62; 72)	64 (62; 66)	*U*=152; *Z*=1.05607483	0.29093
22	Urea, mmol/L	6.3 (5; 7.5)	5.8 (4.8; 7.5)	6.7 (6.4; 7.9)	*U*=147; *Z*=–1.17902195	0.23839
23	Creatinine, μmol/L	89 (79; 97)	88 (77; 96)	94 (83; 99)	*U*=137.5; *Z*=–1.414835	0.157120
24	Cystatin C in blood, mg/L	1.32 (1.08; 1.63)	1.31 (1.04; 1.61)	1.695 (1.3; 2.02)	*U*=95; *Z*=–2.46879	**0.013550**
25	Cystatin C in urine, mg/L	0.28 (0.17; 0.51)	0.25 (0.17; 0.46)	0.94 (0.35; 7.21)	*U*=105; *Z*=–2.22164	**0.026308**
26	CRP, mg/L	96.9 (30.8; 145.2)	101.6 (41.3; 146.6)	89.4 (13.3; 126.7)	*U*=156; *Z*=–0.95507	0.339544
27	Fibrinogen, g/L	4.3 (3.4; 6.84)	4.76 (3.5; 8)	3.79 (3.3; 4.08)	*U*=98.5; *Z*=2.39513	**0.016615**
28	Ferritin, μg/L	684.5 (529.7; 712.7)	671 (422.5; 720.7)	681.7 (579.5; 689.2)	*U*=94; *Z*=0.387332	0.698510
29	Procalcitonin, ng/mL	0.5 (0.5; 0.5)	0.5 (0.5; 0.5)	0.5 (0.5; 0.5)	*U*=162; *Z*=0.00	1.000000
30	D-dimer, mg/L	0.46 (0.28; 0.83)	0.46 (0.28; 0.83)	0.43 (0.19; 0.95)	*U*=189; *Z*=0.13664	0.89130

Note. Q — quartile; CRP — C-reactive protein.

Table 2. Multivariate regression analysis (Cox) of predictors of death.

Selected parameters	B	SE	p-value	Exp (B)	95% CI	
					Lower limit	Upper limit
s-CysC, mg/l	2.789	0.955	0.003	16.273	2.503	105.814
u-CysC, mg/l	0.247	0.121	0.040	1.281	1.011	1.622

Note. Values measured during the first 24 hours after ICU admission. B — coefficient; SE — standard error; Exp (B) — odds ratio (the predicted change in odds for a unit increase in the predictor).

Table 3. ROC analysis of the significance of predictors of death.

Selected parameters	AUC of the ROC-curve	*P*-value	95% CI		Cut-off value	Sensitivity, %	Specificity, %
			Lower limit	Upper limit			
s-CysC, mg/l	0.863	0.000	0.738	0.988	1.44	80	72
u-CysC, mg/l	0.938	0.000	0.867	1.000	0.86	90	90

Note. Values measured during the first 24 h of admission to the ICU.

Using ROC analysis, we identified u-CysC as the most significant predictor of death with 90% sensitivity and 90% specificity (*P*=0.000) (Table 3, Fig.), indicating excellent model quality. For s-CysC, the sensitivity was 80% and the specificity was 72% (*P*=0.000) (Table 3, Figure), corresponding to a good predictive ability for adverse outcomes.

Discussion

The search for promising and advanced laboratory markers that can objectively assess the severity of COVID-19 patients and predict possible poor (fatal) outcomes is ongoing. In our opinion, both s-CysC and u-CysC deserve attention as indicators of systemic inflammation and COVID severity, in addition to their well-established role as reliable biomarkers of renal injury.

The significant increase in s-CysC and u-CysC levels in the group of non-survivors is probably associated with a more severe systemic inflammation and an increase in their production by nucleated cells.

However, a partial or, in some cases, complete dysfunction of the tubular system that interferes with the tubular reabsorption of CysC in the kidneys cannot yet be excluded.

The lack of intergroup differences in the levels of such a common marker of systemic inflammation as C-reactive protein (CRP) may be partially explained by the use of biological and steroid therapy prior to ICU admission in 57.14% (*N*=28) of cases.

Similar results were reported by authors from China (Li Y. et al., Wuhan, China, 2020), citing data from a single-center retrospective study of the prognostic value of s-CysC in patients with severe COVID-19 [31]. Adult patients without renal comorbidities (*N*=101) were evaluated and divided into two groups, including survivors (*N*=64) and non-survivors (*N*=37). The s-CysC was found to be an independent risk factor for death in severe COVID-19 patients (odds ratio=1.812, 95% CI: 1.300–2.527; *P*<0.001). s-CysC had an area under the AUC curve of 0.755 for predicting death (sensitivity 86.5%, specificity 56.2%). The authors concluded that patients with s-CysC of 0.80 mg/L or higher had a greater risk of death.

This is consistent with data from a meta-analysis by Zinellu A. et al. (2021) that included 13 studies (*N*=2.510) comparing s-CysC concentrations in patients with COVID-19. The authors concluded that the severity of COVID-19 and mortality increased with increasing s-CysC [32].

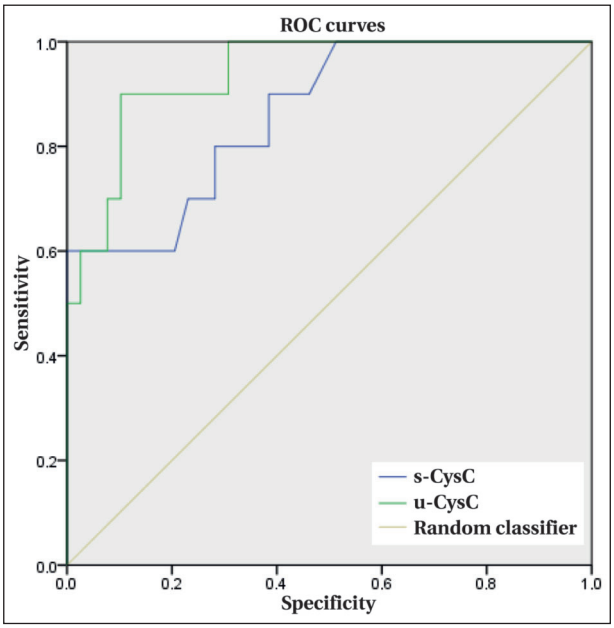

AUC ROC value of s-CysC and u-CysC to predict poor outcome (death).

A retrospective cohort study by Chen D. et al. (2020) evaluated the relationship between s-CysC levels and the severity of COVID-19 in 481 patients [33]. The highest s-CysC level was independently associated with the most severe manifestations of systemic inflammation, multiple organ failure and adverse outcome (*P*<0.05). Similarly, APACHE II and SOFA scores increased with increasing s-CysC (*P*<0.05). Notably, high s-CysC levels correlated significantly with increased lactate, CRP, procalcitonin, high neutrophil/lymphocyte ratio, and leukocytosis (*P*<0.05) and decreased oxygenation index (*P*<0.05). In conclusion, the investigators recommended regular monitoring of s-CysC in patients with COVID-19 to predict the severity of COVID-19.

The results of the study by Ouyang S.-M. et al. (2020) support the idea that increased s-CysC is associated with the risk of death and COVID-19 progression (*P*<0.05) [34].

Similarly, Wang J. et al. (2020) showed that severe COVID-19 is associated with increased s-CysC and hemoglobin and decreased blood oxygen saturation [35].

Similar results were reported by Chen S. et al. (2021), who showed that s-CysC increases earlier

than SCr in patients with impaired renal function in COVID-19 and is also more valuable in predicting disease severity [36].

Another recent study by Yang Z. et al. (2021) demonstrated that an increase in s-CysC may be associated with an increase in infiltration area on lung computed tomography within 6±1 to 24 hours [37].

Thus, the above studies suggest that an increase in s-CysC precedes the progression of pulmonary infiltration and the development of AKI. The level of s-CysC was also found to be significantly higher in the non-survivors than in the survivors.

Conclusion

The study of s-CysC and u-CysC level changes during COVID-19 is a promising trend that will allow to optimize the therapy of pneumonia associated with severe and extremely severe COVID-19, while high levels of s-CysC (more than 1.44 mg/L) and u-CysC (more than 0.86 mg/L) are reliable predictors of death.

An increase in s-CysC concentration to 1.44 mg/L and more and u-CysC concentration to 0.86 mg/L and more is associated with a high risk of death, therefore their increase in pneumonia associated with severe and extremely severe COVID-19 should be considered life-threatening and requires early use of life-saving medicinal and other critical care options.

References

1. *Хаджиева М.Б., Грачева А.С., Ершов А.В., Чурсинова Ю.В., Степанов В.А., Авдейкина Л.С., Гребенчиков О.А., с соавт.* Биомаркеры повреждения структур аэрогематического барьера при COVID-19. *Общая реаниматология*. 2021; 17 (3): 16–31. [*Khadzhieva M.B., Gracheva A.S., Ershov A.V., Chursinova Yu.V., Stepanov V.A., Avdeikina L.S., Grebenchikov O.A. et al.* Biomarkers of Air-Blood Barrier Damage In COVID-19. *General Reanimatology*. 2021; 17 (3): 16–31. (in Russ.)]. DOI: 10.15360/1813-9779-2021-3-2-0.
2. World Health Organization. Weekly epidemiological update on COVID-19 [Электронный ресурс/ Electronic resource]. URL: https://www.who.int/publications/m/item/weekly-epidemiological-update-on-COVID-19---5-april-2022 (дата обращения: 26.05.2022/ Accessed May 26, 2022).
3. Федеральная служба по надзору в сфере защиты прав потребителей [Электронный ресурс]. URL: https://rospotrebnadzor.ru/ about/info/news_time/ news_details.php?ELEMENT_ID=13566 (дата обращения: 08.04.2022). [Federal Service for Supervision of Consumer Rights Protection and Human Well-Being/Federalnaya sluzhba po nadzoru v sfere zashchity prav potrebiteley I blagopoluchiya cheloveka Electronic resource] (in Russ.)]. (Accessed April 8, 2022). https://rospotrebnadzor.ru/about/info/ news_time/ news_details.php?ELEMENT_ID=13566.
4. *Магомедалиев М.О., Корабельников Д.И., Хорошилов С.Е.* Острое повреждение почек при тяжелом течении пневмоний, ассоциированных с новой коронавирусной инфекцией (COVID-19). *Вестник Российской Военно-Медицинской Академии*. 2022; 24 (3): 511–520. [*Magomedaliev M.O., Korabelnikov D.I., Khoroshilov S.E.* Acute kidney injury in severe pneumonia associated with COVID-19. *Bull Russ Mil Med Acad./ Vestnik Rossiyskoy Voenno- Meditsinskoy Akademii*. 2022; 24 (3): 511–520. (in Russ.)]. DOI: 10.17816/brmma109938.
5. *Oliveira E., Parikh A., Lopez-Ruiz A., Goldberg J., Cearras M., Fernainy K., Andersen S.* et al. ICU outcomes and survival in patients with severe COVID-19 in the largest health care system in central Florida. *PLoS One*. 2021; 16 (3): e0249038. DOI: 10.1371/journal.pone.0249038. PMID: 33765049
6. *Wu Z., McGoogan J.M.* Characteristics of and important lessons from the coronavirus disease 2019 (COVID-19) outbreak in China: summary of a report of 72 314 cases from the Chinese Center for Disease Control and Prevention. *JAMA*. 2020; 323 (13): 1239–1242. DOI: 10.1001/jama.2020.2648. PMID: 32091533
7. *Ершов А.В., Сурова В.Д., Долгих В.Т., Долгих Т.И.* Цитокиновый шторм при новой коронавирусной инфекции и способы его коррекции. *Антибиотики и Химиотерапия*. 2020; 65 (11–12): 27–37. [*Ershov A.V., Surova V.D., Dolgikh V.T., Dolgikh T.I.* Cytokine storm in the novel coronavirus infection and methods of its correction. *Antibiotics and Chemotherapy/Antibiotiki i Khimioterapiya* 2021; 65 (11–12): 27–37. (In Russ.)]. DOI: 10.37489/0235-2990-2020-65-11-12-27-37.
8. *Rello J., Belliato M., Dimopoulos M.-A., Giamarellos-Bourboulis E.J., Jaksic V., Martin-Loeches I., Mporas I.* et al. Update in COVID-19 in the intensive care unit from the 2020 HELLENIC Athens International symposium. *Anaesth Crit Care Pain Med*. 2020; 39 (6): 723–730. DOI: 10.1016/j.accpm.2020.10.008. PMID: 33172592
9. *Bone R.C., Balk R.A., Cerra F.B., Dellinger R.P., Fein A.M., Knaus W.A., Schein R.M.* et al. Definitions for sepsis and organ failure and guidelines for the use of innovative therapies in sepsis. The ACCP/SCCM Consensus Conference Committee. American College of chest physicians/ Society of critical care medicine. *Chest*. 1992; 101 (6): 1644–1655. DOI: 10.1378/chest.101.6.1644. PMID: 1303622
10. *Хорошилов С.Е., Никулин А.В.* Эфферентное лечение критических состояний. *Общая реаниматология*. 2012; 8 (4): 30. [*Khoroshilov S.E., Nikulin A.V.* Efferent treatment for critical conditions. *Gen Reanimatol./ Obshchaya Reanimatologya*. 2012; 8 (4): 30. (in Russ.)]. DOI: 10.15360/1813-9779-2012-4-30
11. Временные методические рекомендации «Профилактика, диагностика и лечение новой коронавирусной инфекции (COVID-19)». Версия 13.1 от 17.11.2021. [Temporary Guidelines «Prevention, diagnosis treatment of new coronavirus Infect (COVID-19)» Version 13.1 (11.17. 2021)/ Vremennye metodicheskie rekomendatsyi «Profilaktika, diagnostika i lecheniye novoy koronavirusnoy infektsii (COVID-19)». Versiya 13.1 (17.11.2021). (In Russ.)]. https://www.garant.ru/products/ ipo/prime/doc/ 402985106/. Accessed April 28, 2023.
12. *Зайцев А.А., Чернов С.А., Стец В.В., Паценко М.Б., Кудряшов О.И., Чернецов В.А., Крюков Е.В.* Алгоритмы ведения пациентов с новой коронавирусной инфекцией COVID-19 в стационаре. Методические рекомендации. *Consilium Medicum*. 2020; 22 (11): 91–97. [*Zaitsev A.A., Chernov S.A., Stets V.V., Patsenko M.B., Kudriashov O.I., Chernetsov V.A., Kriukov E.V.* Algorithms for the management of patients with a new coronavirus COVID-19 infection in a hospital. Guidelines. *Consilium Medicum*. 2020; 22 (11): 91–97. (In Russ.)]. DOI: 10.26442/20751753. 2020.11.200520
13. *Магомедалиев М.О., Корабельников Д.И., Хорошилов С.Е.* Прогностическое значение цистатина-С как предиктора развития острого повреждения почек при COVID-19. *Общая реаниматология*. 2023; 19 (2): 14–22. [*Magomedaliev M.O., Korabelnikov D.I., Khoroshilov S.E.* The predictive value of cystatin C for AKI in patients with COVID-19. *General Reanimatology/Obshchaya Reanimatologya*. 2023; 19 (2): 14–22. (In Russ.)]. DOI: 10.15360/1813-9779-2023-2-224
14. *Корабельников Д.И., Магомедалиев М.О.* Современные биомаркеры острого повреждения почек. *ФАРМАКОЭКОНОМИКА. Современная фармакоэкономика и фармакоэпидемиология*. 2023; 16 (1): 87–104. [*Korabelnikov D.I., Magomedaliev M.O.* Modern biomarkers of acute kidney injury. *PHARMACOECONOMICS. Modern Pharmacoeconomics and Pharmacoepidemiology / FARMAKOEKONOMIKA. Sovremennaya Farmakoekonomika I Farmakoekoepidemiologiya* 2023; 16 (1): 87–104. (In Russ.)]. DOI: 10.17749/2070-4909/ farmakoekonomika. 2023.171.
15. *Gharaibeh K.A., Hamadah A.M., El-Zoghby Z.M., Lieske J.C., Larson T.S., Leung N.* Cystatin C predicts renal recovery earlier than creatinine among patients with acute kidney injury. *Kidney Int Rep*. 2018; 3 (2): 337–342. DOI: 10.1016/j.ekir.2017.10.012. PMID: 29725637

16. *Digvijay K., Neri M., Fan W., Ricci Z., Ronco C.* International survey on the management of acute kidney injury and continuous renal replacement therapies: year 2018. *Blood Purif.* 2019; 47 (1–3): 113–119. DOI: 10.1159/000493724. PMID: 30269144
17. *Каюков И.Г., Смирнов А.В., Эмануэль В.Л.* Цистатин С в современной медицине. *Нефрология.* 2012; 16 (1): 22–39. [*Kayukov I.G., Smirnov A.V., Emanuel V.L.* Cystatin C in current medicine. *Nephrology/ Nefrologiya* (Saint-Petersburg). 2012; 16 (1): 22–39. (In Russ.)]. DOI: 10.24884/1561-6274-2012-16-1-22-39.
18. *Магомедалиев М.О., Корабельников Д.И., Хорошилов С.Е.* Способ оценки неблагоприятного исхода пневмонии тяжелого течения, ассоциированной с COVID-19, по уровню s-CysC. Российский патент RU 2779581C2 2022 г. по МПК G01N33/68 G01N33/49 G01N33/53. *Бюллетень.* 2022; 25: 3. [*Magomedaliev M.O., Korabelnikov D.I., Khoroshilov S.E.* A method for assessing the adverse outcome of severe pneumonia associated with COVID-19 by the level of s-CysC. Russian patent RU 2 779581 C2, IPC G01N 33/68, G01N 33/49, G01N 33/53. *Bulletin.* 2022; 25: 3. (in Russ.)]. https://patenton.ru/patent/RU2779581C2
19. *Магомедалиев М.О. Корабельников Д.И. Хорошилов С.Е.* Способ оценки неблагоприятного исхода пневмонии тяжелого течения, ассоциированной с COVID-19, по уровню u-CysC. Российский патент RU 2779579C2 2022 г. по МПК G01N 33/68, G01N 33/493, G01N 33/53. *Бюллетень.* 2022; 25: 3. [*Magomedaliev M.O, Korabelnikov D.I., Khoroshilov S.E.* A method for assessing the adverse outcome of severe pneumonia associated with COVID-19 by the level of u-CysC. Russian patent RU2779579 C2, IPC G01N 33/68, G01N 33/493, G01N 33/53. *Bulletin.* 2022; 25: 3. (in Russ.)]. https://patenton.ru/patent/RU2779579C2
20. *Zi M., Xu Y.* Involvement of cystatin C in immunity and apoptosis. *Immunol Lett.* 2018; 196: 80–90. DOI: 10.1016/j.imlet.2018.01.006. PMID: 29355583
21. *Collins A.R., Grubb A.* Inhibitory effects of recombinant human cystatin C on human coronaviruses. *Antimicrob Agents Chemother.* 1991; 35 (11): 2444–2446. DOI: 10.1128/AAC.35.11.2444. PMID: 1804023
22. *Collins A.R., Grubb A.* Cystatin D, a natural salivary cysteine protease inhibitor, inhibits coronavirus replication at its physiologic concentration. *Oral Microbiol Immunol.* 1998; 13 (1): 59–61. DOI: 10.1111/j.1399-302X.1998.tb00753.x. PMID: 9573825
23. *Clemente V., D'Arcy P., Bazzaro M.* Deubiquitinating enzymes in coronaviruses and possible therapeutic opportunities for COVID-19. *Int J Mol Sci.* 2020; 21 (10): 3492. DOI: 10.3390/ijms21103492. PMID: 32429099
24. *Björck L., Grubb A., Kjellén L.* Cystatin C, a human proteinase inhibitor, blocks replication of herpes simplex virus. *J Virol.* 1990; 64 (2): 941–943. DOI: 10.1128/JVI.64.2.941-943.1990. PMID: 2153254
25. *Vernekar V., Velhal S., Bandivdekar A.* Evaluation of cystatin C activities against HIV. *Indian J Med Res.* 2015; 141 (4): 423–430. DOI: 10.4103/0971-5916.159282. PMID: 26112843
26. *Nakamura S., Hata J., Kawamukai M., Matsuda H., Ogawa M., Nakamura K., Jing H.* et al. Enhanced anti-rotavirus action of human cystatin C by site-specific glycosylation in yeast. *Bioconjug Chem.* 2004; 15 (6): 1289–1296. DOI: 10.1021/bc049838s. PMID: 15546195
27. *Carrasco L.* Picornavirus inhibitors. *Pharmacol. Ther.* 1994; 64 (2): 215–290. DOI: 10.1016/0163-7258(94)90040-X. PMID: 7533301.
28. *Murray P.T., Le Gall J.-R., Miranda D.D.R., Pinsky M.R., Tetta C.* Physiologic endpoints (efficacy) for acute renal failure studies. *Curr Opin Crit Care.* 2002; 8 (6): 519–525. DOI: 10.1097/00075198-200212000-00007. PMID: 12454536
29. *Наркевич А.Н., Виноградов К.А.* Методы определения минимально необходимого объема выборки в медицинских исследованниях. *Социальные аспекты здоровья населения. Электронный научный журнал.* 2019; 65 (6): 2–19. [*Narkevich A.N., Vinogradov K.A.* Methods for determining the minimum required sample size in medical research. *Social Aspects of Public Health. Electronic Scientific Journal/ Socialniye Aspecty Zdorovya Naseleniya. Electronny Nauchny Zhurnal.* 2019; 65 (6): 2–19. (In Russ.)]. DOI: 10.21045/2071-5021-2019-65-6-10
30. *Larner A.J.* Effect size (Cohen's d) of cognitive screening instruments examined in pragmatic diagnostic accuracy studies. *Dement Geriatr Cogn Dis Extra.* 2014; 4 (2): 236–241. DOI: 10.1159/000363735. PMID: 25177332
31. *Li Y., Yang S., Peng D., Zhu H.-M., Li B.-Y., Yang X., Sun X.-L.* et al. Predictive value of serum cystatin C for risk of mortality in severe and critically ill patients with COVID-19. *World J Clin Cases.* 2020; 8 (20): 4726–4734. DOI: 10.12998/wjcc.v8.i20.4726. PMID: 33195640
32. *Zinellu A., Mangoni A.A.* Cystatin C, COVID-19 severity and mortality: a systematic review and meta-analysis. *J Nephrol.* 2022; 35 (1): 59–68. DOI: 10.1007/s40620-021-01139-2. PMID: 34390479
33. *Chen D., Sun W., Li J., Wei B., Liu W., Wang X., Song F.* et al. Serum cystatin C and coronavirus disease 2019: a potential inflammatory biomarker in predicting critical illness and mortality for adult patients. *Mediators Inflamm.* 2020: 3764515. DOI: 10.1155/2020/ 3764515. PMID: 33061826
34. *Ouyang S.-M., Zhu H.-Q., Xie Y-N, Zou Z.-S., Zuo H.-M., Rao Y.-W., Liu X.-Y.* et al. Temporal changes in laboratory markers of survivors and non-survivors of adult inpatients with COVID-19. *BMC Infect Dis.* 2020; 20 (1): 952. DOI: 10.1186/s12879-020-05678-0. PMID: 33308159
35. *Wang J., Guo S., Zhang Y., Gao K., Zuo J., Tan N., Du K. et al.* Clinical features and risk factors for severe inpatients with COVID-19: a retrospective study in China. *PLoS One.* 2020; 15 (12): e0244125. DOI: 10.1371/journal.pone.0244125 PMID: 33332437
36. *Chen S., Li J., Liu Z., Chen D., Zhou L., Hu D., Li M. et al.* Comparing the value of cystatin C and serum creatinine for evaluating the renal function and predicting the prognosis of COVID-19 patients. *Front Pharmacol.* 2021; 12: 587816. DOI: 10.3389/fphar.2021.587816. PMID: 33828483
37. *Yang Z., Shi J., He Z., Lü Y., Xu Q., Ye C., Chen S. et al.* Predictors for imaging progression on chest CT from coronavirus disease 2019 (COVID-19) patients. *Aging (Albany NY).* 2020; 12 (7): 6037–6048. DOI: 10.18632/aging.102999. PMID: 32275643

Received 07.07.2022
Accepted 06.05.2023

https://doi.org/10.15360/1813-9779-2023-3-12-19

Meglumine Sodium Succinate in Diabetic Ketoacidosis

Mikhail I. Neimark[1,2], Evgenij A. Kloster[2]*,
Andrej A. Bulganin[1,2], Andrej V. Ioshhenko[2], Evgenij A. Subbotin[1]

[1] Altai State Medical University, Ministry of Health of Russia,
40 Lenin Av., 656038 Barnaul, Altai District, Russia
[2] Barnaul Clinical Hospital «Russian Railways-Medicine»
20 Molodezhnaya Str., 656038 Barnaul, Russia

For citation: *Mikhail I. Neimark, Evgenij A. Kloster, Andrej A. Bulganin, Andrej V. Ioshhenko, Evgenij A. Subbotin.* Meglumine Sodium Succinate in Diabetic Ketoacidosis. *Obshchaya Reanimatologiya = General Reanimatology.* 2023; 19 (3): 12–19. https://doi.org/10.15360/1813-9779-2023-3-12-19 [In Russ. and Engl.]

***Correspondence to:** Evgenij A. Kloster, e.kloster@mail.ru

Summary

The most common agent used for infusion therapy in patients with diabetic ketoacidosis (DKA) is isotonic 0.9% sodium chloride solution. However, infusion of required volumes can result in development of iatrogenic complications — i. e., worsening of metabolic hyperchloremic acidosis in DKA patients with already altered acid-base balance. Balanced crystalloid solutions can be used as alternative to saline.

Objective. To evaluate the feasibility of using meglumine sodium succinate (MSS) balanced crystalloid solution in DKA.

Material and methods. We examined 2 groups of patients, 30 subjects each, with moderate and severe diabetic ketoacidosis admitted to anesthesiology and intensive care unit. Patients from both groups were administered with insulin and an infusion therapy was employed according to current clinical guidelines for the management of patients with complications of diabetes mellitus. In the comparison group, infusion therapy included 0.9% sodium chloride, 4% potassium chloride, and 5% dextrose. In the study group MSS intravenous drip infusions 10 ml/kg/daily were added to the infusion protocol. Volumes and infusion rates were comparable in both groups. The following indicators were evaluated: time to resolution and DKA resolution rates during thorough monitoring (first 48 hours of therapy), the time (in hours) before discontinuation of insulin infusion; the time to complete consciousness recovery (15 items on the Glasgow Coma scale); the duration (in hours) of stay in the intensive care unit (ICU), dynamics of blood electrolytes; parameters of acid-base balance; levels of glycemia and lactatemia.

Results. All patients improved and were transferred from ICU, the mortality rate was 0%. Infusion of MSS shortened the time to DKA resolution (30.0 h [24.0 h; 36.0 h] in the study group, vs 44.5 h [36.5 h; 51.5 h] in the comparison group (P=0.001)); DKA resolution rates during 48 hours from initiation of therapy achieved 90.0% (27) in the study group, vs 66.7% (20) in the comparison group (P=0.060)); duration of intravenous insulin infusion was 32.0 h [24.5 h; 40.0 h] in the study group vs 48.0 h [40.0 h; 55.5 h] in the comparison group (P=0.001)); duration of ICU stay was 41.0 h [30.0 h; 48.0 h] in the study group, vs 56.0 h [50.0 h; 66.3 h] in the comparison group (P=0.001).

Conclusion. Infusion of a balanced succinate-containing crystalloid solution improves the results of DKA treatment, as compared to traditional infusion of 0.9% sodium chloride.

Keywords: meglumine sodium succinate; diabetic ketoacidosis; diabetes mellitus; infusion therapy; acidosis; crystalloid solution; Reamberin

Conflict of interest. The authors declare that there is no conflict of interest. LLC «NTFF «POLISAN» was not the initiator of the study and had no influence on study design, analysis of obtained data, interpretation of the results and writing of this paper.

Introduction

Diabetic ketoacidosis (DKA) is a serious complication of uncontrolled diabetes mellitus (DM) that requires urgent medical intervention.

The total number of patients with diabetes mellitus in the Russian Federation as of January 1, 2019 was 4,584,575 (3.12% of the Russian population), including 5.6% (256,200) of type 1 diabetes, 92.4% (4.24 million) of type 2 diabetes, and 2% of other types of diabetes. Worldwide, 3–4% of the adult population has diabetes mellitus, 95% of them type 2 DM. It is predicted that its prevalence could reach 552 million people by 2030. The prevalence of DKA is 46 cases per year per 10,000 people with diabetes. The predominant age of onset is less than 30 years [1]. The differences in the risk of DKA in different types of diabetes can be seen in the prevalence of ketoacidotic coma in Russia, which is 1.25% in type 1 DM, while in type 2 diabetes it is 0.05% [2].

DKA is characterized by a clinical and laboratory triad of hyperglycemia, ketonemia, and metabolic acidosis with increased anion gap [3]. Ketones are formed from β-hydroxylated fatty acids during fasting or insulin deficiency. They include acetate, acetoacetic acid, and beta-hydroxybutyrate, which

act as strong ions. In patients with DKA, acidosis is caused by increased ketones and lactate due to tissue hypoperfusion. Due to hyperglycemia-induced increased urine output, dehydration is common in DKA patients [4].

In this context, the primary therapeutic intervention, which precedes the correction of insulin deficiency, is fluid therapy. Its strategy is still under discussion. The use of isotonic crystalloid solutions for the treatment of DKA is a generally accepted principle. Current recommendations for fluid therapy in DKA include isotonic 0.9% sodium chloride with possible addition of potassium chloride [1, 5–7].

However, the use of unbalanced solutions can lead to hyperchloremia and aggravate the preexisting acidosis, promoting disorders of coagulation, cardiac, immune and renal function (due to renal arteriolar narrowing), provoking oliguria and delayed control of acidosis [4, 7–9, 11]. Preference should be given to balanced polyionic solutions [12].

Since meglumine sodium succinate (Reamberin®) has an electrolyte composition close to plasma electrolyte composition and contains succinate as an alkaline reserve, the inclusion of Reamberin® in the treatment is thought to lead to a more rapid resolution of DKA due to the correction of hypoxia associated with most urgent conditions [7, 9, 13]. However, the use of balanced crystalloids in the treatment of DKA is associated with the risk of alkalosis and hyperkalemia, which requires a detailed study of this problem.

The aim of our study was to provide a rationale for the use of a balanced crystalloid solution containing meglumine sodium succinate (Reamberin®) in DKA.

Materials and Methods

A noninterventional prospective study was performed. A total of 60 patients (32 male, 28 female), aged 18 to 75 years, admitted to the emergency department of the Russian Railway Clinical Hospital (Barnaul, Russia) with DM complicated by DKA were enrolled. Diabetes mellitus type 1 was diagnosed in 34 patients and diabetes mellitus type 2 in 26 patients. On admission, 32 patients had moderate DKA, while 28 patients were diagnosed with severe DKA according to the classification of Dedov et al. (2021) [5].

Depending on the type of fluid therapy, patients were divided into 2 groups of 30 patients each. Randomization was performed using the envelope method. Subdivision of patients into subgroups according to the type of DM was considered inappropriate because of the small number of patients. Patients in group 1 received fluid therapy according to the algorithm described in the clinical guidelines [5]. Sodium chloride 0.9% with potassium chloride added if necessary was used. In the second group, the basic fluid therapy was partially replaced by Reamberin® balanced solution 10 ml/kg per day until the ketoacidosis was resolved. When the plasma glucose concentration reached 14 mmol/l (usually by the end of the second day), rehydration was continued with oral fluids and 150–200 ml of 5% dextrose, depending on the actual need [1, 5, 6].

The time of initiation of fluid therapy, its rate and daily volume were comparable in both groups (Table 1).

Fluid therapy was started immediately after the patient was admitted to the ICU. After 2 hours, insulin was administered as follows: an initial dose of rapid-acting insulin 0.1 IU/kg real body weight by bolus injection through an infusion device after the initial infusion load. The rate of intravenous insulin administration was adjusted according to the rate of reduction of hyperglycemia and averaged 3 mmol/l/h (no more than 4 mmol/l/h) [1, 5].

Inclusion criteria were age 18 to 75 years inclusive; documented diabetes mellitus; diagnostic criteria for ketoacidosis such as plasma glucose level >13 mmol/L, hyperketonemia (>5 mmol/L), ketonuria (⩾++), metabolic acidosis (pH <7.3); clinical, functional and laboratory signs of dehydration.

Exclusion criteria were hypersensitivity to components of Reamberin; conditions requiring administration of sodium bicarbonate solution; absence of clinical and laboratory criteria for DKA; urgent diseases of other organs and systems requiring specific drug therapy or surgical intervention.

The clinical assessment of the patient's status and the need for rehydration was based on the volume status according to the results of the PLR test. A 15% increase in the cardiac index (CI) when the patient's legs were elevated, registered by hemodynamic monitoring, and its return to the baseline level when the legs were lowered, indicated «re-

Table 1. The characteristics of the fluid therapy (*M*±*SE*).

Stages	Total volume (composition) of infusion in groups. mL		*P*
	Control	Reamberin	
During the first 2 hours	1413.78±179.18 (KCl 4%; NaCl 0.9%)	1500.8±191.4 (Reamberin; KCl 4%; NaCl 0.9%)	0.094
Day 1	4523.7±313.64 (KCl 4%; NaCl 0.9%)	4802.56±321.31 (Reamberin; KCl 4%; NaCl 0.9%)	0.056
Day 2	2544.48±199.96 (KCl 4%; NaCl 0.9%; Dextrose 5%)	2701.44±213.88 (Reamberin; KCl 4%; NaCl 0.9%; Декстроза 5%)	0.062

sponder» status (all participants were found to have this), which provided a rationale for planned rehydration therapy.

To assess central hemodynamics, including the PLR test, tetrapolar rheovasography was performed with the KM-AR-01 DIAMANT cardio-respiratory and tissue hydration monitor. The following parameters were measured:

— heart rate (HR)
— cardiac index (CI)
— peripheral vascular resistance index (PVRI)
— stroke index (SI)
— extracellular fluid volume (EFV)
— intracellular fluid volume (IFV).

20 healthy subjects were studied as a control group while central hemodynamic parameters were assessed.

Non-invasive blood pressure (NIBP), electrocardiogram, SpO_2, respiratory rate (RR), body temperature, urine output rate were monitored in the intensive care unit, fluid balance was controlled by assessment of administered and excreted fluid.

DKA severity, acid-base status, plasma ion levels, and laboratory criteria for organ and system function were determined at the following intervals

Rapid glycemic test: hourly until plasma glucose (PG) dropped to 13 mmol/L, then, if stable, every 3 hours. Material was capillary blood tested on Biosen C-Line Clinic/GP+.

Urine or plasma analysis for ketone bodies: twice daily for the first 2 days, then once daily on the URILIT-150 device.

Plasma Na^+ and K^+: baseline, then at least twice daily. Venous blood was tested on the EasyLite Calcium Na/K/Ka/pH meter.

Clinical chemistry (urea, creatinine, lactate): baseline, then once daily. Venous blood was tested on Thermo Scientific Indiko Plus.

Blood gases and pH (venous blood): once every 6 hours until resolution of DKA, then once or twice daily until ABB normalized. Mixed venous blood was collected from the central venous catheter near the right atrium and tested using the Abbott i-Stat CG4+Cartridge test system.

The following efficacy endpoints were assessed:

A. Primary efficacy endpoints included:

1) Rate of resolution of DKA during follow-up (within the first 48 hours of therapy).

2) Time (in hours) from initiation of therapy to resolution of DKA. DKA resolution criteria included plasma glucose <11.1 mmol/L and two of the following: plasma bicarbonate $\geqslant 18$ mmol/L, venous blood pH>7.3, or strong ion gap $\leqslant 12$ mmol/L.

3) Time (in hours) to discontinuation of insulin infusion.

4) Time to full recovery of consciousness (15 points on the GCS).

5) Length of stay in the ICU (in hours).

6) Mortality in the ICU.

B. Secondary efficacy endpoints were:

1) Changes in blood electrolytes
2) Changes in acid-base parameters
3) Changes in blood glucose and lactate.

Various statistical methods were employed depending on the distribution type of variables and the aim of the study [14, 15].

We used skewness and kurtosis parameters, which characterized the shape of the distribution curve, to estimate the distribution type of variables. Continuous variables with normal distribution were reported as $M \pm SE$, where M is the sample mean and SE is the standard error of the mean. For variables with non-normal distribution, medians with first and third quartiles were reported. The qualitative variables were reported as observed frequencies and percentages.

In cases of normal distribution and equality of variance, Student's t-test was used to compare means. Equality of variance was assessed using Fisher's F criterion. In the case of non-normal distribution and inequality of dispersion, the Mann–Whitney non-parametric U-criterion was used.

Pearson's χ^2 criterion for four-way contingency tables was used to compare qualitative variables. For small frequencies (5 to 10), Yates' correction for continuity was used. For frequencies less than 5, Fisher's exact method for four-way contingency tables was used.

Differences were considered significant at $P<0.05$, where p is the probability of first-order error in testing the null hypothesis. In all cases, two-tailed versions of the criteria were used.

Data were processed and visualized using Statistica 12.0 (StatSoft) and Microsoft Office Excel 2017.

Results

The baseline characteristics of the patients in the study groups are shown in Table 2.

The baseline status of the patients in the two groups was not comparable in several parameters (age, body mass index (BMI)), baseline glycated hemoglobin, glucose and urea levels, which was related to the variability of the clinical course of DM and a relatively small sample of patients. However, it is noteworthy that blood glucose, glycated hemoglobin, and urea levels were higher in patients in the Reamberin group than in the control group.

Central hemodynamic and fluid compartment parameters were identical between participants and healthy controls. CBV and extracellular fluid compartment were significantly lower by 18.9% (P=0.001) in the patients than in the control group on admission. Intracellular fluid compartment was also lower by 1.9% (P=0.001) and SI was lower by 40.5% (P=0.001). CI values in the patient and healthy control samples did not differ (Table 3), and their maintenance within normal limits in the presence

Table 2. Baseline patient characteristics (*M±SE*, *Me* [*Q1*; *Q3*] or % (*N*)).

Parameter	Values in groups		*P*
	Control, *N*=30	Reamberin, *N*=30	
Age, years	36.67±3.29	49.37±3.09	**0.007**
BMI, kg/m²	24.27±0.90	28.30±1.25	**0.011**
Diabetes mellitus (percentage of type 1 DM)	70.0% (21)	43.3% (13)	0.068
HbA1c, %	9.70 [8.27; 10.70]	11.18 [10.16; 12.24]	**0.025**
DM manifestation as the cause of DKA	6.7% (2)	10.0% (3)	0.999
Disease/surgery/trauma as the cause of DKA	43.3% (13)	46.7% (14)	0.795
Patient non-compliance as the cause of DKA	50.0% (15)	43.3% (13)	0.605
DKA severity			
Glucose, mmol/L	21.74 [19.11; 26.90]	28.82 [21.36; 32.69]	**0.028**
pH	7.21±0.02	7.22±0.02	0.755
Bicarbonate, mmol/L	11.99±1.37	12.88±1.19	0.623
Anion gap, mEq/L	21.70±1.41	21.84±1.33	0.945
Glasgow scale, points	15.00 [15.00; 15.00]	15.00 [13.25; 15.00]	0.844
Severe DKA (percentage)	53.3% (16)	40.0% (12)	0.301
Other parameters prior to treatment initiation			
Na, mmol/L	132.61±0.95	132.56±1.36	0.976
Cl, mmol/L	98.96±0.92	97.83±0.98	0.406
K, mmol/L	4.17±0.17	3.98±0.22	0.489
Lactate, mmol/L	2.86 [2.00; 3.94]	3.01 [2.06; 4.56]	0.291
Urea, mmol/L	9.93±0.89	13.95±1.47	**0.024**
Creatinine, μmol/L	112.5 [95.4; 128.5]	116.7 [86.4; 138.3]	0.247

Table 3. Baseline hemodynamic parameters in the studied patients and healthy controls, *M±SE*.

Parameter	Values in samples		*P*
	Patients, *N*=60	Healthy controls, *N*=20	
Heart rate, bpm	113.9±1.9	67±4.1	**0.001**
Stroke index, mL/m²	22.5±1.5	37.8±3.3	**0.001**
Cardiac index, L/min/m²	2.6±0.2	2.5±0.3	**0.07**
Systemic vascular resistance index, dyn×s×cm^{-5}/m²	2332.6±196.8	3000.2±403.4	**0.001**
Urine output rate, mL/kg/h	0.32±0.09	1.04±0.13	**0.04**
Extracellular fluid, %	81.1±2.6	100.2±0.6	**0.001**
Intracellular fluid, %	98.1±1.0	100±0.1	**0.001**
Circulating blood volume, %	81.1±2.6	100.2±0.6	**0.001**

Table 4. Changes in central hemodynamic parameters in the general patient population during treatment (*N*=60, *M±SE*).

Parameter	Values during fluid therapy		*P*
	Prior to initiation	Two hours after initiation	
Heart rate, bpm	113.9±1.9	91.4±8.3	**0.001**
Stroke index, mL/m²	22.5±1.5	31.7±3.6	**0.001**
Cardiac index, L/min/m²	2.6±0.2	2.8±0.3	0.22
Systemic vascular resistance index, dyn×s×cm^{-5}/m²	2332.6±196.8	2539.6±473.1	0.491
Urine output rate, mL/kg/h	0.32±0.09	0.71±0.18	**0.05**

Table 5. Treatment outcomes by study group (*Me* [*Q1*; *Q3*] or % (*N*)).

Parameters of severity and outcome	Values in groups		*P*
	Control, *N*=30	Reamberin, *N*=30	
Duration of DKA, hours	44.5 [36.5; 51.5]	30.0 [24.0; 36.0]	**0.001**
Resolution of DKA within 48 hours, percentage	66.7% (20)	90.0% (27)	0.060
Duration of insulin infusion, h	48.0 [40.0; 55.5]	32.0 [24.5; 40.0]	**0.001**
Time to complete recovery of consciousness, h	0.0 [0.0; 0.0]	0.0 [0.0; 4.0]	0.627
ICU treatment time, h	56.0 [50.0; 66.3]	41.0 [30.0; 48.0]	**0.001**
Mortality rate in the ICU, %	0	0	—

of reduced stroke volume was achieved by significant tachycardia.

The above results (Table 4) demonstrate the reversal of hemodynamic disturbances caused by fluid therapy.

The treatment efficiency outcomes are shown in Table 5. The data show that the duration of DKA, insulin infusion and ICU treatment was significantly shorter in the Reamberin group than in the control group (*P*=0.001).

Table 6. Changes in acid-base status in the study groups (*M±SE* or *Me* [*Q1*; *Q3*]).

Parameter and time point	Values in the groups				*P*
	N	Control	*N*	Reamberin	
Venous blood pH					
Within the first 24 hours					
1–6 h	30	7.21±0.02	30	7.22±0.02	0.703
7–12 h	29	7.27±0.02	30	7.30±0.02	0.187
13–18 h	25	7.30±0.01	30	7.34±0.01	**0.037**
19–24 h	27	7.33±0.01	30	7.38±0.01	**0.003**
25–48 hours later					
25–30 h	15	7.32±0.01	18	7.38±0.01	**0.003**
31–36 h	25	7.36±0.01	14	7.40±0.01	**0.029**
37–42 h	11	7.35±0.01	6	7.42±0.01	**0.010**
43–48 h	20	7.38±0.01	7	7.43±0.01	**0.010**
Bicarbonate, mmol/L					
Within the first 24 hours					
1–6 h	30	11.99±1.37	30	12.88±1.19	0.623
7–12 h	29	14.05±1.12	30	16.88±0.90	0.053
13–18 h	25	16.83±1.23	30	19.81±0.75	**0.045**
19–24 h	27	17.79±0.99	30	22.38±0.62	**<0.001**
25–48 hours later					
25–30 h	15	17.60±1.34	18	23.04±0.84	**0.001**
31–36 h	25	20.42±0.80	14	24.05±0.71	**0.004**
37–42 h	11	19.39±1.07	6	24.60±0.81	**0.005**
43–48 h	20	22.65±0.55	7	24.61±0.91	0.078
Anion gap, mEq/L					
Within the first 24 hours					
1–6 h	30	21.60±1.40	30	21.67±1.36	0.970
7–12 h	29	21.06±1.18	30	17.91±1.09	0.054
13–18 h	25	18.04±1.27	30	15.37±0.94	0.092
19–24 h	27	16.40 [13.00; 18.95]	30	12.24 [10.43; 15.44]	**0.038**
25–48 hours later					
25–30 h	15	17.36±1.74	18	13.24±0.94	**0.049**
31–36 h	25	14.20 [9.90; 17.79]	14	10.30 [9.53; 11.54]	0.107
37–42 h	11	15.32±1.26	6	11.92±1.11	0.093
43–48 h	20	11.86±1.01	7	9.65±1.26	0.250

Note. *N* — number of measurements.

The changes in blood acid-base status in the groups of patients studied are shown in Table 6.

The addition of Reamberin to the infusion therapy protocol improved the basic parameters of acid-base balance intrinsic to ketoacidosis.

The changes in plasma electrolytes in two groups of patients are summarized in Table 7.

The urea level on day 1 and 2 was higher in the Reamberin group than in the controls. No significant differences between the two groups of patients in plasma electrolytes were found.

Discussion

According to current critical care guidelines for diabetic acidosis, the primary goal is to correct water and electrolyte disturbances. Dehydration is controlled by increasing the volume of extracellular fluid through intravenous infusion of crystalloid solutions. CBV replenishment helps stabilize the cardiovascular system, increases tissue sensitivity to insulin by reducing plasma osmolality, improving tissue perfusion, as well as decreasing the production of insulin antagonists [6, 16], which explains the feasibility of administering crystalloid solutions first, followed by insulin. This is accompanied by a more manageable fall in a blood glucose level in response to insulin administration compared to its use in severe dehydration.

CBV is replenished in patients who respond to infusion therapy, as determined by the PLR test. A good response, indicated by a 15% increase in cardiac index after leg elevation and its return to baseline after leg lowering, suggests dehydration and a likely positive response to fluid therapy.

The fluid deficit in patients with diabetic ketoacidosis is 50–100 ml/kg real body weight and depends on the severity of DKA. In this case, a large volume of fluid must be replenished within 24–48 hours. The recommended solution for infusion therapy is 0.9% sodium chloride or 0.45% sodium chloride for sodium levels above 145 mmol/L [5, 17].

Currently, more clinicians are inclined to a restrictive strategy of fluid therapy, including control of hemodynamic parameters and body fluid compartments. Restrictive fluid therapy in our study implied replenishment of circulating blood volume in case of actual hypovolemia, as well as its continuation in volumes not involving dangerous excessive fluid infusion.

The rate of replenishment of hypovolemia in the first 2 hours was about 10 ml/kg/h and did not depend on the type of fluid. The rate of further

Table 7. Changes in electrolytes and clinical chemistry parameters in the study groups (*M±SE*, *Me* [*Q1*; *Q3*]).

Parameter. mmol/L	Values in groups				*P*
	N	Control	*N*	Reamberin	
Na^+					
12 h	30	134.73±0.97	30	135.16±1.15	0.777
24 h	30	135.60 [133.20; 138.13]	30	136.00 [133.63; 138.65]	0.761
36 h	27	136.63±0.70	20	137.83±1.04	0.324
48	25	137.43±0.69	14	137.69±1.03	0.829
Cl^-					
12 h	30	99.73±0.85	30	100.17±0.76	0.705
24 h	30	102.17±0.79	30	100.63±0.69	0.147
36 h	27	102.11±0.79	20	102.15±0.71	0.972
48 h	25	103.00 [102.00; 105.00]	15	102.00 [99.00; 105.00]	0.275
K^+					
12 h	30	3.92±0.12	30	3.87±0.12	0.764
24 h	30	3.91±0.10	30	4.01±0.08	0.402
36 h	27	3.90±0.11	20	3.94±0.10	0.818
48 h	25	3.87±0.11	15	3.82±0.09	0.785
Lactate					
24 h	29	1.93 [1.21; 2.31]	30	1.29 [0.86; 2.01]	0.576
48 h	24	1.28±0.12	14	1.31±0.19	0.914
Urea					
24 h	30	6.86±0.52	30	9.82±1.00	**0.012**
48 h	25	6.03±0.54	14	9.56±1.35	**0.026**
Creatinine					
24 h	30	86.57 [76.75; 95.79]	30	86.87 [72.83; 105.26]	0.186
48 h	25	79.33±3.38	14	91.42±10.37	0.284

Note. *N* — number of measurements.

rehydration was determined by central hemodynamic parameters and urine output rate. It averaged 2–3 ml/kg/hour during the first day. With positive clinical trends, improved ABB, stabilization of glucose levels, the rate of fluid therapy did not exceed 1–3 ml/kg/hour during the second day. This approach helped to avoid iatrogenic complications such as cerebral or pulmonary edema.

Despite the paramount importance of normal saline in DKA, recent clinical guidelines [1,5] emphasize the risk of hyperchloremic metabolic acidosis due to its high chloride content (154 mmol/L). Increasing the plasma chloride level decreases the bicarbonate concentration, while diluting the blood with a large volume of buffer-free fluid results in dilutional acidosis. Therefore, the use of normal saline in DKA may actually worsen its course [18].

This, together with the antioxidant, antihypoxic, and energy-protective properties of sodium meglumine succinate [19–21], suggests that its use may improve the outcome of intensive care in patients with diabetic ketoacidosis.

In our study, the addition of Reamberin to fluid therapy protocol resulted in a more rapid resolution of ketoacidosis than the use of normal saline alone. Increased bicarbonate buffering capacity due to succinate metabolism resulted in earlier pH normalization. The anion gap in the Reamberin group decreased over time, in contrast to the control group. This explained the faster resolution of DKA, allowing patients to be switched to subcutaneous insulin administration.

Conclusion

The addition of Reamberin (sodium meglumine succinate), a balanced crystalloid solution containing succinate, to fluid therapy protocol for DKA resulted in faster resolution of ketoacidosis, discontinuation of intravenous insulin, and transfer from the intensive care unit. These effects were achieved by increasing blood buffering capacity and earlier normalization of blood pH.

References

1. *Заболотских И.Б., Проценко Д.Н.* Интенсивная терапия: национальное руководство. Т. 2. 2-е изд., перераб. и доп. М.: ГЭОТАР-Медиа; 2022: 1056. [*Zabolotskikh I. B., Protsenko D. N.* Intensive care: national guidelines. Vol. 2. 2nd ed., rev. and exp. M.: GEOTAR-Media; 2022: 1056. (in Russ.)] DOI: 10.33029/9704-5018-5. ISBN 978-5-9704-6259-1.
2. *Шестакова М.В., Викулова О.К., Железнякова А.В., Исаков М.А., Дедов И.И.* Эпидемиология сахарного диабета в Российской Федерации: что изменилось за последнее десятилетие? *Терапевтический архив.* 2019; 91 (10): 4–13. [*Shestakova M.V., Vikulova O.K., Zheleznyakova A.V., Isakov M.A., Dedov I.I.* Diabetes epidemiology in Russia: what has changed over the decade? *Ter. Arkh/Terapevticheskiy Arkhiv.* 2019; 91 (10): 4–13. (in Russ.)]. DOI: 10.26442/00403660.2019.10.000364
3. *Jahangir A., Jahangir A., Siddiqui F.*S., *Niazi M.R.K., Yousaf F., Muhammad M., Sahra S. et al.* Normal saline versus low chloride solutions in treatment of diabetic ketoacidosis: a systematic review of clinical trials. *Cureus* 14 (1): e21324. DOI: 10.7759/cureus.21324. PMID: 35186583
4. *Roizen M. F., Fleisher L. A.* Периоперационное ведение пациентов с сопутствующими заболеваниями. В кн.: «Анестезия» Рональда Миллера *(ред.).* в 4 т. СПб.: Человек; 2015 (2): 1139–1234. [*Roizen M. F., Fleisher L. A.* Perioperative management of patients with concomitant diseases. In the book: «Anesthesia» by Ronald Miller (ed.). in 4 vols. St. Petersburg: Man/Chelovek; 2015 (2): 1139–1234. (in Russ.)]
5. Алгоритмы специализированной медицинской помощи больным сахарным диабетом. Под редакцией Дедова И.И., Шестаковой М.В., Майорова А.Ю. 10-й выпуск (дополненный). М.; 2021. [Standards of specialized diabetes care. Ed. by Dedov I.I., Shestakova M.V., Mayorov A.Yu. 10th ed. (revised). M.; 2021. (in Russ.)]. DOI: 10.14341/DM12802
6. *Коваленко А.Л., Ризаханов Д.М., Яковлев А.Ю., Симутис И.С., Парфенов С.А., Бобовник С.В., Сорокин с соавт.* Предварительные результаты включения меглюмина натрия сукцината в лечение пациентов с острым панкреатитом средней и тяжелой степени. *Общая реаниматология.* 2021; 17 (1): 46–56. [*Kovalenko A.L., Rizakhanov D.M., Yakovlev A.Yu., Simutis I.S., Parfenov S.A., Bobovnik S.V., Sorokin et al.* Preliminary results of adding meglumine sodium succinate to the treatment of patients with moderate and severe acute pancreatitis. *General Reanimatology/Obshchaya Reanimatologya.* 2021; 17 (1): 46–56. (in Russ.)]. DOI: 10.15360/1813-9779-2021-1-0-1
7. *Симутис И.С., Бояринов Г.А., Юрьев М.Ю., Петровский Д.С., Коваленко А.Л., Сапожников К.В.* Новый взгляд на коррекцию COVID-19-опосредованных нарушений лёгочного газообмена. *Казанский медицинский журнал.* 2021; 102 (3): 362–372. [*Simutis I.S., Boyarinov G.A., Yuryev M.Yu., Petrovsky D.S., Kovalenko A.L., Sapozhnikov K.V.* A new look at the correction of COVID-19-mediated pulmonary gas exchange disorders. *Kazan Medical Journal/Kazanskiy Meditsinkiy Zhurnal.* 2021; 102 (3): 362–372. (in Russ.)]. DOI: 10.17816/KMJ2021-362.
8. *Handy J.M., Soni N.* Physiological effects of hyperchloraemia and acidosis. *Br J Anaesth.* 2008; 101 (2): 141–150. DOI: 10.1093/bja/ aen148. PMID: 18534973
9. *Симутис И.С., Бояринов Г.А., Юрьев М.Ю., Петровский Д.С., Коваленко А.Л., Сапожников К.В.* Первый опыт применения меглюмина натрия сукцината в коррекции COVID-19-ассоциированной коагулопатии. *Общая реаниматология.* 2021; 17 (3): 50–64. [*Simutis I.S., Boyarinov G.A., Yuriev M.Yu., Petrovsky D.S., Kovalenko A.L., Sapozhnikov K.V.* Meglumine sodium succinate to correct COVID-19-associated coagulopathy: the feasibility study. *General Reanimatology/ Obshchaya Reanimatologya.* 2021; 17 (3): 50–64. (in Russ)]. DOI: 10.15360/1813-9779-2021-3-50-64.
10. *Федерякин Д.В., Парфенов С.А., Веселов С.В., Колгина Н.Ю., Майоров М.О., Сабитов Т.Ф., Гончарук А.В. и соавт.* Гемодилюция меглюмина натрия сукцинатом при операциях на сердце в условиях искусственного кровообращения. *Кардиология и сердечно-сосудистая хирургия.* 2020; 13 (2): 114–119. [*Federyakin D.V., Parfenov S.A., Veselov S.V., Kolgina N.Yu., Mayorov M.O., Sabitov T.F., Goncharuk A.V. et al.* Hemodilution with meglumine sodium succinate during heart surgery in on-pump cardiac surgery. *Cardiology and cardiovascular surgery/ Kardiologiya i Serdechno-Sosudistaya Khirurgiya.* 2020; 13 (2): 114–119. (in Russ.)]. DOI: 10.17116/kardio202013021114
11. *Carrillo A.R., Elwood K., Werth C., Mitchell J., Sarangarm P.* Balanced crystalloid versus normal saline as resuscitative fluid in diabetic ketoacidosis. *Ann Pharmacother.* 2022; 56 (9): 998–1006. DOI: 10.1177/10600280211063651. PMID: 34986659
12. *Self W.H., Evans C.S., Jenkins C.A., Brown R.M., Casey J.D., Collins S.P., Coston T.D. et al.* Clinical effects of balanced crystalloids vs saline in adults with diabetic ketoacidosis: a subgroup analysis of cluster randomized clinical trials. *JAMA Netw Open.* 2 020; 3 (11): e2024596. DOI: 10.1001/jamanetworkopen.2020.24596. PMID: 33196806.
13. *Белкин А.А., Лейдерман И.Н., Коваленко А.Л., Ризаханова О.А., Парфенов С.А., Сапожников К.В.* Цитофлавин как компонент реабилитационного лечения пациентов с ишемическим инсультом, осложненным ПИТ-синдромом. *Журнал неврологии и психиатрии им. С.С. Корсакова.* 2020; 120 (10): 27–32. [*Belkin A.A., Leiderman I.N., Kovalenko A.L., Ryazanova O.A., Parfenov S.A., Sapozhnikov K.V.* Cytoflavin as a modulator of rehabilitation treatment of patients with ischemic stroke complicated by post-intensive care syndrome. *S.S. Korsakov Journal of Neurology and Psychiatry/ Zh. Nevrol.Psikhiatr. im. S.S. Korsakova.* 2020; 120 (10): 27–32. (in Russ.)]. DOI: 10.17116/jnevro202012010127.
14. *Гланц С.А.* Медико-биологическая статистика. Пер. с англ. М.: Практика; 1998: 459. [*Glantz S.A.* Medico-biological statistics. Translated from English M.: Praktika; 1998: 459]
15. *Боровиков В.П.* STATISTICA: искусство анализа данных на компьютере для профессионалов. СПб.: Питер; 2001: 656. [*Borovikov V.P.* STATISTICA: the art of data analysis on a computer for professionals. St. Petersburg: Peter; 2001: 656. (in Russ.)]
16. *Eledrisi M.S., Elzouki A.-N.* Management of diabetic ketoacidosis in adults: a narrative review. *Saudi J*

Med Med Sci. 2020; 8 (3): 165–173. DOI: 10.4103/sjmms.sjmms_478_19. PMID: 32952507

17. *Besen B.A.M.P, Boer W., Honore P.M.* Fluid management in diabetic ketoacidosis: new tricks for old dogs? *Intensive Care Med*. 2021; 47 (11): 1312–1314. DOI: 10.1007/s00134-021-06527-7. PMID: 34608527
18. *Марино П.Л.* Под ред. Ярошецкого А.И. Интенсивная терапия. Второе издание. Пер. с англ. М.: ГЭОТАР-Медиа; 2022: 1152. ISBN 978-5-9704-7041-1. [*Marino P.L.* Ed. Yaroshevsky A.I. Intensive therapy. Second edition. Translated from English. M.: GEOTAR-Media; 2022: 1152. ISBN 978-5-9704-7041-1]
19. *Спичак И.И., Копытова Е.В.* Применение полиионного раствора реамберина в медицине и опыт его использования в детской онкологии. *Онкология. Журнал им. П.А. Герцена*. 2018; 7 (5): 47–55. [*Spichak I.I., Kopytova E.V.* Application of polyionic reamberin solution in medicine and experience with its use in pediatric oncology. *P.A. Herzen Journal of Oncology/ Oncologiya. Zhurnal im. P.A. Herzena*. 2018; 7 (5): 47 55. (in Russ.)]. DOI; 10.17116/ onkolog2018705147
20. *Тихонова Е.О., Ляпина Е.П., Шульдяков А.А., Сатарова С.А.* Использование препаратов, содержащих сукцинат, в клинике инфекционных болезней. *Терапевтический архив*. 2016; 88 (11): 121–127. [*Tikhonova E.O., Lyapina E.P., Shuldyakov A.A., Sattarova S.A.* Use of succinate-containing agents in the treatment of infectious diseases. *Ter. Arkh/Terapevticheskiy Arkhiv*. 2016; 88 (11): 121–127. (in Russ.)]. DOI: 10.17116/terarkh20168811121-127
21. *Шах Б.Н., Лапшин В.Н., Кырнышев А.Г., Смирнов Д.Б., Кравченко-Бережная Н.Р.* Метаболические эффекты субстратного антигипоксанта на основе янтарной кислоты. *Общая реаниматология*. 2014; 10 (1): 33–42. [*Shah B. N., Lapshin V.N., Kyrnyshev A.G., Smirnov D.B., Kravchenko-Berezhnaya N.R.* Metabolic effects of a succinic acid. *General Reanimatology/Obshchaya Reanimatologya*. 2014; 10 (1): 33–42. (in Russ.)]. DOI: 10.15360/1813-9779-2014-1-33-42

Received 16.01.2023
Accepted 28.04.2023

https://doi.org/10.15360/1813-9779-2023-3-20-27

Risk Factors for COVID-19 Adverse Outcomes in ICU Settings of Various Types Repurposed Hospitals

Alexander A. Avramov[1,2,3]*, Evgeny V. Ivanov[1], Alexander V. Melekhov[2], Ruslan S. Menzulin[4], Andrey I. Nikiforchin[5]

[1] M. V. Lomonosov Moscow State University,
1 Leninskiye gory Str., 119991 Moscow, Russia
[2] National Medical Research Center, Treatment and Rehabilitation Center, Ministry of Health of Russia,
3 Ivankovskoe shosse, 125367 Moscow, Russia
[3] Clinic MedSwiss,
8/4 Lebyazhy lane, bldg. 2, 119019 Moscow, Russia
[4] Medsi Clinical Hospital №1,
2 Otradnoe, bldg.1, Krasnogorsk city district, 143442 Moscow area, Russia
[5] Mercy medical center,
345 St Paul Pl, Baltimore, MD 21202, USA

For citation: *Аврамов А. А., Иванов Е. В., Мелехов А. В., Мензулин Р. С., Никифорчин А. И.* Факторы риска неблагоприятного исхода COVID-19 в ОРИТ перепрофилированных стационаров разного типа. *Общая реаниматология.* 2023; 19 (3): 20–27. https://doi.org/10.15360/1813-9779-2023-3-20-27 [In Russ. and Engl.]

***Correspondence to:** Александр Александрович Аврамов, shurikfta@yandex.ru

Summary

Objective: to study the risk factors for COVID-19 adverse outcomes in repurposed hospitals of various types.

Material and methods. A retrospective study was conducted in the ICUs of three repurposed hospitals: a municipal hospital, a federal center and a private clinic. Data of 369 patients were analyzed for the period from April to December 2020. Gender, age, BMI, NEWS score, severity of lung damage based on CT quantification, blood gases and pH, patterns of antibiotic administration during hospital stay (all classes and number of antimicrobials, regardless the sequence of administration), patterns of main drugs administration (glucocorticosteroids, lopinavir/ritonavir, tocilizumab/ solilumab, hydroxychloroquine) were evaluated as risk factors. Odds ratios (OR) and 95% confidence intervals (95% CI) were calculated by logistic regression.

Results. Patients from repurposed hospitals of various types were distinguishable in terms of distribution by sex, severity of lung damage, administered therapy, blood gases, and the number of antimicrobials used. Mortality rates were 21.8% in the federal center, 41.4% in the private clinic, and 77.2% in the municipal hospital. The most significant risk factors were: the severity of lung damage based on CT quantification (OR=3.694, 95% CI: 1.014–13.455, *P*=0.048) — in the federal center, patient's age (OR=1.385, 95% CI: 1.034–1.854, *P*=0.029) and arterial oxygen tension (OR=0.806, 95% CI: 0.652–0.996) — in the municipal hospital, and patients' age (OR=2.158, 95% CI: 1.616–2.880, *P*<0.0001), number of antibiotics (OR=1.79, 95% CI: 1.332–2.406, *P*=0.0001), and blood pH (OR=0.381, 95% CI: 0.261–0.555, *P*<0.0001) — in the private clinic.

Conclusion. Patient's profiles in municipal, federal, and private ICU settings varied significantly in the first wave of the COVID-19 pandemic. Gender distribution and severity of the diseases were found as the most significant differences among them. Clinical outcomes were also different, with the lowest mortality rate in the federal center and the highest in the municipal hospital. Arterial pO_2, blood pH, and the number of antimicrobials used in the course of treatment were the significant risk factors of fatal outcome (in some hospitals).

Keywords: COVID-19; SARS-CoV-2; ICU; risk factors; logistic regression; hospital repurposing

Conflict of interest. The authors declare no conflict of interest.

Introduction

Despite significant reductions in morbidity and mortality, COVID-19 remains a significant public health problem. Patients admitted to intensive care units are still at high risk of serious complications and death. The 2020–2021 COVID-19 pandemic has provided a wealth of information, the analysis of which will allow important conclusions to be drawn about risk factors in the management of coronavirus infection. A large number of risk factors have been described in the literature, and they vary considerably from country to country and from hospital to hospital. According to a meta-analysis of 40 studies by Y. Li et al., the most significant risk factors for mortality in COVID-19 are male sex (OR = 1.32, 95% CI = 1.18 to 1.48, 20 studies), age (OR = 1.05 for each additional year, 95% CI = 1. 04 to 1.07, 10 studies), obesity (OR = 1.59, 95% CI = 1.02 to 2.48, 4 studies), diabetes mellitus (OR = 1.25, 95% CI = 1.11 to 1.40, 11 studies), and chronic kidney disease (OR = 1.57, 95% CI = 1.27 to 1.93, 6 studies) [1].

According to many studies, age is a risk factor independent of disease severity, hospital type, or department [2, 3]. Gender was found to be a significant risk factor in most published studies, whereas data on smoking and comorbidities are less consistent [3–5]. Among comorbidities, diabetes mellitus, obesity, and cardiovascular disease are the most commonly reported risk factors [6, 7].

A more accurate prognosis of outcome can be obtained from the results of laboratory tests. C-reactive protein, lactate dehydrogenase (LDH), C3, increased CD14+CD16+ monocytes and Th17 cells have been studied as predictors of disease outcome [8–10]. Not all of these markers are available for routine measurement. It is important to find an optimal set of predictors based on clinical and medical history data and routine laboratory tests.

During the 2020–2021 pandemic, coronavirus pneumonia was treated in a variety of hospitals. In addition to city hospitals, converted public and private hospitals were involved. Since the patient populations and treatment efficacy differed in many parameters, it is reasonable to consider patients from different types of hospitals as separate populations unless proven otherwise.

Aim of the present study: to investigate risk factors for adverse COVID-19 outcomes in different types of converted hospitals.

Materials and Methods

A retrospective study of the outcomes of treatment of coronavirus pneumonia in intensive care units of three hospitals involved in the provision of medical care in Moscow in 2020 was conducted. The types of hospitals were abbreviated as follows: city clinical hospital (CCH), converted federal center (CFC), and converted private clinic (CPC). Treatment outcomes for April–June 2020 were obtained from CFC and CCH, and for May–December 2020 from CPC. Inclusion criteria were treatment in the ICU, COVID-19 as the reason for transfer to the ICU, absence of severe neoplastic and neurological disorders not related to infection.

Patients with the minimum required information were selected. For CFC, data were collected on sex, age, duration of ventilatory support, length of ICU stay, BMI, NEWS score, severity on lung CT scan (on admission, initiation of ventilation, last value during hospitalization and «maximum» value during hospitalization), pH, and lactate and glucose levels, arterial blood CO_2 and O_2 pressures before tracheal intubation, number of antibacterial drugs prescribed during treatment (different antibacterial drugs, regardless of the order in which they were prescribed), frequency of administration of major drugs (glucocorticosteroids, lopinavir/ritonavir, tocilizumab/solilumab, hydroxychloroquine).

For CCH, data on sex, age, NEWS score, arterial blood CO_2 and O_2 pressures before tracheal intubation, and number of antibacterial drugs administered during treatment were collected.

For CPC, data were collected on sex, age, duration of mechanical ventilation and ICU stay, pH and lactate levels, arterial blood CO_2 and O_2 pressures before tracheal intubation, number of antibacterial drugs prescribed during treatment, specific drugs prescribed (glucocorticosteroids, lopinavir/ritonavir, tocilizumab/sarilumab, hydroxychloroquine), and tracheotomy.

Statistical analysis of the study results and plotting were performed using the common statistical libraries *sklearn*, *statsmodels*, and *scipy* of Python 3.

Chi-squared test for categorical variables, ANOVA with post hoc comparison by Tukey's test for quantitative parameters (Tukey's HSD test, statsmodels library) were used to assess differences in clinical and laboratory parameters between institutions. Normality of distribution was assessed by the Shapiro–Wilk test (scipy library). Data were described as mean and standard deviation (*SD*), unless otherwise noted.

Logistic regression model with l1 regularization (maximum likelihood estimator of statsmodels library, b. l1 alpha = 1) was used to estimate the studied parameters as risk factors. According to the recommendations for epidemiological data analysis, missing values were imputed by iterative imputation (IterativeImputer function of Ridge Regression in the sklearn library). To assess the accuracy of imputation, we compared the mean and standard deviation in the sample before and after imputation. Covariates whose values could exceed 10 were scaled to a range of 1–10, which was taken into account when interpreting the regression coefficients. Pseudo-R^2, log likelihood and log likelihood ratio *P*-value were evaluated as criteria for model adequacy. A logistic regression model was calculated for all available covariates from individual hospital data. Covariates with a calculated *P*-value < 0.05 were selected as significant predictors of mortality, and odds ratios (OR = expB), 95% confidence intervals (95% CI) were reported for each factor.

Results и discussion

Patient selection. Based on the inclusion and exclusion criteria, 540 patients were selected from 4 450 ICU patients in the three clinical centers, of whom 369 patients had the required minimum information (sex, age, disease outcome, length of stay in the ICU, and duration of mechanical ventilation) and whose data were used for the study (Fig. 1).

Comparison of different clinical facilities. There were differences in almost all parameters of the patient populations between the different types of clinical centers. The most important for further analysis were the differences in adverse outcome rate between the three institutions. It was 21.8% for CFC, 77.2% for CCH, and 41.4% for CPC (chi-squared differences <0.001 for CFC/CCH and CCH/CPC comparisons, $P=0.006$ for CFC/CCH, which is below the set threshold, even when multiple comparisons adjustments were applied).

The sex ratio of patients differed significantly between some clinical centers (67.2%, 43.6%, 62.3% of male patients, $P=0.003$ in CFC, CCH, and CPC,

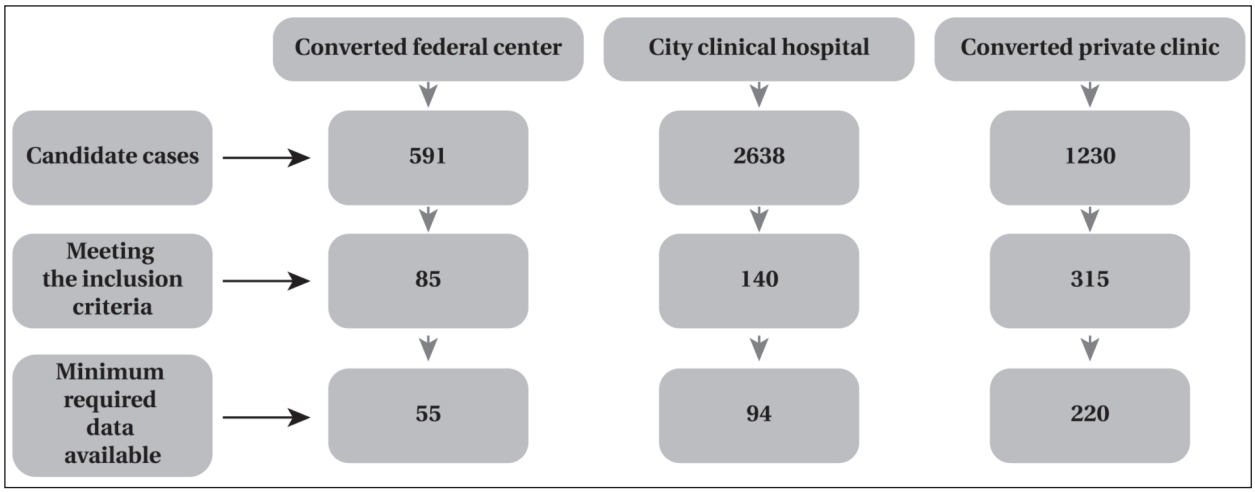

Fig. 1. Flowchart of the patient selection.

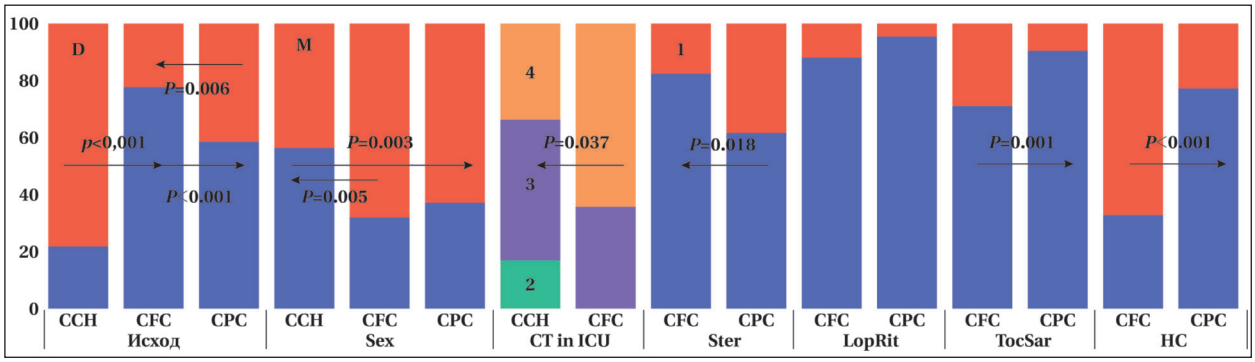

Fig. 2. Comparison of different clinical sites by frequency of categorical variables (%).
Note. CCH — city clinical hospital; CFC — converted federal center; CPC — converted private clinic; CT in ICU — CT severity of pneumonia before intubation (0–4 points); Ster — administration of steroids; LopRit — administration of lopinavir/ritonavir; TocSar — administration of tocilizumab/sarilumab; HC — administration of hydroxychloroquine; D — death; M — male sex. For the administration of drugs, «1» means that the drug was prescribed.

respectively, when compared by chi-squared test in the overall comparison). Pairwise comparisons using the chi-squared test were also significant with *P*=0.005 for CFC and CCH, *P*=0.49 for CFC/CPC, and *P*=0.003 for CCH/CPC. Thus, no gender differences were observed between patients in the ICU of the converted federal center and the private clinic, but significantly fewer males met the study inclusion criteria in the CCH sample.

When comparing the severity of pneumonia on CT scan before tracheal intubation, CFC and CCH differed significantly (*P*=0.037 with more severe disease in CFC), whereas CT severity on admission did not differ significantly (*P*=0.10). Hydroxychloroquine (22.3% vs. 66.7%, *P*<0.001), tocilizumab/sarilumab (10% vs. 39.4%, *P*=0.001) and steroids were prescribed significantly less often in CPC than in CFC (37.8% vs. 17%, *P*=0.018). The frequency of prescribing lopinavir/ritonavir was not significantly different (4.1% vs. 11.4%, *P*=0.11).

The mean age of patients was not significantly different between the three centers (ANOVA *P*>0.1). The mean NEWS score was significantly higher in CCH than in CFC (6.4±3.1 vs. 4.3±3, p=0.001). Mean pH before tracheal intubation was significantly lower (7.36±0.11 vs. 7.47±0.06, *P*=0.001) and lactate level was significantly higher (2.09±1.22 mmol/L vs. 1.18±1.19 mmol/L, p=0.001) in CPC compared to CFC. Significant differences were found between patients of the three institutions in O_2 and CO_2 partial pressure before tracheal intubation (*P*<0.001 and *P*<0.001, respectively), number of antibiotics administered (*P*<0.001). The pO_2 in CPC was significantly higher than in CFC (93.7±31.9 mm Hg versus 48.7±11.7 mm Hg, *P*=0.001) and CCH (93.7±31.9 mm Hg versus 56±18.3 mm Hg, *P*=0.01), no difference was found between CFC and CCH (*P*=0.18). Mean pCO_2 was significantly lower in CFC compared to CCH (32.9±11.7 mm Hg vs 56±18.3 mm Hg, *P*=0.001) and CPC (32.9±11.7 mm Hg vs 42.6±14.1 mm Hg, *P*=0.001). There were no significant differences between CCH and CPC (*P*=0.85). The number of antibiotics prescribed was significantly different between CFC and CPC (2.1±1.4 vs.

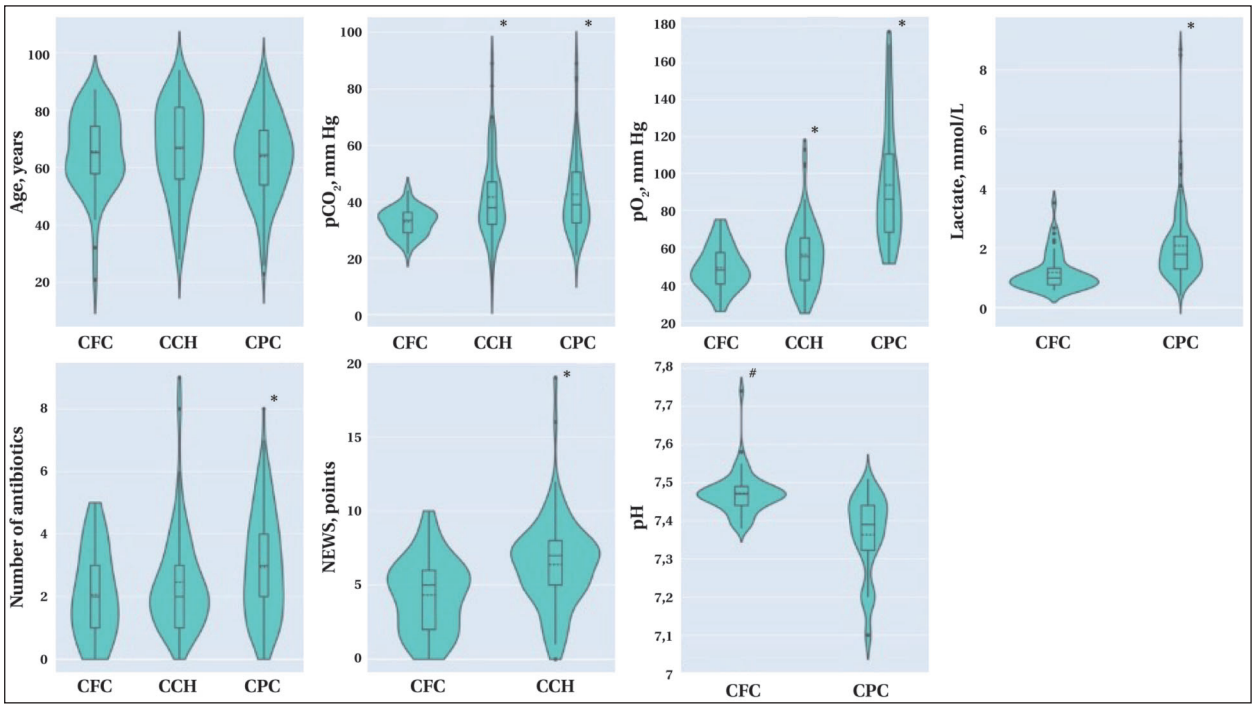

Fig. 3. Comparison of different clinical institutions by mean values of quantitative variables (violin diagrams).
Note. * — the average value is significantly (P<0.01) higher than in the CFC group. # — the average value is significantly (P<0.01) higher than in the CPC group.

Missing values and imputation quality.

Parameter	Institution	Missing values	Mean before imputation	Mean after imputation	SD before imputation	SD after imputation	SD of imputed means
pCO_2	CFC	1	32.88	32.94	4.82	4.79	4.78
pO_2	CFC	1	48.7	48.7	11.73	11.62	11.62
Last CT severity	CFC	3	2.73	2.75	1.03	1.05	1.00
Lactate	CFC	6	1.19	1.14	0.63	0.65	0.59
Number of antibiotics	CFC	10	2.1	1.93	1.42	1.42	1.28
CT severity on admission	CCH	76	3.17	3.15	0.71	0.96	0.3
pH	CPC	5	7.36	7.36	0.11	0.11	0.10
pCO_2	CPC	120	42.6	43.2	14.1	15.0	9.5
pO_2	CPC	120	93.7	94.7	31.9	32.5	21.5
Lactate	CPC	5	2.1	2.1	1.22	1.22	1.2
Number of antibiotics	CPC	88	2.94	2.66	1.7	1.9	1.3

2.9±1.7, P<0.001). The differences between CFC and CCH (P=0.38) and CPC and CCH (P=0.09) were not significant.

Patients in the ICUs of the different types of converted hospitals studied differed significantly in their clinical characteristics. On the one hand, a higher score on the NEWS scale in CCH compared to CFC indicates greater severity of illness. On the other hand, patients in CFC had greater severity on CT scan before tracheal intubation, and the proportion of males was maximal among them. A pH shift towards acidosis in CPC patients compared to CFC patients could also be a sign of greater disease severity.

The reasons for the discrepancy in the characteristics of the samples could be different, since the treatment was performed in 2020, before the full standardization of the treatment of COVID-19 patients. Importantly, the results of the risk factor study need to be interpreted in light of the specifics of the inpatient setting. The results of individual epidemiologic studies may not be applicable because of such differences, so it is better to be guided by the results of meta-analyses.

Analysis of Significant Mortality Factors

Imputation of missing values. Logistic regression methods cannot handle data with missing values, so we iteratively imputed missing values for each criterion used in the model (Table). Conformity of the new sample form to the original data was tested using means and standard deviations (SDs).

The standard deviations of one of the basic methods for imputing missing values, the mean for the parameters (see table), were reported. The mean values for the parameters differed insignificantly, the standard deviations differed significantly less from the baseline values than the mean imputation. A significant improvement was obtained by imputing the parameters with a large number of missing values.

Because of the small number of patients selected for CFC, a number of parameters were not included in the logistic regression model due to uneven class distribution. The following variables were included in the model: age, NEWS score, pCO_2, pO_2, admission lung CT severity score, last available CT severity score, lactate level, and number of antimicrobials administered. For the model, the pseudo-R^2 value was 0.73, LL = –7.88, LLR $P<0.001$. Severity according to the last CT scan was a significant risk factor (p=0.048). With a score of 1 to 4, each additional point increased the risk of death by a factor of 3.694 (OR = 3.694; 95% CI, 1.014–13.455). Most of the other parameters included in the model were not significant due to the wide confidence interval. Due to the proximity of significant differences, the possible importance of pCO_2, pO_2, NEWS, and lactate level should be considered in further studies (Fig. 4, *a*).

Risk factors in CCH. Sex, age, lung CT severity at ICU transfer and pO_2 were included in the model predicting the odds of fatal outcome based on data from CCH. The adequacy of the model can be assessed by pseudo-R^2 = 0.11, LL = –44.27, LLR *p*-value of 0.010. For age, the OR was 1.385, i.e., each year in the model increased the odds of death by a factor of 1.385 (95% CI, 1.034–1.854; P=0.029; 66.7±15.7 years). The other significant predictor was pO_2 56±32 mm Hg, OR = 0.806 (95% CI, 0.652-0.996), indicating that each additional 10 mm Hg of pO_2 in the blood reduced the odds of death by 1.24-fold (Fig. 4, *b*).

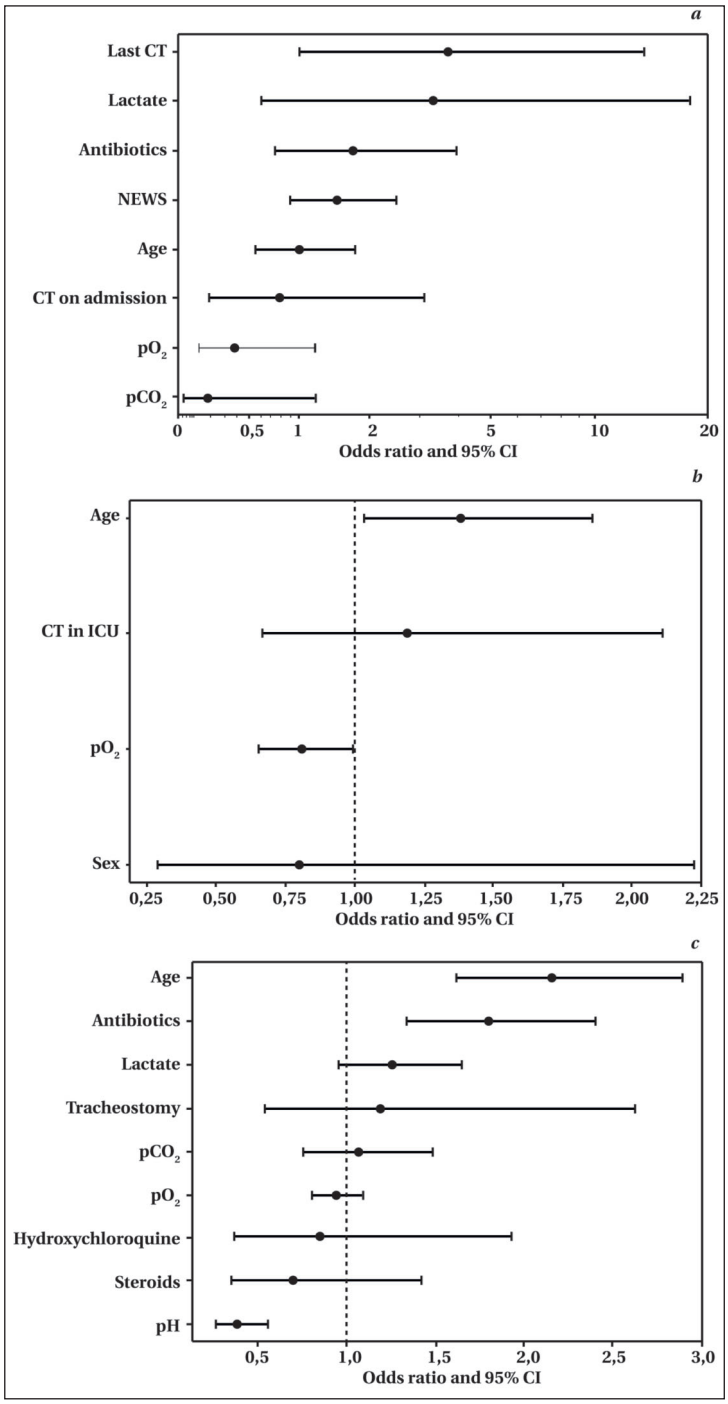

Fig. 4. Forest plot of risk factors for death in the ICU of the CFC (*a*), CCH (*b*), CPC (*c*).

Risk factors in CPC. From the CPC data, age, pH, pCO_2, pO_2, use of steroids, hydroxychloroquine, lactate level, tracheostomy, and number of antimicrobial agents used were included in the logistic regression model. For the model, the pseudo-R2 value was 0.24, LL = –113.95, LLR $P<0.001$. Three risk factors were significant, including pH, age, and number of antibiotics prescribed. For age (63.9±14.4 years), the OR was 2.158 (95% CI 1.616 to 2.880, $P<0.0001$), i.e. each year increased the odds of death by a factor of 2.158. For pH (7.36±0.11), the OR was 0.381 (95% CI 0.261 to 0.555, $P<0.0001$), i.e. a decrease in pH by 1 increased the odds of death by 2.62 times. For the number of antibiotics (2.9±1.7 drugs), the OR was 1.79 (95% CI 1.332 to 2.406, P=0.0001), i.e., each additional antibacterial drug was associated with a 1.79-fold increase in the odds of death (Fig. 4, *c*).

Analysis of blood acid-base balance and blood gases is an important method of assessing patient

status in the ICU. Several studies have confirmed that arterial pO_2 and pCO_2 may be predictors of mortality to some extent [11]. However, they, as well as pH, were not included in meta-analyses of significant predictors of COVID-19 outcome [12, 13]. Significant variation in blood gas measurements between clinical centers may be explained by lack of strict adherence to blood collection protocols. Therefore, the use of such parameters as predictors requires strict standardization of techniques.

There is no information in the literature on the relationship between the number of antibacterial agents administered and the risk of mortality in the ICU. A number of studies have shown that the administration of antibacterial drugs itself may be an independent risk factor for adverse outcomes [14]. In ICU patients, a high number of antibiotics indicates the development of septic complications. Interestingly, more antibiotics were prescribed in a private clinic, which was also a significant risk factor for mortality.

The drugs used to treat coronavirus pneumonia in 2020 had no significant effect on the odds of death, regardless of the type of hospitalization. Currently, the failure of most etiologic therapies has been demonstrated in numerous clinical trials. Moiseev S. et al. demonstrated a lack of effect of tocilizumab [15]. The meta-analysis by Amani B. et al. showed no effect of lopinavir/ritonavir [16]. Later, Axfors C. et al. showed a lack of efficacy for hydroxychloroquine in a meta-analysis [17]. The results obtained with the above drugs are consistent with the literature. However, we found no effect of steroids, contrary to the results of many other studies in severe patients [18, 19]. A relatively small number of patients received steroids (treatment was prescribed before the clinical guidelines were updated), which may explain the lack of significant differences.

Ermokhina L. et al. analyzed risk factors in the ICU of Moscow City Hospital No. 68 during the first pandemic wave. With an average mortality of 44.9%, significant risk factors included age and length of stay in the ICU. Mortality did not differ between men and women and did not depend on BMI. None of the etiologic medications affected mortality. The results presented by the authors are similar to those we obtained from the CCH and CPC data [20].

It should be noted that the results of our study were obtained in 2020, during the first wave of the COVID pandemic. Coronavirus strains and approaches to treatment management changed during the second wave and thereafter. For example, in the study by Bychinin M. V. et al., ICU mortality during the «second wave» increased from 50.5% to 62.7% compared to the first wave, and the structure of comorbidity changed slightly [21].

Conclusion

During the first wave of COVID-19, ICUs of different types of hospitals (city, federal and private) received patients with significantly different clinical characteristics. Treatment outcomes were also significantly different.

Arterial blood pO_2 and pH before tracheal intubation were significant predictors of mortality in patients with coronavirus pneumonia in the ICU.

The number of antibiotics administered may be a significant predictor of mortality in some medical centers.

References

1. *Li Y., Ashcroft T., Chung A., Dighero I., Dozier M., Horne M., McSwiggan E. et al.* Risk factors for poor outcomes in hospitalised COVID-19 patients: a systematic review and meta-analysis. *J Glob Health*. 2021; 11: 10001. DOI: 10.7189/jogh.11.10001. PMID: 33767855
2. *Telle K.E., Grøsland M., Helgeland J., Håberg S.E.* Factors associated with hospitalization, invasive mechanical ventilation treatment and death among all confirmed COVID-19 cases in Norway: prospective cohort study. *Scand J Public Health*. 2021; 49 (1): 41–47. DOI: 10.1177/1403494820985172. PMID: 33461404
3. *Macedo M.C.F., Pinheiro I.M., Carvalho C.J.L., Fraga H.C.J.R., Araujo I.P.C., Montes S.S., Araujo O.A.C. et al.* Correlation between hospitalized patients' demographics, symptoms, comorbidities, and COVID-19 pandemic in Bahia, Brazil. *PLoS One*. 2020; 15 (12): e0243966. DOI: 10.1371/journal.pone.0243966. PMID: 33318711
4. *Allameh S.F., Nemati S., Ghalehtaki R., Mohammadnejad E., Aghili S.M., Khajavirad N., Beigmohammadi M-T. et al.* Clinical characteristics and outcomes of 905 COVID-19 patients admitted to Imam Khomeini hospital complex in the capital city of Tehran, Iran. *Arch Iran Med*. 2020; 23 (11): 766–775. DOI: 10.34172/AIM.2020.102. PMID: 33220695
5. *Jiménez E., Fontán-Vela M., Valencia J., Fernandez-Jimenez I., Álvaro-Alonso E.A., Izquierdo-García E., Cebas A.L. et al.* Characteristics, complications and outcomes among 1549 patients hospitalised with COVID-19 in a secondary hospital in Madrid, Spain: a retrospective case series study. *BMJ Open*. 2020; 10 (11): e042398. DOI: 10.1136/bmjopen-2020-042398. PMID: 33172949
6. *Миронов П.И., Лутфарахманов И.И., Сырчин Е.Ю., Домбровская А.А., Пушкарев В.А., Ширяев А.П.* Предикторы гибели пациентов с COVID-19, находящихся на искусственной вентиляции легких. *Медицинский Вестник Башкортостана*. 2020; 15 (6): 86–92 [*Mironov P.I., Lutfarakhmanov I.I., Syrchin E.Yu., Dombrovskaya A.A., Pushkarev V.A., Shiryaev A.P.* Predictors of death in patients with COVID-19 on artificial lung ventilation. *Bashkortostan Medical Journal/ Meditsinskiy Vestnik Bashkortostana*. 2020; 15 (6): 86–92 (In Russ.).]
7. *Глыбочко П.В., Фомин В.В., Авдеев С.Н., Моисеев С.В., Яворовский А.Г., Бровко М.Ю. и соавт.* Клиническая характеристика 1007 больных тяжелой SARS-CoV-2 пневмонией, нуждавшихся в респираторной поддержке. *Клиническая Фармакология и Терапия*. 2020; 29: 21–29. [*Glybochko P., Fomin V., Avdeev S.,Moiseev S.,Yavorovskiy A., Brovko M.* et al. Clinical Characteristics of 1007 Intensive Care Unit Patients with Sars-Cov-2 Pneumonia. *Clinical Pharmacology and Therapy/ Clinical Pharmacology and Therapy/Klinicheskaya Farmakologiya i Terapiya*. 2020; 29: 21–29 (In Russ.).] DOI: 10.32756/0869-5490-2020-2-21-29
8. *Клыпа Т.В., Бычинин М.В., Мандель И.А., Андрейченко С.А., Минец А.И., Колышкина Н.А., Троицкий А.В.* Клиническая характеристика пациентов с COVID-19, поступающих в отделение интенсивной терапии. Предикторы тяжелого течения. *Клиническая Практика*. 2020; 11 (2): 6–20. [*Klypa T.V., Bychinin M.V., Mandel I.A., Andreichenko S.A., Minets A.I., Kolyshkina N.A., Troitsky A.V.* Clinical characteristics of patients admitted to an ICU with COVID-19. Predictors of the severe disease. *Clinical practice/Klinicheskaya Praktika*. 2020; 11 (2): 6–20. (In Russ.).]. DOI: 10.17816/clinpract34182
9. *Elamari S., Motaib I., Zbiri S., Elaidaoui K., Chadli A., Elkettani C.* Characteristics and outcomes of diabetic patients infected by the SARS-CoV-2. *Pan Afr Med J*. 2020; 37: 32. DOI: 10.11604/pamj. 2020.37.32.25192. PMID: 33209159
10. *Payán-Pernía S., Pérez L.G., Remacha Sevilla Á.F., Gil J.S., Canales S.N.* Absolute lymphocytes, ferritin, C-reactive protein, and lactate dehydrogenase predict early invasive ventilation in patients with COVID-19. *Lab Med*. 2021; 52 (2): 141–145. DOI: 10.1093/labmed/ lmaa105. PMID: 33336243
11. *Gupta B., Jain G., Chandrakar S., Gupta N., Agarwal A.* Arterial blood gas as a predictor of mortality in COVID pneumonia patients initiated on noninvasive mechanical ventilation: a retrospective analysis. *Indian J Crit Care Med*. 2021; 25 (8): 866–871. DOI: 10.5005/jp-journals-10071-23917. PMID: 34733025
12. *Tian W., Jiang W., Yao J., Nicholson C.J., Li R.H., Sigurslid H.H., Wooster L. et al.* Predictors of mortality in hospitalized COVID-19 patients: a systematic review and meta-analysis. *J Med Virol*. 2020; 92 (10): 1875–1883. DOI: 10.1002/jmv.26050. PMID: 32441789
13. *Shi C., Wang L., Ye J., Gu Z., Wang S., Xia J., Xia Y., Li Q. et al.* Predictors of mortality in patients with coronavirus disease 2019: a systematic review and meta-analysis. *BMC Infect Dis*. 2021; 21 (1): 663. DOI: 10.1186/s12879-021-06369-0. PMID: 34238232
14. *Bendala Estrada A.D., Parra J.C., Carracedo E.F., Míguez A.M., Martínez A.R., Rubio E.M., Rubio-Rivas M.,* Inadequate use of antibiotics in the COVID-19 era: effectiveness of antibiotic therapy. *BMC Infect Dis*. 2021; 21 (1): 1144. DOI: 10.1186/s12879-021-06821-1. PMID: 34749645
15. *Моисеев С.В., Авдеев С.Н., Тао Е.А., Бровко М.Ю., Яворовский А.Г., Умбетова К.Т.* Эф-

фективность тоцилизумаба у пациентов с COVID-19, госпитализированных в ОРИТ: ретроспективное когортное исследование. *Клиническая Фармакология и Терапия*. 2020; 29 (4): 17–25. [*Moiseev S.V., Avdeev S.N., Tao E.A., Brovko M.Yu., Yavorovsky A.G., Umbetova K.T.* Efficacy of tocilizumab in the intensive care unit patients with COVID-19: a retrospective cohort study. *Clinical Pharmacology and Therapy/ Klinicheskaya Farmakologiya i Terapiya*. 2020; 29 (4): 17–25. 10.32756/0869-5490-2020-4-17-25. (In Russ.).] DOI: 10.32756/ 0869-5490-2020-4-17-25

16. *Amani B., Khanijahani A., Amani B., Hashemi P.* Lopinavir/ritonavir for COVID-19: a systematic review and meta-analysis. *Pharm Sci*. 2021; 24: 246–257. DOI: 10.18433/jpps31668. PMID: 34048671
17. *Axfors C., Schmitt A.M., Janiaud P, van't Hooft J., Abd-Elsalam S., Abdo E.F., Abella B.S. et al.* Mortality outcomes with hydroxychloroquine and chloroquine in COVID-19 from an international collaborative meta-analysis of randomized trials. *Nat Commun*. 2021; 12 (1): 2349. DOI: 10.1038/s41467-021-22446-z. PMID: 33859192
18. *Yu G.Q., Jiang Z-.H., Yang Z.-B., Jiang S.-Q., Quan X.-Q.* The effect of glucocorticoids on mortality in severe COVID-19 patients: evidence from 13 studies involving 6612 cases. *Medicine (Baltimore)*. 2021; 100 (40): e27373. DOI: 10.1097/MD.0000000000027373. PMID: 34622840
19. *Sterne J.A.C., Murthy S., Diaz J. V., Slutsky A.S., Villar J., Angus D.C., Annane D. et al.* Association between administration of systemic corticosteroids and mortality among critically ill patients with COVID-19: a meta-analysis. *JAMA*. 2020; 324 (13): 1330–1341. DOI: 10.1001/jama.2020.17023. PMID: 32876694
20. *Ермохина Л.В., Митяшов А.С., Переходов С.И., Чаус Н.И., Карпун Н.А., Баева А.А., Ядгаров М.А. с соавт.* Эффективность некоторых методов лечения COVID-19 в ОРИТ: одноцентровое ретроспективное когортное исследование. *Вестник Интенсивной Терапии Имени А.И. Салтанова*. 2021; (3): 69–79. [*Ermokhina L.V., Mityashov A.S., Perekhodov S.N., Chaus N.I., Karpun N.A., Baeva A.A., Yadgarov M.Ya. et al.* What treatment really make sense for critically ill patients with COVID-19: single-center retrospective cohort study. *Ann Crit Care/ Vestnik Intensivnoy Terapii im AI Saltanova*. 2021; (3): 69–79. (In Russ.).] DOI: 10.21320/1818-474X-2021-3-69-79
21. *Бычинин М.В., Клыпа Т.В., Мандель И.А., Коршунов Д.И., Колышкина Н.А., Джелиев Р.А.* Сравнительная клинико-лабораторная характеристика пациентов реанимационного профиля первой и второй волн пандемии COVID-19. *Анестезиология и Реаниматология (Медиа Сфера)*. 2022; (4): 57–65. [*Bychinin M.V., Klypa T.V., Mandel I.A., Korshunov D.I., Kolyshkina N.A., Dzheliev R.A.* Clinical and laboratory characteristics of intensive care patients of the first and second waves of the COVID-19 pandemic. *Russian Journal of Anaesthesiology and Reanimatology/ Anesteziologiya i Reanimatologiya*. 2022; (4): 57–65. (In Russ.).] DOI: 10.17116/anaesthesiology202204157

Received 22.11.2022
Accepted 20.03.2023

https://doi.org/10.15360/1813-9779-2023-3-28-38

Modified Supraclavicular and Pectoral Nerves Blocks for Implantation of Intravenous Port System in Cancer Patients

Maxim P. Yakovenko[1]*, Eduard E. Antipin[2], Nadezhda A. Bochkareva[1], Natalia I. Koroleva[1], Ekaterina F. Drobotova[1], Eduard V. Nedashkovsky[1]

[1] Northern State Medical University, Ministry of Health of Russia,
51 Troitsky prospect, 163069 Arkhangelsk, Russia
[2] Research Center for Medical and Biological Problems of Human Adaptation in the Arctic, Kola Scientific Center RAS
41a microdistrict Akademgorodok, 184209 Apatity, Murmansk area, Russia

For citation: *Maxim P. Yakovenko, Eduard E. Antipin, Nadezhda A. Bochkareva, Natalia I. Koroleva, Ekaterina F. Drobotova, Eduard V. Nedashkovsky.* Modified Supraclavicular and Pectoral Nerves Blocks for Implantation of Intravenous Port System in Cancer Patients. *Obshchaya Reanimatologiya = General Reanimatology.* 2023; 19 (3): 28–38. https://doi.org/10.15360/1813-9779-2023-3-28-38 [In Russ. and Engl.]

***Correspondence to:** Maxim P. Yakovenko, alter83@mail.ru

Summary

Ultrasound-guided regional anesthesia can be an effective way to achieve analgesia during implantation of permanent intravenous port systems.

The aim of the study was to improve the quality of perioperative analgesia during placement of permanent intravenous port systems.

Material and methods. The prospective randomized study included 93 patients with malignant neoplasms. Patients were randomized into 3 groups, 31 people each, who were implanted with a permanent intravenous port system in 2019–2022. Group 1 patients were implanted under local infiltration anesthesia (LIA). Ultrasound-guided pectoral nerves block (PECS1) in group 2 was supplemented by LIA. In group 3 ultrasound-guided selective supraclavicular (SC) nerve block was supplemented with LIA. Pain intensity was assessed on a 100 mm visual analog scale (VAS) at rest and while moving at 8, 16, 32 and 72 hours after implantation. The inflammatory postoperative stress response was assessed by the dynamics of C-reactive protein (CRP), interleukin 1-β (IL 1-β), interleukin-6 (IL-6). We also analyzed the correlation of proinflammatory cytokines levels with VAS-measured pain intensity at the stages of the study taking into account a potential relationship between IL-6 and IL-1β fluctuations and the severity of inflammatory and neuropathic pain.

Results. In groups 2 (PECS1) and 3 (SC nerve block), pain intensity measured by VAS at rest and while conducting daily activities was significantly lower than in group 1 (LIA). CRP levels were also significantly lower in group 2 and 3 patients as compared to group 1. The lowest IL-6 and IL-1β concentrations after port implantation were revealed in a group 3 in 24 hours after the procedure, persisting through day 3. There was a correlation between proinflammatory cytokines levels and pain intensity.

Conclusion. Implantation of an intravenous port system under local infiltration anesthesia causes a significant inflammatory response in cancer patients, which can be balanced by regional techniques. Selective supraclavicular nerve block in combination with a local anesthesia for intravenous port implantation demonstrated the greatest analgesic potential and requires significantly reduced amounts of local anesthetic compared to pectoral nerves block in combination with LIA, or only local infiltration anesthesia.

Keywords: intravenous port system; oncology; pain; implantation; analgesia; PECS1; modified blockage; supraclavicular nerve; pectoralis nerves; ultrasound-guided; regional anesthesia

Conflict of interest. The authors declare no conflict of interest.

Funding. The study had no sponsorship.

Introduction

A recent large descriptive study of procedural pain in adult cancer patients reported that more than 50% of these patients experienced moderate to severe pain during procedures [1]. Implantation of an intravenous port system is a routine procedure in daily practice, usually performed by an anesthesiologist. Currently available literature, however, does not provide guidance on the perioperative anesthetic strategy for patients undergoing this procedure [2]. Local infiltration anesthesia (LIA) is a widely used technique for procedures such as drain placement, pacemaker or intravenous port system implantation [3, 4]. Cancer patients usually have previous experience with invasive procedures and often suffer from chronic pain syndrome directly related to the tumor and/or due to previous treatment. As a result, most of them experience anxiety and fear before the procedure [5].

The pain experienced by cancer patients during procedures can be excruciating for the patient, family, and caregivers. In addition, painful procedures can cause pain breakthrough or worsening in patients receiving analgesic therapy [6].

Nociceptive stimulation associated with any type of invasive procedure in cancer patients cannot be completely blocked by local anesthesia alone [7]. According to Renzini et al. and Sansone et al. [8–10], the LIA technique is insufficient when a subcutaneous «pocket» is created. Taxbro K. et al.

[11] believe that a quarter of patients experience severe pain and discomfort during implantation of an intravenous port system using only local anesthesia. Chang D. et al. point out that the combination of local anesthesia and sedation may also be insufficient for patients with high levels of anxiety and distress, and the level of distress is often underestimated by the operator [12].

Mehmet et al. [13] report that patients complain of pain after port system implantation within the next few days and most of them require additional analgesia [13]. However, according to Mehmet et al. [13], little attention has been paid to the importance of postoperative analgesia after portosystemic implantation. Byager et al. [14] reported that infiltration of the surgical wound with local anesthetic does not provide analgesia in the early postoperative period.

These facts warrant further research into the possibilities of improving the control of the pain associated with an invasive procedure in cancer patients.

Currently, there are several regional anesthesia techniques that provide more effective perioperative analgesia compared to LIA [15–18]. One of the disadvantages of LIA is the need for relatively large doses of local anesthetics (up to 30–40 ml [8]), which increases the risk of systemic toxicity.

In 2011, R. Blanco introduced a new type of fascial plane block, the neurofascial pectoralis nerve block, or PECS [19]. It is a block of the medial and lateral pectoral nerves, which, although considered motor, have both nociceptive and proprioceptive fibers [20, 21]. In addition, according to Munshey et al. and Sansone et al., this type of analgesia also blocks the intercostal nerves at the level of the Th3 to Th6 segments [9, 10]. It is worth mentioning that all thoracic motor nerves have postganglionic fibers from cervical and thoracic ganglia, which may be additional conductors of pain impulses and participate in the development of postoperative neuropathic pain [22]. The use of the PECS block provided a relatively simple and safe technique to achieve high quality postoperative anesthesia for breast surgery. Selective supraclavicular nerve (SSCN) block is another regional anesthesia technique that can be used for port system implantation. This ultrasound-guided technique was first described in 2011 by Maybin et al [23]. It was designed to avoid additional phrenic nerve block, which is particularly relevant in patients with comorbidities and in the outpatient setting. Traditionally, the supraclavicular nerve has been blocked by proximal spread of the solution during brachial plexus block via interscalene approach in shoulder and clavicle surgery [24, 25], but the technique of proximal compression failed to avoid the associated phrenic nerve block [26]. Selective block of the supraclavicular nerve and upper trunk of the brachial plexus (SCUT block) is known to allow clavicle surgery without additional anesthesia [27].

There are no studies comparing wound infiltration by a surgeon with any selective cutaneous nerve block. However, many comparative studies between standard mixed nerve block and wound infiltration show superiority of the former [28–31].

Given the extent of sensory anesthesia in selective supraclavicular nerve block, it can be effectively used for perioperative pain control during implantation of intravenous port systems (Fig. 1).

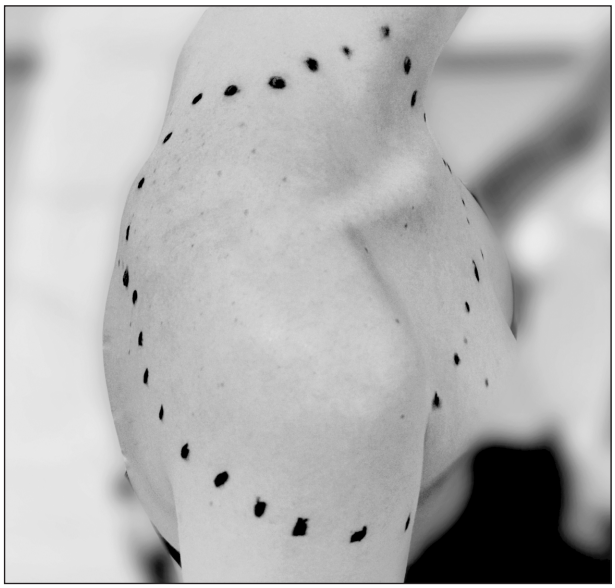

Fig. 1. Area of sensory anesthesia during supraclavicular nerve block.

Response to a noxious stimulus, such as surgery, involves changes in the hepatic production of acute-phase proteins, such as C-reactive protein (CRP), and various cytokines, which initiate and/or maintain an inflammatory response. High levels of proinflammatory cytokines (mainly IL-6) and lack of compensatory expression of anti-inflammatory cytokines can cause a systemic inflammatory response in cancer patients [32, 33].

Interleukin-1β and interleukin-6 are proinflammatory cytokines involved in autoimmune reactions, inflammation and pain processes, which also play an important role in evaluating the acute phase of postoperative stress response [34–38]. According to Ke Ren, Richard Torres and Zhou et al., interleukin-1β and interleukin-6 are critical in these processes [34, 35]. These cytokines also significantly influence the induction and maintenance of pain as chronic pain develops. Blocking the synthesis of these interleukins may have an analgesic effect [34–37]. Postoperative pain is associated with an inflammatory response, the reduction of which is an important determinant of both the

severity of acute pain and the persistence of pain after surgery [39].

Inflammatory pain is a multifaceted cellular response involving the development of abnormal hyperalgesia in response to tissue damage and inflammation (e.g., postoperative pain, trauma, ischemia, metabolic dysfunction, or infection) [40].

The choice of regional anesthesia for intravenous port system implantation can be challenging because each of the currently used blocks, including local infiltration anesthesia, «covers» only one part of the surgical field, leaving the other unaffected. Janc J. et al. used a modified block in their study, combining a thoracic nerve block with local anesthesia, and showed the superiority of such a combination [41].

We also used modified versions of the block combining local and regional anesthesia. The rationale behind the study was the assumption that regional anesthesia techniques ensure less response to surgical stress due to a more pronounced analgesic potential and reduce the need for postoperative analgesia.

The aim of the study was to improve the quality of perioperative analgesia during placement of permanent intravenous port systems.

Materials and Methods

The prospective, randomized, single-blind study included 93 patients aged 31 to 73 years (mean age, 59.5 years) assessed according to ASA III–IV [42]. The study flow chart is shown in Fig. 2. Patients were implanted with the intravenous Power Port™ isp M.R.I.™ Implantable Port System. The Mindray DC-N6 with L12-4 (3–13 MHz) linear transducer was used for ultrasound guidance.

The study was approved by the Ethics Committee of Northern State Medical University (Arkhangelsk) No. 04/10-19 dated October 30, 2019.

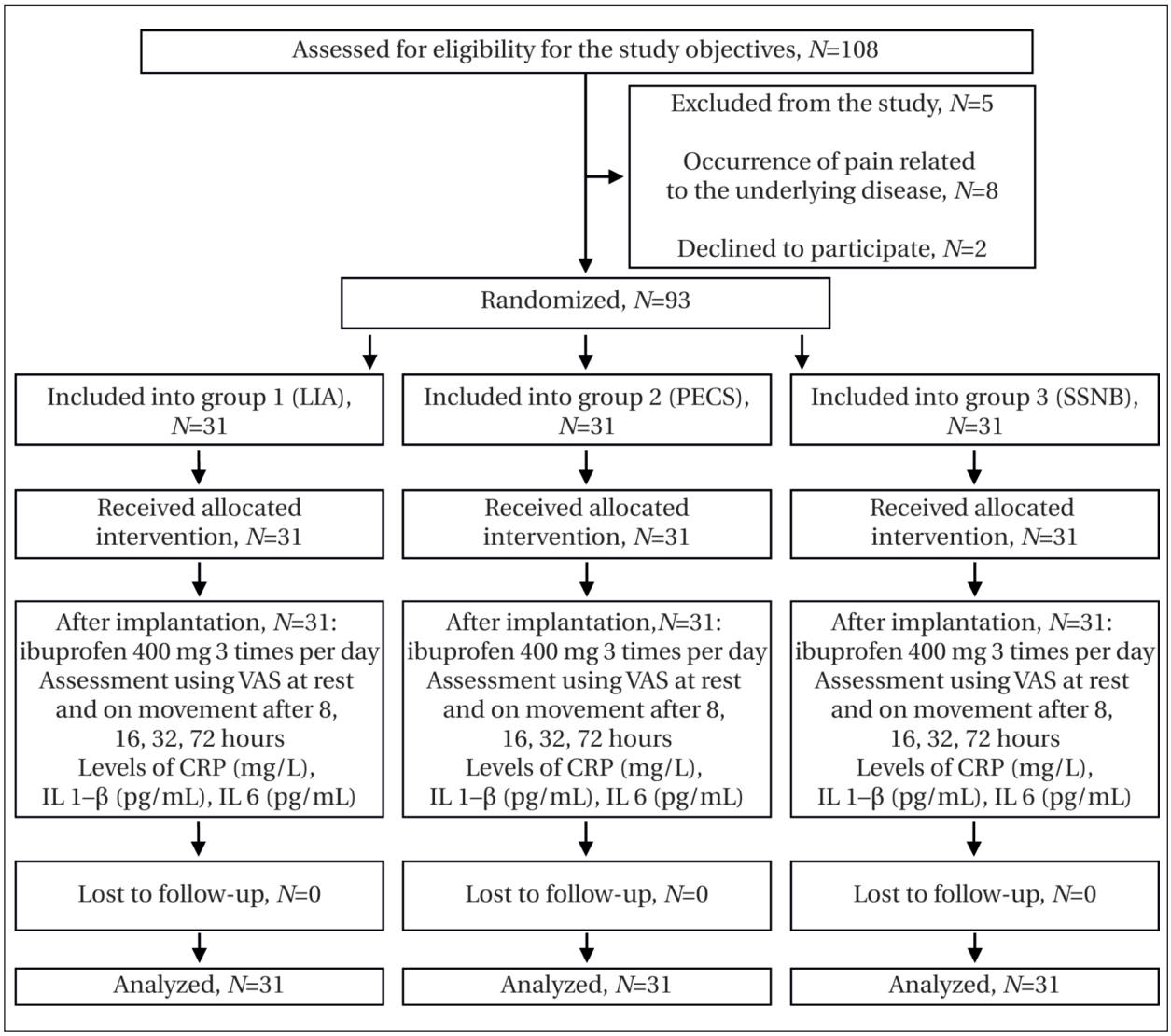

Fig. 2. The study flowchart.

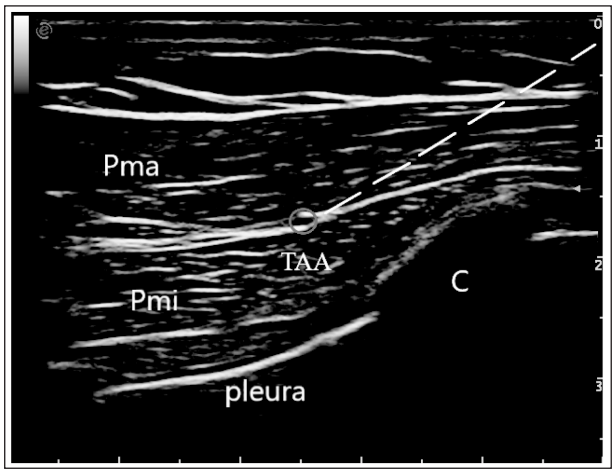

Fig. 3. Thoracic nerve block.
Note. Pma — pectoralis major muscle; TAA — thoracoacromial artery; Pmi — pectoralis minor muscle; C — costa (rib), dotted line indicates the direction of the needle movement.

Inclusion criteria for the study were:

1. Presence of indications for port system placement
2. Absence of pain
3. Absence of psychiatric disorders
4. Age older than 18 years
5. Absence of coagulopathy or systemic anticoagulant therapy
6. Absence of tissue changes at the site of port system implantation (complications after radiation therapy such as radiation dermatitis, infection foci, anatomical malformations, etc.)
7. Absence of allergy to local anesthetics.

Exclusion criteria were:

1. Refusal of the patient to participate in the study
2. Presence of pain related to the underlying disease or treatment immediately prior to port system implantation and during the study
3. Immunologic comorbidities requiring administration of systemic immunomodulatory drugs
4. Daily use of NSAIDs
5. Failure to meet the inclusion criteria.

Depending on the type of regional anesthesia, the participants were divided into three groups of 31 patients each. In group 1 patients, the port system was placed under local infiltration anesthesia (LIA) using the «creeping infiltration» technique with 35±5 mL of 0.5% ropivacaine. In group 2, local anesthesia was used in combination with pectoral block (PECS) under ultrasound guidance. The correct distribution of the local anesthetic between the fasciae was verified by visualizing the separation of the fascial layers between the pectoral muscles [19] (Fig. 3). The 0.5% ropivacaine 0.2 ml/kg and local anesthesia with 0.5% ropivacaine (20±5 ml) were used. In group 3, selective supraclavicular nerve block (SSNB) was performed under ultrasound guidance (2 mL of 0.5% ropivacaine) with additional local infiltration anesthesia along the dermatomes of the ventral branches of Th1–3 with 0.5% ropivacaine (10±5 mL) [23] (Fig. 4).

Postoperative analgesia in all groups was provided by ibuprofen 400 mg three times a day.

The port system was placed under the skin in the subclavian region at the level of 2–3 ribs. For successful implantation of the venous port system, percutaneous catheterization of the superior vena cava was done, using the subclavian vein for catheterization, which was performed under ultrasound guidance. After catheter insertion, a subcutaneous «pocket» was created and the catheter was connected to the port. The port was then inserted into the pocket with separate sutures, and the skin incision was sutured.

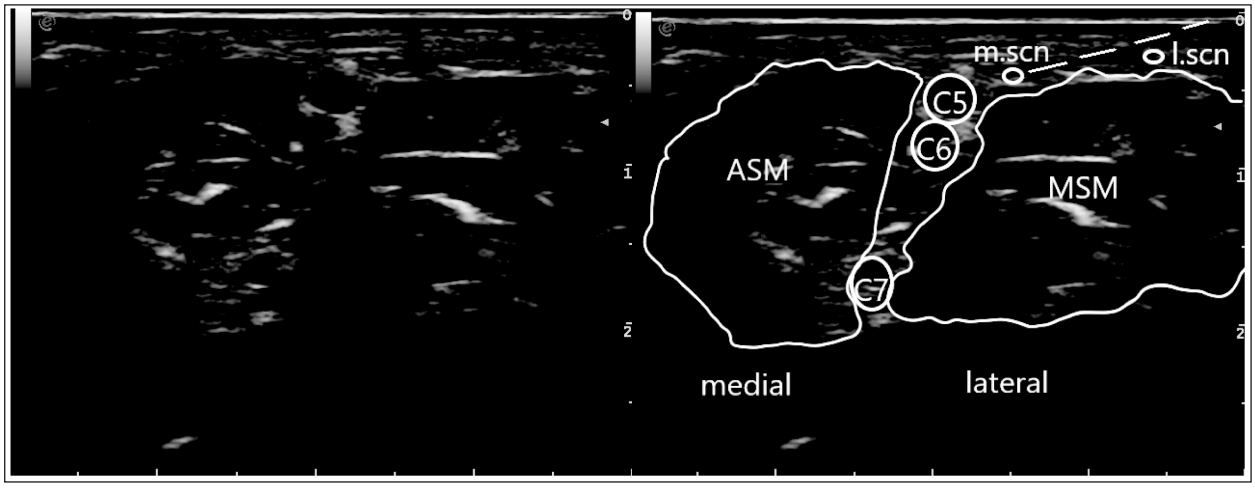

Fig. 4. Selective supraclavicular nerve block
Note. ASM — anterior scalenus muscle; MSM — middle scalenus muscle; m.scn — medial supraclavicular nerve; l.scn — lateral supraclavicular nerve; C5–C7 — cervical nerve roots.

Table 1. Patient characteristics **Me* [25; 75 percentile].

Parameter	Values in the groups			*P*-value
	1 (LIA), *N*=31	2 (PECS), *N*=31	3 (SSNB), *N*=31	
Age, years*	60 [53; 64]	63 [57; 68]	63 [54; 69]	0.267
ASA, points*	3 [3; 4]	4 [3; 4]	3 [3; 4]	0.216
Sex, number/%				
male	18/58	16/51.6	16/51.6	
female	13/42	15/48.4	15/48.4	

Table 2. Localization of the neoplasms.

Localization	Number/%
Gastrointestinal tract	40/43
Breast	16/17.2
Uterus	12/12.9
Lungs	11/11.8
ENT	4/4.3
Lymph nodes	3/3.2
Skin	3/3.2
Prostate	2/2.2
Kidneys	1/1.1
Liver	1/1.1

The intravenous port system was implanted in patients of both sexes, mean age 59.3 years, ASA III/IV, with different localization of neoplasms (Tables 1, 2). The main indication for implantation was chemotherapy.

In the postoperative period, pain was assessed using a visual analog scale (VAS) at rest and during movement at 8, 16, 32, and 72 hours after port placement. To assess the inflammatory response, the changes in the levels of CRP, interleukin-1β (IL-1β), interleukin-6 (IL-6) before the procedure and 24, 72 hours after surgery were measured. A semi-automated ELISA Rideret «Anthos 2020»(Sweden) and reagent kits from Vector-Best (Russia) were used.

The power of the study was assessed using G*Power 3.1.9.7 software, taking into account the number of patients (*N*=93) included in the study to compare the three groups. The effect size (ES) was 0.4, corresponding to a large effect according to Cohen's criteria, with α=0.05 and a sample size of 31 patients in each group. The a posteriori power (1-β) was 0.93.

Statistical analysis of the data was performed using the IBM SPSS Statistics software package (version 26.0). Normality of the distribution of quantitative variables was determined using the Shapiro–Wilk criterion. Quantitative data were described using median (*Me*) and interquartile range. For normal distribution, one-way analysis of variance (ANOVA) with Bonferroni correction was used to compare groups. For non-normal distributions, the non-parametric analog, Kruskal–Wallis test, and the Mann–Whitney test for pairwise a posteriori comparison were used. Parameters in groups 1 (LIA), 2 (PECS), and 3 (SSNB) were compared. When significance was reached, pairwise comparisons were made between groups 1 and 2, 1 and 3, and 2 and 3. The relationship between variables was quantitatively assessed using Spearman's rank correlation coefficient. The critical significance level for rejecting the null hypotheses was 0.05.

Results

The local anesthetic dose (0.5% ropivacaine hydrochloride) in group 1 (LIA) was 150 mg, additional LIA Me (25; 75 percentiles) was 25 (18.7; 31.2) mg, in group 2 (PECS) 75 mg with additional LIA Me of 95 (90.5;105.5) mg, in group 3 (SSNB) 10 mg with additional LIA Me of 20 (15; 39.8) mg.

In group 1 (LIA), the postoperative pain score on VAS at rest and during movement was significantly higher than in groups 2 (PECS) and 3 (SSNB) at all stages of the study, i. e. 8, 16, 36 and 72 hours after port system implantation ($P<0.001$). There were no significant differences in pain intensity at rest and during movement between groups 2 (PECS) and 3 (SSNB) at the same time points (Fig. 5).

According to the study design, all patients were prescribed ibuprofen 1200 mg/day after port system implantation, and the need for medication was then recorded in all groups. The ibuprofen requirement (*Me* [25; 75 percentiles]) was 1200 mg (1200; 1200) for three days in the LIA group, 800 mg (400; 800) in the PECS group, and 400 mg (0; 400) for one day in the SSNB group. A greater need for ibuprofen in the LIA group (P=0.001) was associated with persistent pain greater than 30 VAS points 48 hours after port system implantation.

Baseline CRP levels did not differ between groups.

In the LIA group, the increase in CRP 24 hours after port placement was significantly higher than in the PECS and SSNB groups ($P<0.001$) (Fig. 6a). On day 3, significant differences in CRP levels persisted between these groups (P=0.004). Notably, the CRP level in the LIA group was significantly higher than the reference values (8.05±2.97 mg/L) on day 1 after surgery, in contrast to the PECS and SSNB groups (5.45±2.16 and 4.97±2.59, respectively). The increase in CRP 24 hours after surgery was not significant in the PECS and SSNB groups. In 8 patients of the LIA group, the CRP concentration exceeded 10 mg/L, indicating clinically significant inflammation [43].

No significant differences in CRP levels were found in the PECS and SSNB groups ($P\geqslant0.05$), indicating a similar effect of these regional techniques on the inflammatory stress response (Table 4).

At baseline, there were no significant differences in interleukin-1β levels between groups.

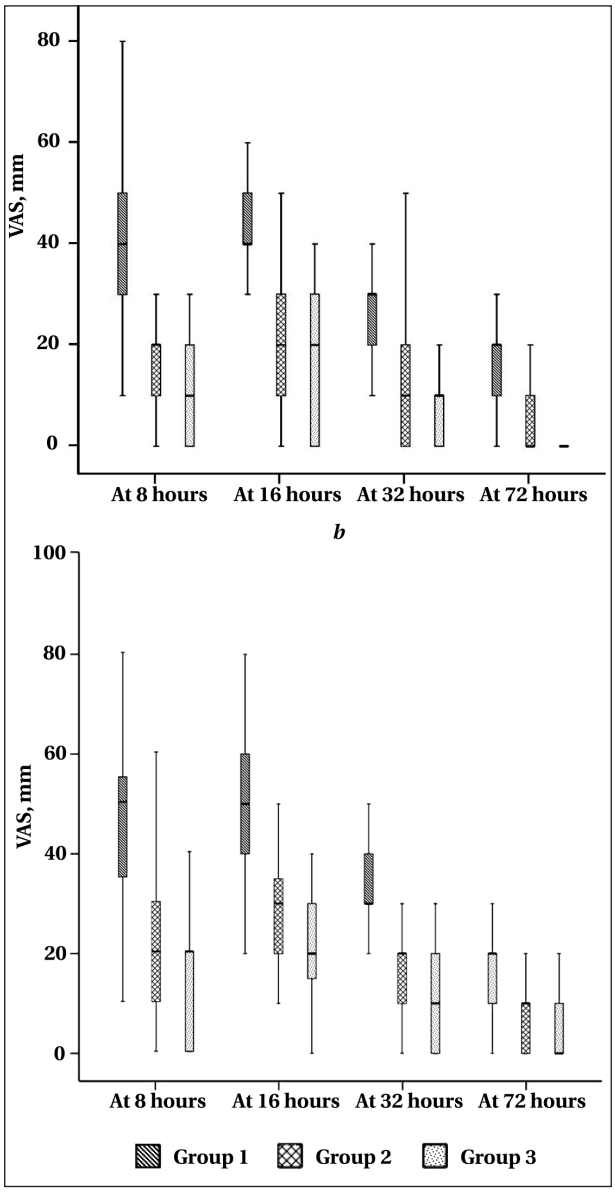

Fig. 5. Boxplot («whisker box») diagram of pain intensity according to VAS at rest (*a*) and during movement (*b*).
Note. Mann–Whitney test was used.

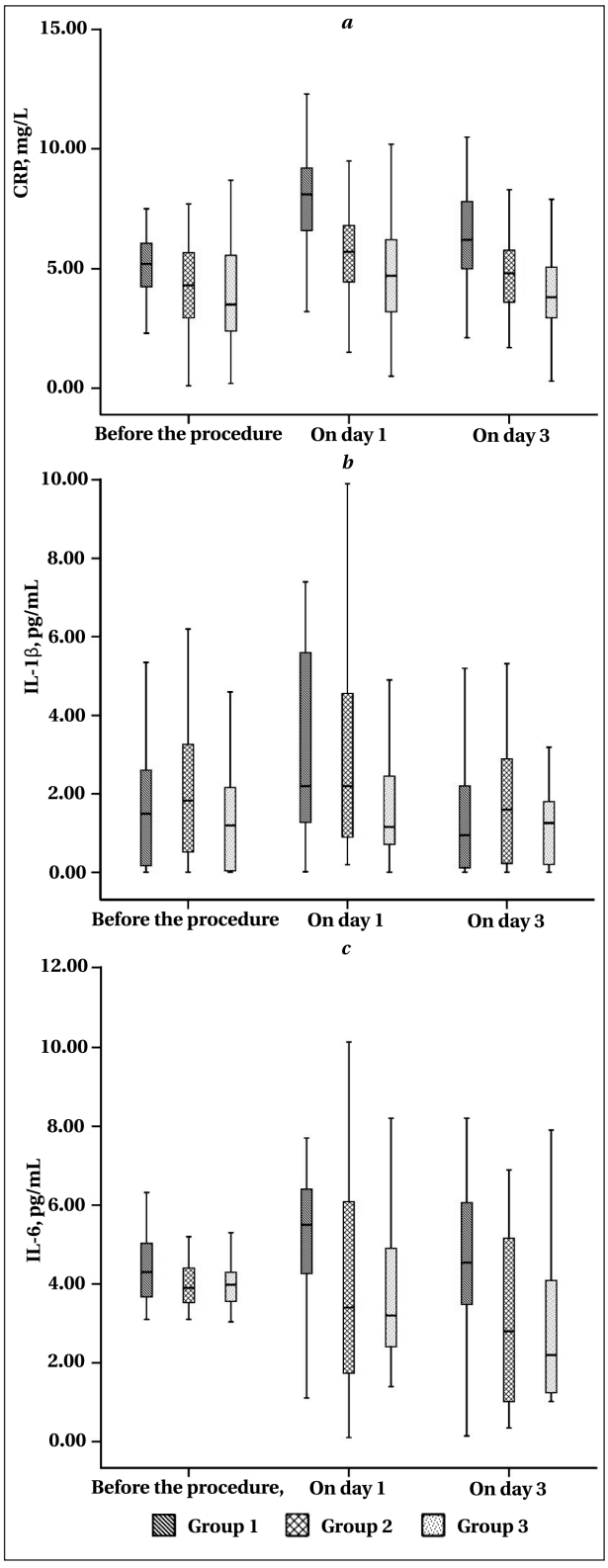

Fig. 6. Intergroup comparison of CRP (*a*) and interleukin (*b, c*) levels during the study phases.
Note. *a* — ANOVA test with Bonferroni correction; *b, c* — Kruskall–Wallis test.

On postoperative day 1, interleukin-1β levels were lower in groups 1 (LIA) and 2 (PECS) than in group 3 (SSNB), 2.1 (1.04; 5.8) and 1.9 (0.9; 4.02) vs. 1.14 (0.51; 2.64), respectively ($P<0.05$) (Table 5). There were no differences in this parameter between groups at day 3 (Fig. 6, *b*).

There were no significant differences in IL-1β between groups 1 (LIA) and 2 (PECS) at any time point ($P>0.05$).

Baseline IL-6 levels in the study groups did not differ and were above reference values due to the concurrent severe malignancy. Significant differences in IL-6 levels were found in groups 1 (LIA) and 2 (PECS) on day 1 after surgery, 5.5 (4.25;6.5) vs. 3.2 (2.32; 5.3) pg/mL, respectively, and on day 3, 4.54 (3.44; 6.1) vs. 2.2 (1.24; 4.1) pg/mL ($P<0.05$) (Fig. 6, *c*). The most significant differences in interleukin-6 concentrations on days 1 and 3 after surgery were found between the LIA and SSNB groups, 5.5 (4.25; 6.5) and 4.54 (3.44; 6.1) versus 3.2 (2.32; 5.3) and 2.2 (1.24; 4.1), respectively (Table 5).

Table 3. Paired comparison of CRP levels, difference of means (standard error).

Time point	Intergroup comparison of CRP levels (mg/l)			P_{1-2}	P_{1-3}	P_{2-3}
	1 (LIA) — 2 (PECS)	1 (LIA) — 3 (SSNB)	2 (PECS) — 3 (SSNB)			
Before the procedure	0.77 (0.47)	1.02 (0.47)	0.25 (0.47)	0.329	0.103	1.00
On day 1	2.6 (0.66)	3.08 (0.66)	0.48 (0.66)	0.0001	0.001	1.00
On day 3	1.16 (0.59)	2.03 (0.59)	0.87 (0.59)	0.152	0.003	0.43

Note. A posteriori comparisons with Bonferoni correction were used ($P<0.05$).

Table 4. Changes in IL-1β and IL-6 levels, *Me* [25th; 75th percentile].

Time point	Interleukin levels (pg/ml) in groups			P_{1-2}	P_{1-3}	P_{2-3}
	1 (LIA), *N*=31	2 (PECS), *N*=31	3 (SSNB), *N*=31			
		IL-1β				
Before the procedure	1.3 [0.15;2.62[	1,6 [0.36;3.09]	1.15 [0.04;2.32]	0.367	0.397	0.076
On day 1	2.1 [1.04;5.8]	1,9 [0.9;4.02]	1.14 [0.51;2.64]	0.573	0.011	0.03
On day 3	0.93 [0.09;2.33]	1,57 [0.18;2.5]	1.23 [0.12;1.88]	0.345	0.866	0.172
		IL-6				
Before the procedure	4.3 [3.65;5.1]	3.9 [3.5;4.45]	3.98 [3.5;4.3]	0.054	0.106	0.805
On day 1	5.5 [4.25;6.5]	3.4 [1.5;6.25]	3.2 [2.32;5.3]	0.019	0.002	0.751
On day 3	4.54 [3.44;6.1]	2.8 [1.0;5.21]	2.2 [1.24;4.1]	0.05	0.015	0.899

Note. Mann–Whitney test was used.

There were no significant differences in this parameter between the PECS and SSNB groups. Interestingly, in the supraclavicular nerve regional block group, IL-6 levels decreased 2-fold on day 3 after port system implantation compared to baseline (Table 5).

A significant correlation was found between the severity of pain according to VAS and the level of proinflammatory cytokines at all stages of the study. We found the most significant positive correlation between the difference in IL-6 concentrations in the first day after surgery and before surgery, as well as between IL-6 concentrations in the first day after surgery and pain severity according to VAS after 72 hours with *rho*=0.511 ($P<0.001$) and *rho*=0.542 ($P<0.001$), respectively (Fig. 7).

Discussion

When choosing the regional anesthesia technique for the implantation of intravenous port systems, we should consider the innervation of the anterior surface of the chest wall up to the third rib as the most common implantation site. This area is most often used for «pocketing» and direct insertion of the port receiving chamber [44].

The role of cutaneous nerve blocks in regional anesthesia is often underestimated. Such blocks are performed less frequently or in addition to conventional nerve blocks. Cutaneous nerves are involved in the development of acute postoperative pain, but they are also the most common cause of chronic postoperative neuropathic pain [45].

Taking into account the results of pain assessment by VAS in the study groups, SSNB was found to possess the greatest analgesic efficacy during intravenous port system implantation compared to LIA and PECS. The advantages of PECS block over local anesthesia for intravenous port system implantation have been

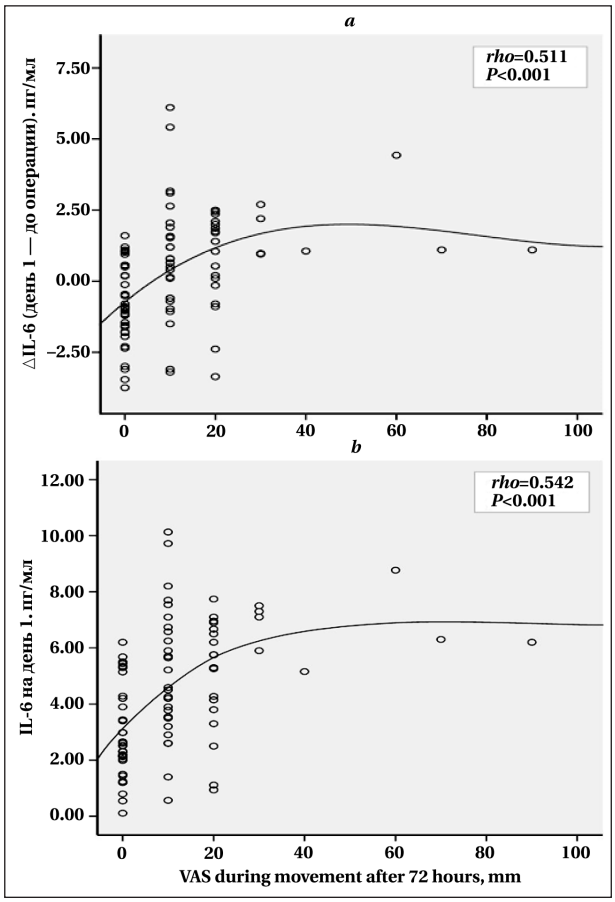

Fig. 7. Correlation of VAS pain severity with IL-6 levels during movement after 72 hours.
Note. Correlation: *a* — with the change in IL-6 level between day 1 after surgery and baseline; *b* — with the IL-6 level on day 1 after surgery.

demonstrated in several studies [13, 41]. In our study, PECS block also had a rather strong analgesic potential, comparable to that of selective supraclavicular nerve

block (SSNB). However, it was the SSNB that significantly reduced the local anesthetic dose and minimized the postoperative stress response.

According to Thomas Dahl Nielsen of Aarhus University Hospital (Denmark), «…whether or not cutaneous nerve blocks should be of relevance to the regional anaesthetist in regard to acute postoperative pain, depends on the objective of the postoperative pain treatment. If future improvements towards opioid-free, painless, fast track procedures are an ambition, then cutaneous nerves and knowledge of cutaneous nerve blocks seem like an unavoidably part that equation» [45]. This study confirms the above statement and also shows that the use of regional anesthesia techniques reduces the need for postoperative anesthesia. This is in agreement with the results of other authors [41].

The use of regional anesthesia is known to reduce the inflammatory response induced during surgery in cancer patients [46, 47]. When local anesthesia was used for intravenous port system implantation, a significant postoperative stress response was obtained on the first day after implantation. The levels of CRP and interleukin-6 significantly exceeded the reference values and did not decrease to the preoperative values even on the third day after surgery only in the local anesthesia group. The data obtained are consistent with the suggestion that CRP is an acute-phase protein induced primarily by the action of IL-6 on the gene responsible for CRP transcription in the acute phase of inflammation/infection [43].

CRP and IL-6 have been reported to have the strongest correlation with the severity of surgical injury, although CRP is probably the most clinically useful of them (Watt D. G. et al.) [48]. It can be concluded that even minimally invasive procedures in cancer patients can induce a significant inflammatory response when only local anesthesia is used.

One day after surgery under local anesthesia, an increase in interleukin-1β was observed compared to the group using selective supraclavicular nerve block combined with local anesthesia. Interleukin-1β, a 17.5 kDa polypeptide, is thought to play an important role in modulating neuronal excitability in the peripheral and central nervous systems. In addition to its immunoregulatory effects, IL-1β has a specific relevance to the development of persistent pain, including peripheral tissue injury (inflammatory pain) and nerve injury (neuropathic pain) [49].

In the acute immune response, tumor necrosis factor-alpha (TNF-α) and interleukin (IL)-1β are released first. They induce a secondary immune response in which IL-6 is produced [50]. Given the association of IL-1β and IL-6 with inflammatory and neuropathic pain, the findings reflect both the superior analgesic effect of cutaneous nerve block and the greatest nociceptive stimulation with local anesthesia alone.

A correlation between pain intensity and the expression of proinflammatory cytokines and CRP has been demonstrated. The study by Amano K et al. also reported a direct correlation between CRP and pain scores on a digital rating scale. In addition, serum levels of CRP have been identified as a «surrogate» for systemic inflammation in relation to survival, activities of daily living, and physical and psychological signs and symptoms [51].

The use of regional anesthesia was found to reduce the inflammatory response; in the cutaneous nerve block group, IL-6 levels were reduced 2-fold on day 3 compared to baseline. Pérez-González O. et al. reported that regional anesthesia in breast cancer surgery was associated with lower levels of inflammation and better immune response compared with general anesthesia and opioid analgesia [52].

In a recent review of perioperative anesthesia strategies in oncology, the authors conclude that regional anesthesia can be considered as a technique to potentially decrease the response to surgical stress, improve pain control, and reduce postoperative complications, providing significant benefit for cancer patients [53].

There is a growing interest in how perioperative strategies can alter cancer outcomes. Literature in recent years has suggested that regional anesthesia can increase recurrence-free survival in cancer patients, leading to the birth of a new specialty, oncoanesthesiology [54]. Mary Thomas, professor of anesthesiology at the Regional Cancer Center of India, argues that «anesthetic strategy could have significant oncological sequel is a quantum leap forward» [54]. Our study also underscores the importance of this point.

Conclusion

Implantation of an intravenous port system under local anesthesia induces a significant inflammatory stress response due to surgical trauma (CRP 8.05 mg/L, IL-6 5.5 pg/mL, IL-1β 2.1 pg/mL at 24 hours), while local anesthesia cannot provide sufficient analgesia after implantation in cancer patients.

The use of regional anesthesia techniques under ultrasound guidance helps to achieve a significant reduction in postoperative pain, the need for additional postoperative analgesia, and to counteract the inflammatory stress response after implantation of the intravenous port system.

Selective supraclavicular nerve block during implantation of the intravenous port system has the greatest analgesic potential and requires significantly less local anesthetic (additional 10 mg LIA median of 20 [5; 39.8] mg) compared to local infiltration anesthesia (additional 150 mg LIA median of 25 [18.7; 31.2] mg) and PECS block (additional 75 mg LIA median of 95 [90.5; 105.5] mg).

References

1. *Portnow J., Lim C., Grossman S.A.* Assessment of pain caused by invasive procedures in cancer patients. *J Natl Compr Canc Netw*. 2003; 1 (3): 435-439. DOI: 10.6004/jnccn.2003.0037. PMID: 19761075
2. *Seifert S., Taxbro1 K., Hammarskjold F.* Patient-controlled sedation in port implantation (PACSPI 1) — a feasibility trial. *Elsevier*. 2022; 3: 100026. DOI: 10.1016/j.bjao.2022.100026
3. *Byager N., Hansen M.S., Mathiesen O., Dahl J.B.* The analgesic effect of wound infiltration with local anaesthetics after breast surgery: a qualitative systematic review. *Acta Anaesthesiol Scand*. 2014; 58 (4): 402–410. DOI: 10.1111/aas.12287. PMID: 24617619
4. *Kaya E., Südkamp H., Lortz J., Rassaf T., Jánosi R.A.* Feasibility and safety of using local anaesthesia with conscious sedation during complex cardiac implantable electronic device procedures. *Sci Rep*. 2018; 8 (1): 7103. DOI: 10.1038/s41598-018-25457-x. PMID: 29740019
5. *Akelma H. Salýk F., Býçak M., Erbatur M.E.* Local anesthesia for port catheter placement in oncology patients: an alternative to landmark technique using ultrasound-guided superficial cervical plexus block — a prospective randomized study. *J Oncol*. 2019: 2585748. DOI: 10.1155/2019/2585748. PMID: 31467534
6. *Vellucci R., Mediati R.D., Gasperoni S., Mammucari M., Marinangeli F., Romualdi P.* Assessment and treatment of breakthrough cancer pain: from theory to clinical practice. *J Pain Res*. 2017; 10: 2147–2155. DOI: 10.2147/JPR.S135807. PMID: 29066928
7. *Bozyel S., Yalnýz A., Aksu T., Guler T.E., Genez S.* Ultrasound-guided combined pectoral nerve block and axillary venipuncture for implantation of cardiac implantable electronic devices. *Pacing Clin Electrophysiol*. 2019; 42 (7): 1026–1031. DOI: 10.1111/pace.13725. PMID: 31106438
8. *Renzini M., Ripani U., Golia L., Nisi F., Gori F.* Pectoralis (PecS) block 1 for port-a-cath removal and central venous catheter (CVC) replacement. *Med Glas (Zenica)*. 2020; 17 (2): 352–355. DOI: 10.17392/1158-20. PMID: 32253905
9. *Munshey F., Ramamurthi R.J., Tsui B.* Early experience with PECS 1 block for Port-a-Cath insertion or removal in children at a single institution. *J Clin Anesth*. 2018; 49: 63–64. DOI: 10.1016/j.jclinane.2018.06.010. PMID: 29894919
10. *Sansone P., Pace M.C., Passavanti M.B., Pota V., Colella U., Aurilio C.* Epidemiology and incidence of acute and chronic post-surgical pain. *Ann Ital Chir*. 2015; 86 (4): 285–292. PMID: 26343897
11. *Taxbro K., Hammarskjöld F., Thelin B., Lewin F., Hagman H., Hanberger H. et al.* Clinical impact of peripherally inserted central catheters vs implanted port catheters in patients with cancer: an open-label, randomised, two-centre trial. *Br J Anaesth*. 2019; 122 (6): 734–741. DOI: 10.1016/j.bja.2019.01.038. PMID: 31005243
12. C*hang D.-H., Hiss S., Herich L., Becker I., Mammadov K., Franke M., Mpotsaris A. et al.* Implantation of venous access devices under local anesthesia: patients' satisfaction with oral lorazepam. *Patient Prefer Adherence*. 2015; 9: 943–949. DOI: 10.2147/PPA.S80330. PMID: 26185424
13. *Ince M.E., Sir E., Eksert S., Ors N., Ozkan G.* Analgesic effectiveness of ultrasound-guided Pecs II block in central venous port catheter implantation. *J Pain Res*. 2020; 13: 1185–1191. DOI: 10.2147/JPR.S258692. PMID: 32547181
14. *Byager N., Hansen M.S., Mathiesen O., Dahl J.B.* The analgesic effect of wound infiltration with local anaesthetics after breast surgery: a qualitative systematic review. *Acta Anaesthesiol Scand*. 2014; 58 (4): 402–410. DOI: 10.1111/aas.12287. PMID: 24617619
15. *Cassi L.C., Biffoli F., Francesconi D., Petrella G., Buonomo O.* Anesthesia and analgesia in breast surgery: the benefits of peripheral nerve block. *Eur Rev Med Pharmacol Sci*. 2017; 21 (6): 1341–1345. PMID: 28387892
16. *Woodworth G.E., Ivie R.M.J., Nelson S.M., Walker C.M., Maniker R.B.* Perioperative breast analgesia: a qualitative review of anatomy and regional techniques. *Reg Anesth Pain Med*. 2017; 42 (5): 609–631. DOI: 10.1097/AAP.0000000000000641. PMID: 28820803
17. *Oksuz G., Bilgen F., Arslan M., Duman Y., Urfalýoglu A., Bilal B.* Ultrasound-guided bilateral erector spinae block versus tumescent anesthesia for postoperative analgesia in patients undergoing reduction mammoplasty: a randomized controlled study. *Aesthetic Plast Surg*. 2019; 43 (2): 291–296. DOI: 10.1007/s00266-018-1286-8. PMID: 30535555
18. *Sato M., Shirakami G., Fukuda K.* Comparison of general anesthesia and monitored anesthesia care in patients undergoing breast cancer surgery using a combination of ultrasound-guided thoracic paravertebral block and local infiltration anesthesia: a retrospective study. *J Anesth*. 2016; 30 (2): 244–251. DOI: 10.1007/s00540-015-2111-z. PMID: 26661141
19. *Blanco R.* The 'pecs block': A novel technique for providing analgesia after breast surgery. *Anaesthesia*. 2011; 66 (9): 847-8. DOI: 10.1111/j.1365-2044.2011.06838.x. PMID: 21831090
20. *Mense S.* Nociception from skeletal muscle in relation to clinical muscle pain. *Pain*. 1993; 54 (3): 241–289. DOI: 10.1016/0304-3959 (93)90027-M. PMID: 8233542
21. *Porzionato A., Macchi V., Stecco C., Loukas M., Tubbs R.S., De Caro R.* Surgical anatomy of the pectoral nerves and the pectoral musculature. *Clin Anat*. 2012; 25 (5) 559–575. DOI: 10.1002/ca.21301. PMID: 22125052
22. *Wallace A.M., Wallace M.S.* Postmastectomy and postthoracotomy pain. *Anesthesiol Clin North Am*. 1997; 15: 353–370. DOI: 10.106/ S0889-8537 (05)70338-2
23. *Maybin J., Townsley P., Bedforth N., Allan A.* Ultrasound guided supraclavicular nerve blockade: first technical description and the relevance for shoulder surgery under regional anaesthesia. *Anaesthesia*. 2011; 66 (11): 1053–1055. DOI: 10.1111/j.1365-2044.2011.06907.x PMID: 22004208
24. *Russon K., Pickworth T., Harrop-Griffiths W.* Upper limb blocks. *Anaesthesia*. 2010; 65 Suppl. 1: 48–56. DOI: 10.1111/j.1365-2044.2010.06277.x. PMID: 20377546
25. *Vester-Andersen T., Christiansen C., Hansen A., Sorensen M., Meisler C.* Interscalene brachial plexus block: area of analgesia, complications and blood concentrations of local anesthetics. *Acta Anaesthesiol Scand*. 1981; 25 (2): 81–84. DOI: 10.1111/j.1399-6576.1981.tb01612.x. PMID: 7324828

26. *Urmey W.F., Grossi P., Sharrock N.E., Stanton J., Gloeggleer P.J.* Digital pressure during interscalene block is clinically ineffective in preventing anesthetic spread to the cervical plexus. *Anesth Analg.* 1996; 83 (2): 366–370. DOI: 10.1097/00000539-199608000-00028. PMID: 8694320
27. *Sivashanmugam T., Areti A., Selvum E., Diwan S., Pandian A.* Selective blockade of supraclavicular nerves and upper trunk of brachial plexus «The SCUT block» towards a site-specific regional anaesthesia strategy for clavicle surgeries — a descriptive study. *Indian J Anaesth.* 2021; 65 (9): 656–661. DOI: 10.4103/ija.ija_255_21. PMID: 34764500
28. *Wang Q., Zhang G., Wei S., He Z., Sun L., Zheng H.* Comparison of the effects of ultrasound-guided erector spinae plane block and wound infiltration on perioperative opioid consumption and postoperative pain in thoracotomy. *J Coll Physicians Surg Pak*. 2019; 29 (12): 1138–1143. DOI: 10.29271/jcpsp.2019.12.1138. PMID: 31839083
29. *Jeske H.C., Kralinger F., Wambacher M., Perwanger F., Schoepf R., Oberladstaetter J., Krappinger D. et al.* A randomized study of the effectiveness of suprascapular nerve block in patient satisfaction and outcome after arthroscopic subacromial decompression. *Arthroscopy*. 2011; 27 (10): 1323–1328. DOI: 10.1016/j.arthro. 2011.05.016. PMID: 21868190
30. *Hadzic A., Williams B.A., Karaca P.E., Hobeika P., Unis G., Dermksian G., Yufa M. et al.* For outpatient rotator cuff surgery, nerve block anesthesia provides superior same-day recovery over general anesthesia. *Anesthesiology.* 2005; 102 (5): 1001–1007. DOI: 10.1097/00000542-200505000-00020. PMID: 15851888
31. *Terkawi A.S., Mavridis D., Sessler D.I., Nunemaker M.S., Doais K.S., Terkawi R.S., Terkawi Y.S. et al.* Pain management modalities after total knee arthroplasty: a network meta-analysis of 170 randomized controlled trials. *Anesthesiology.* 2017; 126 (5): 923–937.DOI: 10.1097/ALN.0000000000001607. PMID: 28288050
32. *Novitsky Y.W., Litwin D.E., Callery M.P.* The net immunologic advantage of laparoscopic surgery. *Surg Endosc*. 2004; 18 (10): 1411–1419. DOI: 10.1007/s00464-003-8275-x
33. *Smajic J., Tupkovic L.R., Husic S., Avdagic S.S., Hodzic S., Imamovic S.* Systemic inflammatory response syndrome in surgical patients. *Med Arch.* 2018; 72 (2): 116–119. DOI: 10.5455/medarh.2018.72.116-119. PMID: 29736100
34. *Ren K., Torres R.* Role of interleukin-1β during pain and inflammation. *Brain Res Rev.* 2009; 60 (1): 57–64. DOI: 10.1016/j.brainresrev. 2008.12.020. PMID: 19166877
35. *Zhou Y.Q., Liu Z., Liu Z.-H., Chen S.-P., Li M., Shahveranov A., Ye D-W. et al.* Interleukin-6: an emerging regulator of pathological pain. *J Neuroinflammation.* 2016; 13 (1): 141. DOI: 10.1186/s12974-016-0607-6. PMID: 27267059
36. *Dos Santos G.G., Delay L., Yaksh T. L., Corr M.* Neuraxial cytokines in pain states. *Front Immunol.* 2020; 10: 3061. DOI: 10.3389/fimmu.2019.03061. PMID: 32047493
37. *Zhang J.-M., An J.* Cytokines, inflammation, and pain. *Int Anesthesiol Clin.* 2007; 45 (2): 27–37. DOI: 10.1097/AIA.0b013e318034194e. PMID: 17426506
38. *Marsland A.L., Walsh C., Lockwood K., John-Henderson N.A.* The effects of acute psychological stress on circulating and stimulated inflammatory markers: a systematic review and meta-analysis. *Brain Behav Immun*. 2017: 64: 208–219. DOI: 10.1016/j.bbi. 2017.01.011. PMID: 28089638
39. *Bugada D., Lavand'homme P., Ambrosoli A.L., Cappelleri G., Saccani Jotti G.M., Meschi T., Fanelli G. et al.* Effect of preoperative inflammatory status and comorbidities on pain resolution and persistent postsurgical pain after inguinal hernia repair. *Mediators Inflamm*. 2016; 2016: 5830347. DOI: 10.1155/2016/5830347. PMID: 27051077
40. *Guan Z., Hellman J., Schumacher M.* Contemporary views on inflammatory pain mechanisms: TRPing over innate and microglial pathways. *F1000Res.* 2016; 5: F1000 Faculty Rev-2425. DOI: 10.12688/f1000research.8710.1. PMID: 27781082
41. *Janc J., Szamborski M., Milnerowicz A., Łysenko L., Leśnik P.* Evaluation of the effectiveness of modified pectoral nerve blocks type II (PECS II) for vascular access port implantation using cephalic vein venesection. *J Clin Med.* 2021; 10 (24): 5759. DOI: 10.3390/jcm10245759. PMID: 34945054
42. ASA physical status classification system. https://www.asahq.org/standards-and-guidelines/asa-physical-status-classification-system
43. *Nehring S.M., Goyal A., Patel B.C.* C reactive protein. [updated 2022 Jul 18]. In: StatPearls [Internet]. Treasure Island (FL): StatPearls Publishing; 2022. Available from: https://www.ncbi.nlm.nih.gov/books/NBK441843/
44. *Zerati A.E., Wolosker N., de Luccia N., Puech-Leão* P. Cateteres venosos totalmente implantáveis: histórico, técnica de implante e complicações [Portuguese]. *J Vasc Bras.* 2017; 16 (2): 128–139. DOI: 10.1590/1677-5449.008216. PMID: 29930637
45. *Nielsen T.D.* Relevance of cutaneous nerve blocks. *Regional Anesthesia & Pain Medicine* 2022; 47: A15-A16. https://rapm.bmj.com/ content/rapm/47/Suppl_1/A15.full.pdf
46. *Deegan C.A., Murray D., Doran P., Moriarty D.C., Sessler D.I., Mascha E., Kavanagh B.P. et al.* Anesthetic technique and the cytokine and matrix metalloproteinase response to primary breast cancer surgery. *Reg Anesth Pain Med.* 2010; 35; (6): 490–495. DOI: 10.1097/AAP. 0b013e3181ef4d05. PMID: 20975461
47. *Zhao J., Mo H.* The impact of different anesthesia methods on stress reaction and immune function of the patients with gastric cancer during peri-operative period. *J Med Assoc Thai.* 2015; 98 (6): 568–573. PMID: 26219161
48. *Watt D.G., Horgan P.G., McMillan D.C.* Routine clinical markers of the magnitude of the systemic inflammatory response after elective operation: a systematic review. *Surgery.* 2015; 157 (2): 362–380. DOI: 10.1016/j.surg.2014.09.009. PMID: 25616950
49. *Prossin A.R., Zalcman S.S., Heitzeg M.M., Koch A.E., Campbell O.L., Phan K.L., Stohler C.S. et al.* Dynamic interactions between plasma IL-1 family cytokines and central endogenous opioid neurotransmitter function in humans. *Neuropsychopharmacology.* 2015; 40 (3): 554–565. DOI: 10.1038/npp.2014.202. PMID: 25139063

50. *Guisasola M.C., Alonso B., Bravo B., Vaquero J., Chana F.* An overview of cytokines and heat shock response in polytraumatized patients. *Cell Stress Chaperones*. 2018; 23 (4): 483–489. DOI: 10.1007/s12192-017-0859-9. PMID: 29101529
51. *Amano K., Ishiki H., Miura T., Maeda I., Hatano Y., Oyamada S., Yokomichi N. et al.* C-reactive protein and its relationship with pain in patients with advanced cancer cachexia: secondary cross-sectional analysis of a multicenter prospective cohort study. *Palliat Med Rep*. 2021; 2 (1): 122–131. DOI: 10.1089/pmr.2021.0004. PMID: 34223511
52. *Pérez-González O., Cuéllar-Guzmán L.F., Soliz J., Cata J.P.* Impact of regional anesthesia on recurrence, metastasis, and immune response in breast cancer surgery: a systematic review of the literature. *Reg Anesth Pain Med*. 2017; 42 (6): 751–756. DOI: 10.1097/AAP. 0000000000000662. PMID: 28953508
53. *Ballestín S.S., Bardaji A.L., Continente C.M., Bartolomé M.J.L.* Antitumor anesthetic strategy in the perioperatory period of the oncological patient: a review. *Front Med (Lausanne)*. 2022; 9: 799355. DOI: 10.3389/fmed.2022.799355. PMID: 35252243
54. *Thomas M.* Advances in oncoanaesthesia and cancer pain. *Cancer Treat Res Commun*. 2021: 29: 100491. DOI: 10.1016/j. ctarc. 2021.100491. PMID: 34837798

Received 03.11.2022
Accepted 30.05.2023

https://doi.org/10.15360/1813-9779-2023-3-39-45

The Analgesic Efficacy of Prolonged Erector Spinae Fascial Plane Block in Patients with Multiple Rib Fractures

Visolat H. Sharipova, Ivan V. Fokin*

Republican Research Centre of Emergency Medicine,
2 Farhad Str., Chilanzar district, 100115 Tashkent, Republic of Uzbekistan

For citation: *Visolat H. Sharipova, Ivan V. Fokin.* The Analgesic Efficacy of Prolonged Erector Spinae Fascial Plane Block in Patients with Multiple Rib Fractures. *Obshchaya Reanimatologiya = General Reanimatology. Общая реаниматология.* 2023; 19 (3): 39–45. https://doi.org/10.15360/1813-9779-2023-3-39-45 [In Russ. and Engl.]

***Correspondence to:** Ivan V. Fokin, vafanya3@yandex.ru

Summary

Objctive. To evaluate the analgesic efficacy of prolonged erector spinae fascial plane (ESFP) block in patients with multiple rib fractures.

Material and methods. The study included 40 patients with multiple rib fractures. Based on anesthesia methods, patients were divided into 2 groups, where systemic analgesics were used for pain management in the control group (*N*=20), and additional supplementation with prolonged erector spinae fascial plane (ESFP) block in the main group (*N*=20). The study monitored the severity of pain measured by the numeric rating scale (NRS) at rest and during coughing, forced vital capacity (FVC), and the need for injectable narcotic analgesics.

Results. The NRS measures at rest in the main group were statistically significantly superior to the control group results: at stage II — 1.5 points (IQR: 1.0–3.0) vs 3.0 points (IQR: 3.0–4.0); at stage III — 2.0 points (IQR: 1.0–2.0) vs 4.0 points (IQR: 3.0–5.0); at stage IV — 1.5 points (IQR: 0.8–2.2) vs. 4.5 points (IQR: 4.0–5.0); at stage V — 1 point (IQR: 0–2,0) vs. 3.0 points (IQR: 2.8–4.0), respectively ($P<0.001$). Percentages of predicted FVC depending on patient's gender, age, height and weight in the control group were as follows: at stage II — 38± 8% (95%CI: 34–41); stage III — 44± 8% (95%CI: 40–47); stage IV — 41±10% (95%CI: 36–45) and stage V — 49±10% (95%CI: 45–53). In the main group, the following FVC values were obtained: 49±15% at stage II (95%CI: 42–56), 50±13% at stage III (95%CI: 44–57), 53±13% at stage IV (95%CI: 47–59), and 57±11% at stage V (95%CI: 52–63). Therefore, statistically significant FVC reduction in the control group vs the main group came up to 22%, 14%, 24% and 15% at stages II-V, respectively ($P<0.05$). The amounts of injected narcotic analgesics on day 1 and day 2 after initiation of the study were 5.0 mg (IQR: 5–10) and 5.0 mg (IQR: 0–5.0) in the main group vs 10.0 mg (IQR: 5.0–15.0) and 7.5 mg (IQR: 5.0–10.0) in the control group, respectively ($P<0.05$).

Conclusion. The prolonged erector spinae fascial plane block improves the quality of analgesia and FVC values in patients with multiple rib fractures.

Key words: long-term continuous block; erector spinae muscle; fascial plane; anesthesia; multiple fractures; ribs

Conflict of interest. The authors declare no conflict of interest.

Introduction

Rib fractures account for 10–12% of all trauma events and are generally a marker of serious injury [1]. Fractures of three or more ribs are defined as multiple and account for up to 68% of all rib fractures [2]. Despite timely and state-of-the-art medical care, this condition is associated with various severe pleural and pulmonary complications in 33%, including pulmonary atelectasis, pneumonia, ARDS, hydro- and pneumothorax, and pleural empyema, significantly prolonging hospital stay [3]. Pain in multiple rib fractures is very intense, and simple physiological actions such as deep breathing, productive coughing, and changes in body position lead to an increase in pain intensity. As a result, chest stiffness and the likelihood of atelectasis and pneumonia increase [4]. Accordingly, the selection and use of the optimal method of emergency pain management in patients with multiple rib fractures is an essential component of the comprehensive management of these patients [5]. In our opinion, multimodal analgesia with systemic analgesics combined with regional analgesia, such as erector spinae plane block (ESPB), seems to be the best method to treat patients with multiple rib fractures.

The erector spinae plane block was first described by Forero M. et al. in 2016 as a new method of regional block of thoracic nerves for the treatment of neuropathic pain [6]. The target of the block when injecting local anesthetic (LA) is the «fascial plane», which is located along the spine, between the anterior surface of the erector spinae muscle and the posterior part of the transverse processes of the vertebrae. Thus, when LA spreads along the fascia, it affects the posterior branches of the spinal nerves, and when it spreads anteriorly into the paravertebral space, it also affects the anterior branches of the spinal nerves, providing analgesia to the posterior, lateral, and anterior chest wall [6–9]. Available publications report broad indications for the use of ESPB, including pain relief for multiple rib fractures [10–14].

ESPB in a patient with multiple rib fractures was first described by Hamilton et al. who noted a

decrease in pain intensity scores on a numeric rating scale from 6 out of 10 at rest and 10 out of 10 on cough (despite prior multimodal analgesia) to 0 out of 10 at rest and 1 out of 10 on cough after only a few minutes of ESPB [15].

Other papers describing a series of clinical observations have also reported good pain relief after ESPB in patients with multiple rib fractures [16, 17]. A retrospective cohort study without a control group demonstrated the efficacy of pain management in 79 patients with multiple rib fractures after ESPB, as measured by reduced pain intensity, increased inspiratory volume on incentive spirometry, and reduced use of narcotic analgesics [18]. The persistent problem of inadequate pain relief in patients with multiple rib fractures, the search for an optimal method of pain relief, and the need to overcome the shortcomings of previous studies, such as the small number of patients and lack of a control group, provide a rationale for conducting our study.

Aim of the study: To evaluate the efficacy of extended erector spinae plane block in patients with multiple rib fractures.

Materials and Methods

A prospective study was conducted at the Republican Scientific Center for Emergency Medical Care in 2019 on 40 patients admitted for emergency indications with multiple rib fractures in the context of combined or isolated thoracic trauma.

Inclusion criteria: age 18 years and older, two and more rib fractures, conservative therapy.

Exclusion criteria: impaired consciousness (Glasgow Coma Score less than 14 points), Injury Severity Score greater than 25 points, need for mechanical ventilation or surgery under general anesthesia. All patients were divided into two groups according to the type of anesthesia. Patients in the control group (*N*=20) were prescribed with systemic analgesics such as Diclofenac 75 mg intramuscularly (i.m.) twice daily or Ketoprofen 100 mg i.m. or intravenously (i.v.) three times daily, Acetaminophen 1 g, administered i.v., four times daily. In addition, a ketoprofen patch was applied to the injured rib area and changed once a day, while Promedol 20 mg or Morphine 10 mg or Omnopon 20 mg i.m. or i.v. were administered for severe pain. Patients in the main group (*N*=20) received systemic analgesics in the same regimen as in the control group, supplemented by prolonged ESPB on day 1 after admission.

No differences were found between the groups in age, sex, frequency of injury causes, number of ribs injured, injury severity according to the Injury Severity Score (ISS), and injury characteristics (Table 1, $P>0.05$).

Before performing the block, the patients were informed about the upcoming manipulation, and after obtaining the patient's consent, an extended ESPB was performed under aseptic and antiseptic conditions.

Routine monitoring (BP, pulse, ECG, SpO_2) was performed during the first day after the patient's admission to the hospital. The patient's position during the block was chosen according to the patient's activity: lying on the side, opposite to the block, or sitting up. The level of the block was determined by the transverse process of the vertebra corresponding to the underlying injured ribs (Fig. 1).

Ultrasound guidance was performed with a 7–12 MHz linear transducer on a portable ultrasound device (Samsung Medison R3, South Korea). The appropriate transverse process was visualized 2.5–3 cm lateral to the spinous processes in the longitudinal position of the transducer. After determining the appropriate transverse process and marking the point of needle insertion, we performed aseptic preparation of the manipulation field and local infiltration anesthesia of the area of needle insertion with 4–5 mL of 1% lidocaine. A Tuohy 18G

Table 1. The main demographic and clinical parameters in groups of patients.

Parameter	Values in groups		*P*
	Control, *N*=20	Study, N=20	
Age, years (*M*±*SD*; 95%CI)	47.3±14.9; 40.3–54.3	48.8±15.6; 41.4–56.1	0.766
Sex, *N* (%)			
Female	5 (25.0)	5 (25.0)	1.000
Male	15 (75.0)	15 (75.0)	
Number of damaged ribs (*Me*; IQR)	4.0; 4.0–6.0	4.5; 4.0–6.0	0.707
Type of trauma, *N* (%)			
Single	10 (50.0)	9 (45.0)	1.000
Multiple	10 (50.0)	11 (55.0)	
Injury Severity Scale (ISS), points (*Me*; IQR)	14.0; 11.0–14.8	14.0; 11.0–17.0	0.423
Cause of trauma, *N* (%)			
Traffic accident	12 (60.0)	10 (50.0)	0.346
High altitude trauma	3 (15.0)	4 (20.0)	
Occupational injury	1 (5.0)	0 (0.0)	
Domestic injury	2 (10.0)	5 (25.0)	
Beating	0 (0.0)	1 (5.0)	
Other	2 (10.0)	0 (0.0)	

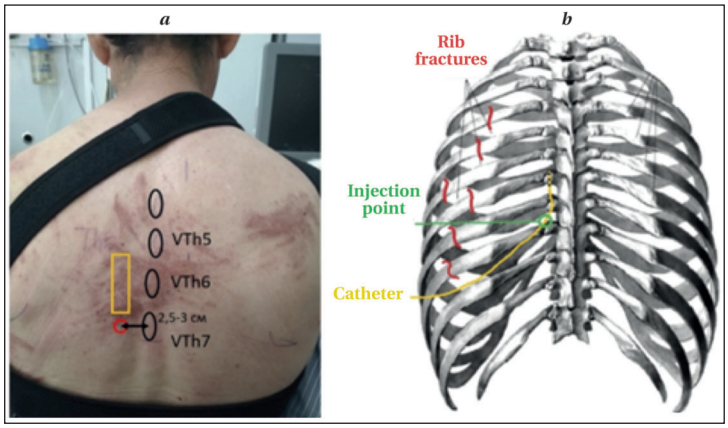

Fig. 1. Selection of injection site for catheter placement based on rib injury.
Note. *a* — clinical case. The red circle indicates the injection point of the needle, the yellow rectangle indicates the location of the base of the linear transducer. *b* — author's scheme of mutual positioning of the catheter tip and bony structures of the thorax (Fig. Bony structures, http://instruktor-fiz.org/wp-content/uploads/image/theory/clip_image023.jpg, Access date 2023.05.03).

needle was inserted in the cranial direction cranially under ultrasound guidance until contact was made with the distal part of the transverse process. The correct position of the needle tip in the fascial plane was determined by injecting up to 5 mL of normal saline, visualizing the linear spread of the solution beyond the erector spinae muscle and its separation from the surface of the transverse process. A 20 G catheter from the epidural kit was then inserted 4–5 cm cranially through the Tuohy needle and secured to the skin with a plaster. A 20 mL bolus of 1% lidocaine with 4 mg dexamethasone was injected through the catheter. For prolonged analgesia, an elastomeric pump was connected to the catheter immediately after the bolus administration, and a continuous infusion of 250 mL of 1% lidocaine was administered at a rate of 5 mL/h. Prolonged analgesia was maintained for three to seven days, depending on the patient's condition.

Pain intensity was assessed by numerical pain rating scale (NPRS) at rest and during coughing, and forced vital capacity (FVC) was measured by a portable spirometer as a percentage of predicted value based on the patient's sex, age, height, and weight. These values were recorded in both groups at several stages of the study: stage 1 — before the study (in both groups primary analgesia with NSAIDs and narcotics was administered), stage 2 — 1 hour later (in the control group after multimodal analgesia, in the main group after multimodal analgesia and block), stage 3 — 6 hours later, stage 4 — 24 hours later, stage 5 — 48 hours after the start of the study. The need for parenteral narcotic analgesics, calculated as the total dose of narcotic analgesics in parenteral morphine equivalent between 0–24 hours and 24–48 hours after the start of the study, was also assessed in the groups. Narcotic analgesic equivalence was calculated as follows: 10 mg Morphine = 20 mg Omnopon = 40 mg Promedol.

The results were analyzed using parametric and non-parametric methods. The collection, adjustment, organization of raw data and visualization of the obtained results were performed in Microsoft Office Excel 2020. Statistical analysis was performed using StatTech v. 2.8.4 (StatTech LLC, Russia). The Shapiro–Wilk criterion was used to assess the normality of the distribution. In case of normal distribution, the data were pooled into variation series, in which the means (*M*) and standard deviations (*SD*) and the 95% confidence interval (95%CI) were calculated. For non-normal distribution, quantitative variables were reported as median (*Me*) and interquartile range (IQR). The Mann–Whitney *U* test was used to compare independent populations when non-normal distribution was present. The nonparametric Friedman criterion with Holm-Bonferroni correction was used to compare more than two dependent samples with distribution different from normal. When the number of expected observations in any cell of the four-way table was less than 5, Fisher's exact test was used to estimate the significance of differences. When comparing means in samples of quantitative variables with normal distribution, Student's *t*-criterion was calculated. The paired Student's *t*-test was used to compare means calculated for paired samples.

Results

Pain intensity at rest as assessed by the NPRS did not differ between groups at stage 1 of the study (Table 2, P=0.128), but significant differences were found at all subsequent stages. The NPRS score at stage 2 was 1.5 points (IQR, 1.0 to 3.0) in the main group vs. 3.0 points (IQR, 3.0 to 4.0) in the control group, at stage 3 it was 2.0 points (IQR, 1.0 to 2.0) versus 4.0 points (IQR, 3.0 to 5.0), at stage 4, 1.5 points (IQR, 0.8 to 2.2) versus 4.5 points (IQR, 4.0 to 5.0), at stage 5, 1.0 point (IQR, 0 to 2.0) versus 3.0 points (IQR, 2.8 to 4.0), respectively (P<0.001). In the control group, there was a significant decrease in NPRS score only at stages 2 and 4 of the study (P<0.001). In the main group, the NPRS score decreased significantly by more than 50% at study stage 2 and remained significantly lower through and including study stage 5, when it reached its lowest point of 1.0 (IQR, 0 to 2.0) (P<0.001).

The NPRS values on cough in stages 2, 3, 4, and 5 of the study in the main group were significantly lower than those in the control group by more than 40% (Table 2, P<0.001). A significant de-

Table 2. Changes in the main parameters.

Group	Values in groups at the study stages					*P*
	1	2	3	4	5	
NPRS at rest, points (*Me*; IQR)						
Control	4.0; 3.0–5.0	3.0; 3.0–4.0	4.0; 3.0–5.0	4.5; 4.0–5.0	3.0; 2.8–4.0	<0.001[2*]
Study	5.0; 4.0–6.2	1.5; 1.0–3.0	2.0; 1.0–2.0	1.5; 0.8–2.2	1; 0–2.0	<0.001[2*] <0.001[3*] <0.001[4*] <0.001[5*]
P	0.128	<0.001*	<0.001*	<0.001*	<0.001*	—
NPRS on coughing, points (*Me*; IQR)						
Control	9.0; 9.0–10.0	9.0; 8.0–10.0	8.0; 8.0–9.0	7.0; 6.0–8.0	8.0; 8.0–8.2	<0.001[3*] <0.008[4*] 0.001[5*]
Study	10.0; 9.0–10.0	6.0; 5.0–7.0	5.0; 5.0–6.2	5.0; 4.0–6.0	5.5; 4.8–6.0	<0.001[2*] 0.001[3*] <0.001[4*] <0.001[5*]
P	0.390	<0.001*	<0.001*	<0.001*	<0.001*	—
FVC, % (*M*±*SD*; 95%CI)						
Control	38.1±8.3; 34.3–42.0	37.6±8.1; 33.8–41.5	43.5±7.7; 39.9–47.2	40.6±9.9; 36.0–45.2	49.0±9.5; 44.6–53.5	0.001[5*]
Study	41.9±11.5; 36.5–47.3	48.5±14.9; 41.6–55.5	50.5±13.1; 44.4–56.6	53.1±13.4; 46.9–59.4	57.4±11.3; 52.1–62.7	<0.001[2*] <0.001[3*] <0.001[4*] <0.001[5*]
P	0.244	0.007*	0.048*	0.002*	0.016*	—

Note. Significant differences, $P<0.05$: * — between groups; [2*] — between stages 1 and 2; [3*] — between stages 1 and 3; [4*] — between stages 1 and 4; [5*] — between stages 1 and 5. NPRS — numerical pain rating scale; FVC — forced vital capacity.

crease in the NPRS on cough in the control group was observed only from stage 3 of the study and reached a minimum in stage 4 of the study ($P<0.001$). In the main group, the reduction in this parameter was more dramatic, starting as early as stage 2, when it decreased by 40% and remained significantly lower until the end of the study ($P<0.001$).

From stage 2 of the study, FVC was significantly lower in the control group than in the main group (Table 2). While the FVC in the main group was 49±15% (95%CI, 42 to 56) at stage 2, 50±13% (95%CI, 44 to 57) at stage 3, 53±13% (95%CI, 47 to 59) at stage 4, and 57±11% (95%CI, 52 to 63) at stage 5, the FVC in the control group was 38±8% (95%CI, 34 to 41) at stage 2, 44±8% (95%CI, 40 to 47) at stage 3, 41±10% (95%CI, 36 to 45) at stage 4, and 49±10% (95%CI, 45 to 53) at stage 5, which were 22%, 14%, 24%, and 15% less than in the main group, respectively ($P<0.05$).

Both groups showed an increase in FVC of 22% in the control group and 27% in the main group from stage 1 to stage 5 of the study ($P<0.05$).

Changes in narcotic analgesic consumption in morphine equivalents are shown in Fig. 2. On day 1 after study initiation, this value was 5.0 mg (IQR, 5–10) in the main group versus 10.0 mg (IQR, 5.0–15.0) in the control group, which was significantly lower by 50% ($P<0.05$). On day 2, it was 5.0 mg (IQR, 0–5.0), also 33% lower than in the control group, where it was 7.5 mg (IQR, 5.0–10.0) ($P<0.05$).

Discussion

The lack of differences in the NPRS at rest and on cough between the groups during stage 1 of the study indicates their comparability. In the subsequent stages of the study, more effective pain relief was achieved with prolonged ESPB used in combination

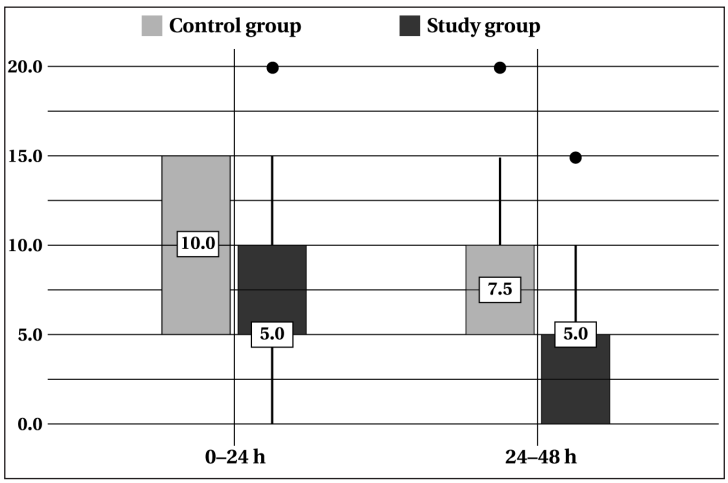

Fig. 2. The use of narcotic analgesics in morphine equivalent on days 1 and 2 after the start of the study.

with the multimodal systemic analgesic therapy. Similar trends in pain severity and respiratory parameters before and after ESPB were found in a study by Adhikari et al. where the NPRS score decreased by 39% in the first 3 hours and inspiratory volume on incentive spirometry increased by a mean of 545 mL (95% CI, 319 to 770 mL) in the first 24 hours after the block [18]. In another study with a smaller number of patients (*N*=10), NPRS at rest and on movement also decreased by 70% and 67%, respectively, within 96 hours [17].

Some authors argue that in fractures of two or less ribs and moderate pain, regional analgesia is not necessary and systemic analgesia alone is sufficient because of the increased risk of various complications associated with regional analgesia [19].

There is no doubt that the individual choice of a specific regional analgesia technique is determined by its efficacy, safety and ease of performance. The risk of complications with epidural analgesia and paravertebral blocks is higher than with fascial blocks. Unstable hemodynamic parameters and prior anticoagulant therapy may limit the use of epidural and paravertebral analgesia, whereas equally effective prolonged ESPB may serve as an alternative [20–22]. No complications of prolonged ESPB were observed in our study.

We used the method of dosed prolonged local anesthetic administration through a catheter connected to a microinfusion pump, the use of which requires staff training, based on literature data suggesting its advantages over fractional or single injection [23–25]. The 1% lidocaine was administered because of a wider therapeutic window compared to bupivacaine or ropivacaine used for fractional or single block, and a lower risk of systemic and cardiac toxicity.

The lack of a pre-specified sample size can be considered a limitation of our study.

Conclusion

Reduced pain perception scores, decreased narcotic analgesic consumption and increased FVC with prolonged erector spinae plane block suggest its efficacy in patients with multiple rib fractures.

References

1. *May L., Hillermann C., Patil S.* Rib fracture management. *BJA Education*. 2016; 16: 26–32. DOI: 1093/bjaceaccp/mkv011
2. *Хаджибаев А.Н., Рахманов Р.О., Султанов П.К., Шарипова В.Х.* Диагностика и хирургическая тактика при неотложных состояниях, обусловленных травмой и заболеваниями органов грудной полости. Общая реаниматология. 2016; 12 (4): 57–67. [*Khadjibaev A.N., Rakhmanov R.O., Sultanov P.K., Sharipova V.K.* Diagnosis and treatment of chest injury and emergency diseases of chest organs. *General Reanimatology/Obshchaya Reanimatologya*. 2016; 12 (4): 57–67. (in Russ.)]. DOI: 10.15360/1813-9779-2016-4-57-67
3. *Chapman B.C., Herbert B., Rodil M., Salotto J., Stovall R.T., Biffl W., Johnson J. et al.* RibScore: a novel radiographic score based on fracture pattern that predicts pneumonia, respiratory failure, and tracheostomy. *J Trauma Acute Care Surg*. 2016; 80 (1): 95–101. DOI: 10.1097/TA.0000000000000867. PMID: 26683395
4. *Witt C.E., Bulger E.M.* Comprehensive approach to the management of the patient with multiple rib fractures: a review and introduction of a bundled rib fracture management protocol. *Trauma Surg Acute Care Open*. 2017; 2 (1): e000064. DOI: 10.1136/tsaco-2016-000064. PMID: 29766081
5. *Galvagno Jr. S.M., Smith C.E., Varon A.J., Hasenboehler E.A., Sultan S., Shaefer G., To K.B. et al.* Pain management for blunt thoracic trauma: a joint practice management guideline from the Eastern Association for the Surgery of Trauma and Trauma Anesthesiology Society. *J Trauma Acute Care Surg*. 2016; 81 (5): 936–951. DOI: 10.1097/TA.0000000000001209. PMID: 27533913
6. *Forero M., Adhikary S.D., Lopez H., Tsui C., Chin K.J.* The erector spinae plane block: a novel analgesic technique in thoracic neuropathic pain. *Reg Anesth Pain Med*. 2016; 41 (5): 621–627. DOI: 10.1097/AAP.0000000000000451. PMID: 27501016
7. *Шарипова В.Х., Фокин И.В., Саттарова Ф.К., Парпибаев Ф.О.* Фасциальная блокада мышцы, выпрямляющей спину, при множественных переломах ребер (клиническое наблюдение). *Общая реаниматология*. 2020; 16 (5): 22–29. [*Sharipova V.Kh., Fokin I.V., Sattarova F.K., Parpibayev F.O.* Erector spinae plane fascial block in multiple rib fractures (case report). *General Reanimatology/Obshchaya Reanimatologya*. 2020; 16 (5): 22–29. (in Russ.)]. DOI: 10.15360/1813-9779-2020-5-22-29
8. *Schwartzmann A., Peng P., Maciel M.A., Forero M.* Mechanism of the erector spinae plane block: insights from a magnetic resonance imaging study. *Can J Anaesth*. 2018; 65 (10): 1165–1166. DOI: 10.1007/s12630-018-1187-y. PMID: 30076575
9. *Cho T.-H., Kim S.H., O J., Kwon H.-J., Kim K.W., Yang H.-M.* Anatomy of the thoracic paravertebral space: 3D micro-CT findings and their clinical implications for nerve blockade. *Reg Anesth Pain Med*. 2021; 46 (8): 699–703. DOI: 10.1136/rapm-2021-102588. PMID: 33990438
10. *Lopez M.B., Cadorniga Á.G., Gonzales J.M.L., Suarez E.D., Carballo C.L., Sobrino F.P.* Erector spinae block. A narrative review. *Central Eur J Clin Res*. 2018; 1 (1): 28–39. DOI: 10.2478/cejcr-2018-0005
11. *Tulgar S., Selvi O., Ozer Z.* Clinical experience of ultrasound guided single and bi-level erector spinae plane block for postoperative analgesia in patients undergoing thoracotomy. *J Clin Anesth*. 2018; 50: 22–23. DOI: 10.1016/j.jclinane.2018.06.034. PMID: 29940470
12. *Chin K.J., Adhikary S., Sarwani N., Forero M.* The analgesic efficacy of pre-operative bilateral erector spinae plane (ESP) blocks in patients having ventral hernia repair. *Anaesthesia* 2017; 72 (4): 452–460. DOI: 10.1111/anae.13814. PMID: 28188621
13. *Chung K., Kim E.D.* Continuous erector spinae plane block at the lower lumbar level in a lower extremity complex regional pain syndrome patient. *J Clin Anesth*. 2018; 48: 30–31. DOI: 10.1016/j.jclinane.2018.04.012. PMID: 29727760
14. *Thiruvenkatarajan V., Hillen C.E., Adhikary S.D.* An update on regional analgesia for rib fractures. *Curr Opin Anaesthesiol*. 2018; 31 (5): 601–607. DOI: 10.1097/ACO.0000000000000637. PMID: 30020155
15. *Hamilton D.L., Manickam B.* Erector spinae plane block for pain relief in rib fractures. *Br J Anaesth*. 2017; 118 (3): 474–475. DOI: 10.1093/bja/aex013. PMID: 28203765
16. *Luftig J., Mantuani D., Herring A.A., Dixon B., Clattenburg E., Nagdev A.* Successful emergency pain control for posterior rib fractures with ultrasound-guided erector spinae plane block. *Am J Emerg Med*. 2018; 36 (8): 1391–1396. DOI: 10.1016/j.ajem.2017.12.060. PMID: 29301653
17. *Syal R., Mohammed S., Kumar R., Jain N., Bhatia P.* Continuous erector spinae plane block for analgesia and better pulmonary functions in patients with multiple rib fractures: a prospective descriptive study. *Braz J Anesthesiol*. 2021: S0104-0014 (21)00361-4. DOI: 10.1016/j.bjane.2021.09.010. PMID: 34624374
18. *Adhikary S.D., Liu W.M., Fuller E., Cruz-Eng H., Chin K.J.* The effect of erector spinae plane block on respiratory and analgesic outcomes in multiple rib fractures: a retrospective cohort study. *Anaesthesia* 2019; 74 (5): 585– 93. DOI: 10.1111/anae.14579. PMID: 30740657
19. *Ho A.M.-H., Karmakar M.K., Critchley L.A.H.* Acute pain management of patients with multiple fractured ribs: a focus on regional techniques. *Curr Opin Crit Care*. 2011; 17 (4): 323–327. DOI: 10.1097/MCC.0b013e328348bf6f. PMID: 21716105
20. *Forero M., Rajarathinam M., Adhikary S., Chin K.J.* Continuous erector spinae plane block for rescue analgesia in thoracotomy after epidural failure: a case report. *A A Case Rep*. 2017; 8 (10): 254–256. DOI: 10.1213/XAA.0000000000000478. PMID: 28252539
21. *Adhikary S.D., Prasad A., Soleimani B., Chin K.J.* Continuous erector spinae plane block as an effective analgesic option in anticoagulated patients after left ventricular assist device implantation: a case series. *J Cardiothorac Vasc Anesth*. 2018; 33 (4): 1063–1067. DOI: 10.1053/j.jvca.2018.04.026. PMID: 29753668
22. *Elawamy A., Morsy M.R., Ahmed M.A.Y.* Comparison of thoracic erector spinae plane block with thoracic paravertebral block for pain management in patients with unilateral multiple fractured ribs. *Pain Physician*. 2022; 25 (6): 483–490. PMID: 36122257
23. *Richman J.M., Liu S.S., Courpas G., Wong R., Rowlingson A.J., McGready J., Cohen S.R. et al.* Does con-

tinuous peripheral nerve block provide superior pain control to opioids? A meta-analysis. *Anesth Analg*. 2006; 102 (1): 248–257. DOI: 10.1213/01.ANE.0000181289. 09675.7D. PMID: 16368838

24. *De La Cuadra-Fontaine J.C., Altermatt F.R.* Continuous erector spinae plane (ESP) block: optimizing the analgesia technique. *J Cardiothorac Vasc Anesth*. 2018; 32 (5): e2–3. DOI: 10.1053/j.jvca.2018. 03.034. PMID: 29706569
25. *Chou R., Gordon D.B., de Leon-Casasola O.A., Rosenberg J.M., Bickler S., Brennan T., Carter T. et al.* Management of postoperative pain: a clinical practice guideline from the American Pain Society, the American Society of Regional Anesthesia and Pain Medicine, and the American Society of Anesthesiologists' Committee on Regional Anesthesia, Executive Committee, and Administrative Council. *J Pain*. 2016; 17 (2): 131–157. DOI: 10.1016/j.jpain.2015.12.008. PMID: 26827847

Received 17.12.2022
Accepted 04.04.2023

https://doi.org/10.15360/1813-9779-2023-3-46-53

Experimental Study of Neuroprotective Properties of Inhaled Argon-Oxygen Mixture in a Photoinduced Ischemic Stroke Model

Ekatherine A. Boeva[1]*, Denis N. Silachev[2], Elmira I. Yakupova[2], Marina A. Milovanova[1], Lydia A. Varnakova[1], Sergey N. Kalabushev[1], Sergey O. Denisov[1], Victoria V. Antonova[1], Ivan A. Ryzhkov[1], Konstantin N. Lapin[1], Alexandra A. Grebenchikova[3]

[1] V. A. Negovsky Research Institute of General Reanimatology, Federal Research and Clinical Center of Intensive Care Medicine and Rehabilitology, 25 Petrovka Str., Bldg. 2, 107031 Moscow, Russia
[2] A.N. Belozersky Research Institute of Physical and Chemical Biology, M. V. Lomonosov Moscow State University, 1 Leninskie gory, Bldg 40, 119992 Moscow, Russia
[3] A.I. Evdokimov Moscow State University of medicine and dentistry, Ministry of Health of Russia 20 Delegatskaya Str., Build 1, 127473 Moscow, Russia

For citation: *Ekatherine A. Boeva, Denis N. Silachev, Elmira I. Yakupova, Marina A. Milovanova, Lydia A. Varnakova, Sergey N. Kalabushev, Sergey O. Denisov, Victoria V. Antonova, Ivan A. Ryzhkov, Konstantin N. Lapin, Alexandra A. Grebenchikova.* Experimental Study of Neuroprotective Properties of Inhaled Argon-Oxygen Mixture in a Photoinduced Ischemic Stroke Model. *Obshchaya Reanimatologiya = General Reanimatology.* 2023; 19 (3): 46–53. https://doi.org/10.15360/1813-9779-2023-3-46-53 [In Russ. and Engl.]

***Correspondence to:** Ekatherine A. Boeva, eboeva@fnkcrr.ru

Summary

Acute ischemic stroke is a serious problem for healthcare systems worldwide. Searching for the optimal neuroprotector is a contemporary challenge. Various studies have demonstrated neuroprotective properties of argon in ischemic brain damage models. However, the published data are inconsistent.

The aim of the study was to evaluate the effect of 24-hour argon-oxygen mixture (Ar 70%/O_2 30%) inhalation on the severity of neurological deficit and the extent of brain damage in rats after a photoinduced ischemic stroke.

Material and methods. The experiments were carried out on male Wistar rats weighing 430–530 g (*N*=26). Focal ischemic stroke was modeled in the sensorimotor cortex of the rat brain using photochemically induced vascular thrombosis. The animals were randomly divided into 3 groups: sham procedure + N_2 70%/O_2 30% inhalation (SP, *N*=6); stroke + N_2 70%/O_2 30% inhalation (Stroke, *N*=10); Stroke + Ar 70%/O_2 30% inhalation (Stroke+iAr, *N*=10). The limb placement test (LPT) was used for neurological assessment during 14 days. Additionally, on day 14 after the stroke, brain MRI with lesion size morphometry was performed. Summarized for days 3,7 and 14 LPT scores were lower in the Stroke and Stroke + iAr groups as compared to the SP group.

Results. Statistically significant differences in LPT scores between SP, Stroke, and Stroke+iAr groups were revealed on day 3 post-stroke: (scores: 14 (13; 14), 6.5 (4; 8), and 5 (3; 8), respectively, *P*=0.027). However, there was no statistical difference between the Stroke and Stroke+iAr groups.

Conclusion. 24-hour inhalation of argon-oxygen mixture (Ar 70%/O_2 30%) after stroke does not reduce the extent of brain damage or the severity of neurological deficit.

Keywords: argon; neuroprotection; photochemically induced ischemic stroke; organoprotection

Conflict of interest. The authors declare no conflict of interest.

Introduction

Stroke is the second leading cause of morbidity and mortality worldwide. The incidence of stroke is increasing due to the prevalence of diabetes mellitus and obesity [1, 2]. The pathophysiology of ischemic brain injury involves the activation of several signaling cascades. Oxygen deprivation leads to the cessation of energy-dependent ion pumps and channels, resulting in the release of neurotransmitters and subsequent neuronal death. Evidence suggests that post-ischemic inflammation is the major cause of a secondary brain damage, which determines the severity of stroke outcome [3]. Therefore, the search for clinically effective neuroprotective agents is relevant. Many therapeutic agents are currently being evaluated in preclinical studies using ischemic injury models [3, 4].

Research with inert (noble) gases is a promising direction in the search for neuroprotective agents. Xenon has been approved for clinical use as a general anesthetic and its neuroprotective properties have been confirmed in numerous *in vitro* and *in vivo* studies [5–13]. Argon may be another promising neuroprotective agent. Over several decades, data on cardio-, neuro-, and nephroprotective properties of argon in various diseases have been obtained in experimental models *in vivo* and *in vitro* [14–20].

A literature review revealed conflicting data on the neuroprotective properties of argon in different models [21–35].

In a study by Grüßer L. (2017), the cytoprotective effect was obtained after argon inhalation for 2 h in a model of traumatic brain injury [36]. In 2021, 2 papers were published evaluating the neuropro-

tective properties of argon in a closed TBI model. In this study, argon inhalation was administered for 24 hours [8, 37]. However, another study [8] showed a significant improvement in neurological status, whereas the study by Creed J. (2021) showed no positive effects [37]. Despite the neuroprotective effect in predominantly ischemic injury, argon did not provide protection after TBI, emphasizing the importance of careful selection of the study model and the time of argon exposure. Studies using models of ischemic injury based on oxygen-glucose deprivation have shown positive results after argon inhalation with different exposure times. Recovery of neurological status and a decrease in the extent of brain injury were observed on histological examination [17–25, 27–50]. Notably, the majority of studies were conducted *in vitro*. Ma S. et al (2019) first performed an *in vivo* study in a model of ischemic injury by middle cerebral artery occlusion with/without reperfusion [48]. The study confirmed the neuroprotective properties of argon, but revealed a discrepancy between the improved neurological outcome and the total area of injury [48]. Given the equivocal results of studies in various models of ischemic injury, photochemically induced thrombosis appears to be one of the most promising experimental models of stroke. Unlike other methods of thrombosis induction, photochemically induced thrombosis can be used in small animals, as this model is characterized by persistent sensorimotor deficits and low postoperative mortality [42].

Thus, based on the literature data, argon may be a promising tool for brain protection against ischemia. However, the lack of consistent results indicates the need for a comprehensive study of this gas as a neuroprotective agent.

The aim of our study was to evaluate the effect of 24 h inhalation of argon-oxygen mixture after photoinduced ischemic stroke on the severity of neurological deficit and the degree of brain injury in rats.

Materials and Methods

Experimental animals. Experiments were performed on male Wistar rats weighing 430–530 g (*N*=26). The animals were deprived of food for 8 h before the experiment, but had free access to water. The study protocol was approved by the Local Ethical Committee of the Federal Research and Clinical Center of Intensive Care Medicine and Rehabilitology, No. 3/22/3 of December 14, 2022. The experiments were performed in accordance with the requirements of Directive 2010/63/EU of the European Parliament and Council of the European Union on the protection of animals used for scientific purposes.

Animals were randomly divided into 3 groups according to the interventions performed:

— sham-operated animals under anesthesia and preparation without stroke + N_2 70%/O_2 30% inhalation (SO group), *N*=6;

— control group with stroke + N_2 70%/O_2 30% inhalation (stroke group), *N*=10;

— experimental group with stroke + Ar 70%/O_2 30% inhalation (stroke+iAr group), *N*=10.

Photoinduced ischemic stroke simulation. Under general anesthesia with sevoflurane 7.0–8.0 ml (2–4 vol%) using the SomnoSuite (Kent Scientific Corporation, USA) low-flow anesthesia system for small laboratory animals with oxygen flow of 1 L/min, ischemic stroke with photochemically induced cortical vascular thrombosis was simulated according to [45]. Photosensitive rose Bengal dye (3%, 40 mg/kg intravenously; Sigma-Aldrich, St. Louis, Missouri, USA) was injected into the jugular vein. The rat head was then fixed in a stereotactic frame (Bregma stereotactic coordinates: 0.5 mm distal and 2.5 mm lateral), and the skull was exposed through a midline incision free of periosteum. The cerebral hemisphere in the area of the sensorimotor cortex was then irradiated with green light at λ=550 nm for 15 min. After skin suture, the rats were placed in a cage under an infrared heating lamp until they recovered from anesthesia. Body temperature was maintained at 37±0.5°C throughout the experiment. The temperature was measured by installing a rectal body temperature sensor, and thermoregulation was maintained in automatic mode by connecting a heating module to a thermoregulator and setting limit values. The sham operation included a paratracheal incision with isolation of the internal jugular vein and exposure of the skull through a midline incision [45].

Argon exposure. Fifteen minutes after the stroke simulation, the animal was placed in a 15 L transparent plastic chamber continuously supplied with a fresh gas mixture (N_2 70%/O_2 30% for SO and stroke groups; Ar 70%/O_2 30% for the stroke+iAr group) at a flow rate of 0.5 L/min per animal. No more than 5 animals of the same group were in the chamber at the same time to avoid hypoxia and hypercapnia.

The exposure time in the chamber was 24 hours. Throughout the experiment, the O_2 and CO_2 levels in the animal chamber were continuously monitored using a closed atmosphere control device (INSOVT, St. Petersburg, Russia). At the end of the exposure period, the general condition of the animal (level of alertness, mobility) was assessed and anesthesia with paracetamol at a dose of 50 mg/kg, subcutaneously, was administered. The animal was then placed in its cage with free access to water and food.

Assessment of neurological status. The neurological status of the animals was assessed one day before the experiment (D0), on day 3 (D3), day 7 (D7), and day 14 (D14) after stroke.

We used a protocol based on the method described by De Rieck et al. (1989) [43] and modified by Yolkkonen J. et al. (2000) [44]. Rats were hand-trained for one week prior to testing. The test consisted of seven tests assessing sensorimotor integration of the forelimbs and hindlimbs in response to tactile, proprioceptive and visual stimulation. Each test was scored as follows: normal performance, 2 points; delayed (>2 s) and/or incomplete performance, 1 point; no performance, 0 points. The scores were summed, and the results were presented as the sum of the test scores.

On day 14 after stroke, animals underwent MRI examination on a 7 Tesla magnetic field induction tomograph with a gradient system of 105 mTl/m (BioSpec 70/30, Bruker, Germany). Anesthesia was performed with isoflurane (1.5–2%), after which the rat was placed in a positioning device with stereotaxis and thermoregulation system as described previously [45].

A standard protocol for rat brain examination was used, including the acquisition of T2-weighted images. A linear transmitter with an internal diameter of 72 mm was used for radiofrequency (RF) signal transmission, and a receiving coil on the rat brain surface was used for RF signal detection. The following pulse sequences (PS) were used: RARE, a spin echo-based PS with the following parameters: TR = 6000 ms, TE = 63.9 ms, 0.8 mm slice thickness in 0.8 mm increments, 256×384 matrix size, 0.164×0.164 mm/pixel resolution. Total scanning time per animal was approximately 25 minutes. The extent of brain injury was assessed by graphical analysis of MRI images with calculation of brain lesion volume. For this purpose, one slide with the largest brain lesion area in a series of MR images was selected. The lesion area in mm^2 was calculated using ImageJ software (National Institutes of Health image software, Bethesda, MD, USA). The brain lesion area was then similarly calculated on four additional slides (two cranial and two caudal). The volume of brain lesions was calculated using the formula: $V = \sum Sn \times d$, where d is the thickness of one section (0.8 mm), $\sum Sn$ is the sum of the lesion areas on five slides (mm^2) [45]. Mortality in the groups of animals was assessed at 24 h, 7 and 14 days after stroke.

Statistical analysis of the data was performed using STATISTICA 7.0 (StatSoft. Inc., USA) and GraphPad Prizm. The distribution of variables was assessed using the Shapiro–Wilk criterion. All data were presented as median and interquartile range. Statistical differences between groups in data with at least one non-normal distribution were analyzed using the Mann–Whitney *U* test with Bonferroni correction for comparison of three or more groups, and the Kruskal–Wallis or Mann–Whitney *U* test for analysis of no more than two groups. The significance level was set at $P<0.05$.

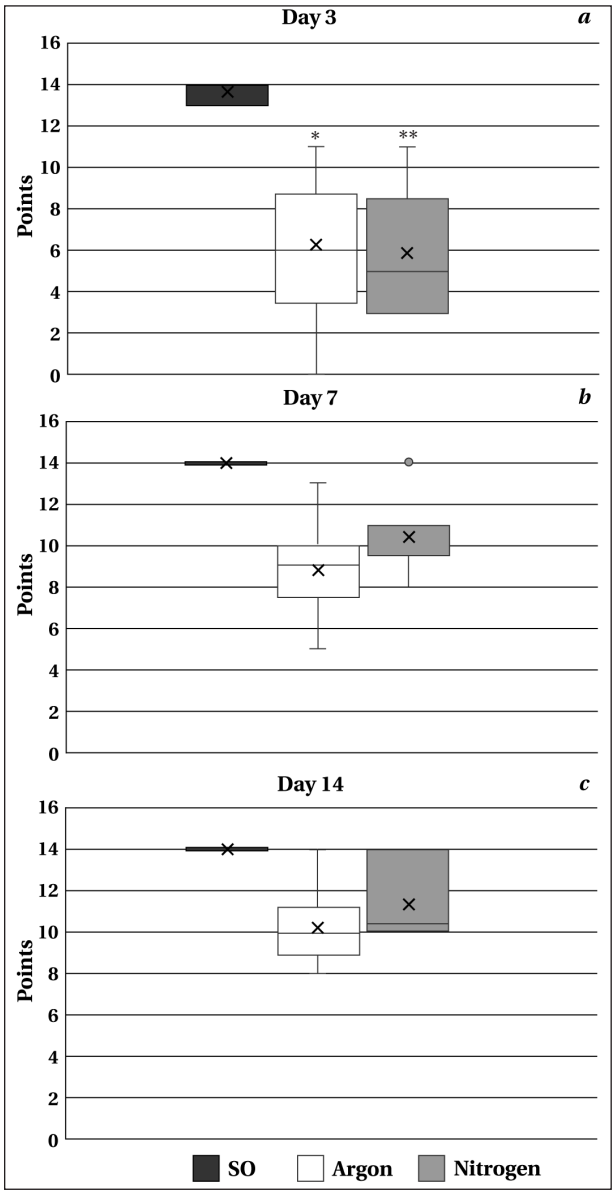

Fig. 1. Results of the limb-placing test (LPT).
Note. *a* — Results on day 3 after simulated stroke; *P*=0.027 between SO and stroke* groups, SO and stroke+iAr** groups. *b* — Results on day 7 after simulated stroke. *c* — Results on day 14 after simulated stroke. Data are presented as median and interquartile range [25%; 75%]. Mann–Whitney *U* test with Bonferroni correction, Kruskel–Wallis test was used to compare three or more groups.

Results

No animals were withdrawn from the study for 14 days and no humane endpoint was reached. There were no lethal outcomes.

Neurological evaluation. The limb-placing test (LPT). At each of the time points (D3, D7, and D14), the sum of LPT scores in animals from both experimental groups was lower than in the SO group. We obtained significant differences between the SO group and the stroke and stroke+iAr groups on day 3 (14 (13; 14), 6.5 (4; 8), 5 (3; 8), respectively, *P*=0.027). The stroke and stroke+iAr groups did

not differ (day 3, *P*=0.57; day 7, *P*=0.70; day 14, *P*=0.71) (Fig. 1).

Over time, the values of this parameter in the SO group of animals did not change from D3 to D14 (Fig. 2, *a*). The changes in LPT scores in the stroke and stroke+iAr groups were almost identical: the lowest values were at time point D1 (5.9 (3; 8) in the stroke group and 6.3 (7; 9.5) in the stroke+iAr group; *P*=0.73). At D7, there was a trend toward increasing the score values in both groups (10.4 (10; 10.8) in the stroke group and 8.8 (8; 10) in the stroke+iAr group, *P*=0.59). At D14, the total LPT score exhibited a trend to be higher in the stroke group (11.4 (10; 14)) (Fig. 2, *b*) and stroke+iAr (10.3 (9; 11)) (Fig. 2, *c*) group compared to both D1 (*P*=0.56 for the stroke group, *P*=0.63 for the stroke+iAr group) and D7 (*P*=0.68 for the stroke group, *P*=0.61 for the stroke+iAr group). However, the differences were not significant.

Brain MRI. The mean lesion volumes in the stroke+iAr group and the stroke group were 9.68 (7.42; 12.2) mm3 and 9.34 (8.74; 12.90) mm^3, respectively. No significant differences were found between the groups (*P*=0.500) (Fig. 3, 4 *a*, *b*, *c*).

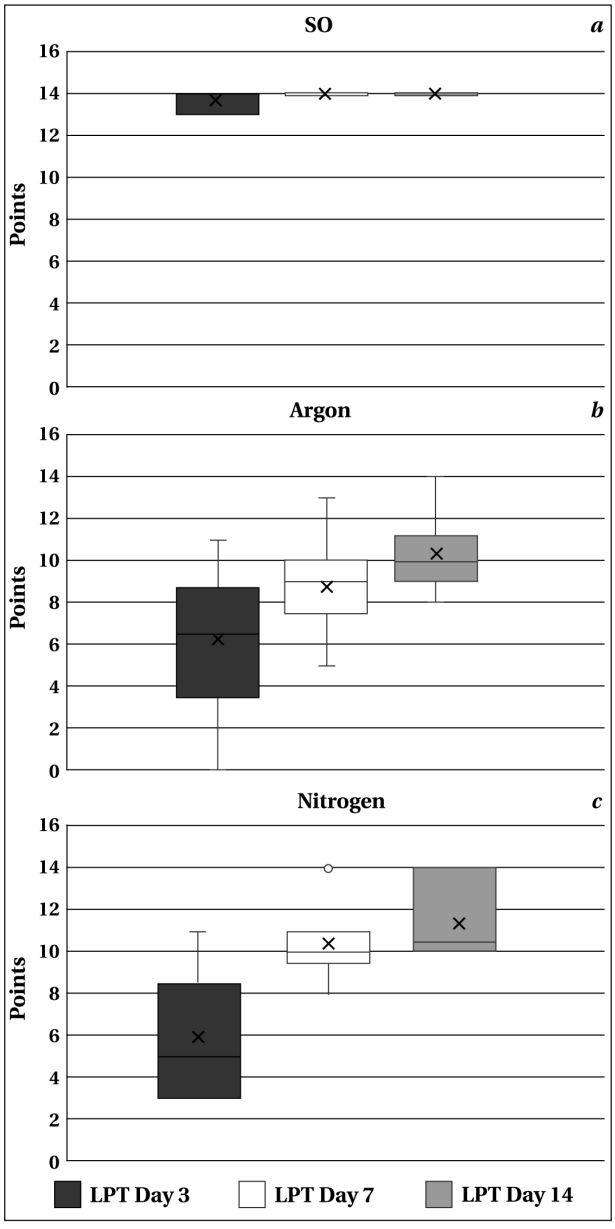

Fig. 2. Limb-placing test.
Note. *a* — changes in LPT results in the SO group; *b* — changes in LPT results in the stroke+iAr group; *c* — changes in LPT results in the stroke group. Data are expressed as median and interquartile range. Mann–Whitney *U* test with Bonferroni correction and Kruskal–Wallis test were used to compare three or more groups.

Discussion

This study was designed to evaluate the neuroprotective effect of argon on important outcome parameters after ischemic stroke. According to the literature, the most pronounced neuroprotective effect of this gas has been demonstrated in models of ischemic neuronal injury *in vitro*. Thus, in an in vitro model of traumatic brain injury [50], 50-percent argon showed a strong neuroprotective profile compared to 6-percent desflurane. Meanwhile, a small number of preclinical studies of the protective effects of argon in vivo have shown conflicting results.

Our study of the neuroprotective effect of 24 h argon inhalation starting from the first hours of photoinduced ischemic stroke in rats showed no significant effect on the severity of neurological deficit during the 2-week postischemic period and on the lesion volume according to MRI data at day 14.

The negative result of the study could be due to several factors.

First, argon, unlike xenon, may not have clinically significant neuroprotective effects in ischemic stroke, which is confirmed by negative results in other in vivo studies [24, 37]. Second, experimental modeling of stroke and other brain injury is almost always performed in anesthetized animals, so it is

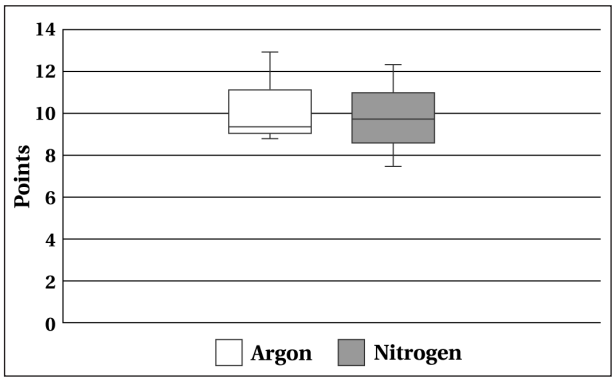

Fig. 3. Extent of brain injury in rats on day 14 of follow-up according to MRI.
Note. The data were presented as medians and quartiles.

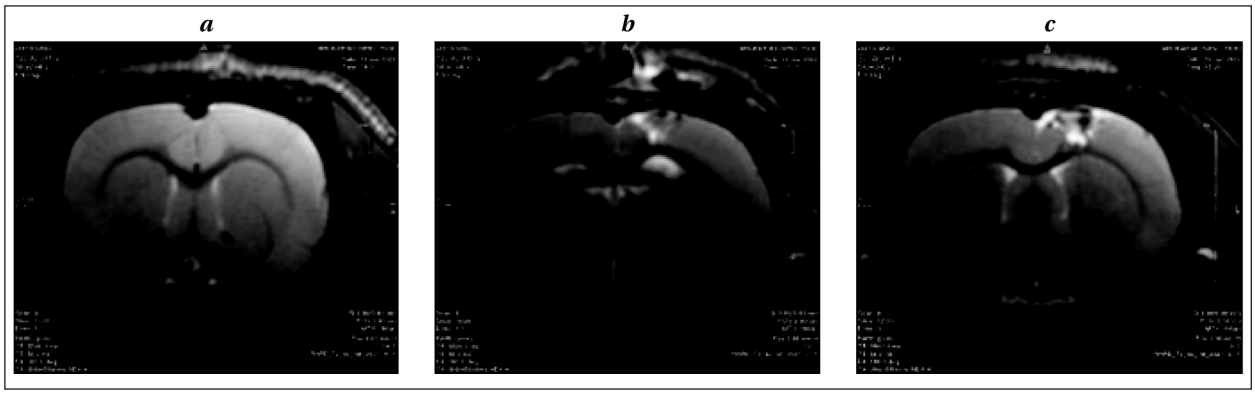

Fig. 4. MRI examination of the rat brain.
Note. *a* — T2-weighted coronal MR image of the animal from the SO group. *b* — T2-weighted coronal MR image of an animal from the stroke group. *c* — T2-weighted coronal MR image of an animal from the stroke+iAr group.

imperative to consider the effects of the anesthetic used. According to the literature, comparative studies of sevoflurane, isoflurane, and argon in the ischemic injury model have not been performed. Both groups of stroke animals had high limb-placing test scores, which may be a manifestation of the neuroprotective effect of sevoflurane. Experimental and clinical studies confirm the strong neuroprotective properties of sevoflurane [51–53]. In this regard, the use of another anesthetic without apparent organoprotective effects (e. g., chloral hydrate [54]) may reveal the neuroprotective effects of argon in a similar experimental model. Another factor that could influence the results of the study is the duration and conditions of exposure. On the one hand, 24 h exposure should have been sufficient to obtain a positive result. However, a number of studies [55, 56] have suggested that argon, due to its specific heat capacity, which is twice lower than that of air, causes moderate hyperthermia, exacerbating ischemic brain injury. In the present study, the temperature of the animals in the postoperative period and the volume of fluid consumed by the animal were not evaluated. In this regard, a long duration of argon inhalation in a closed chamber may have influenced the results obtained. However, the lack of significant differences between the groups suggests that prolonged argon inhalation did not have a deleterious effect.

Considering the data obtained and the review of the literature, we can conclude that further studies with a modified design that takes into account the above-mentioned limitations of this study are needed to evaluate the neuroprotective effect of argon.

Conclusion

Inhalation of an argon-oxygen mixture (Ar 70%/O_2 30%) for 24 hours after photochemically induced stroke does not reduce the extent of brain injury and the severity of neurological deficits.

References

1. *Jurcau A., Simion A.* Neuroinflammation in cerebral ischemia and ischemia/reperfusion injuries: from pathophysiology to therapeutic strategies. *Int J Mol Sci.* 2021; 23 (1): 14. DOI: 10.3390/ijms23010014. PMID: 35008440.
2. *Черпаков Р.А., Гребенчиков О.А.* Влияние концентрации хлорида лития на его нейропротекторные свойства при ишемическом инсульте у крыс. *Общая реаниматология*. 2021; 17 (5): 101–110. [*Cherpakov R.A., Grebenchikov O.A.* Effect of lithium chloride concentration on its neuroprotective properties in ischemic stroke in rats. General Reanimatology /Obshchaya Reanimatologiya. 2021; 17 (5): 101–110. (In Russ.)]. DOI: 10.15360/1813-9779-2021-5-101-110
3. *Paul S., Candelario-Jalil E.* Emerging neuroprotective strategies for the treatment of ischemic stroke: an overview of clinical and preclinical studies. *Exp Neurol.* 2021; 335: 113518. doi: 10.1016/j.expneurol.2020.113518. PMID: 33144066
4. *Rabinstein A.A.* Update on treatment of acute ischemic stroke. *Continuum (Minneap Minn)*. 2020; 26 (2): 268–286. DOI: 10.1212/CON.0000000000000840. PMID: 32224752.
5. *Campos-Pires R., Koziakova M., Yonis A., Pau A., Macdonald W., Harris K., Edge C.J. et al.* Xenon protects against blast-induced traumatic brain injury in an in vitro model. *J Neurotrauma.* 2018; 35 (8): 1037–1044. DOI: 10.1089/neu.2017.5360. PMID: 29285980.
6. *Campos-Pires R., Hirnet T., Valeo F., Ong B.E., Radyushkin K., Aldhoun J., Saville J. et al.* Xenon improves long-term cognitive function, reduces neuronal loss and chronic neuroinflammation, and improves survival after traumatic brain injury in mice. *Br J Anaesth*. 2019; 123 (1): 60–73. DOI: 10.1016/j.bja.2019.02.032. PMID: 31122738
7. *Filev A.D., Silachev D.N., Ryzhkov I.A., Lapin K.N., Babkina A.S., Grebenchikov O.A., Pisarev V.M.* Effect of xenon treatment on gene expression in brain tissue after traumatic brain injury in rats. *Brain Sci.* 2021; 11 (7): 889. DOI: 10.3390/brainsci11070889. PMID: 34356124
8. *Moro F., Fossi F., Magliocca A., Pascente R., Sammali E., Baldini F., Tolomeo D. et al.* Efficacy of acute administration of inhaled argon on traumatic brain injury in mice. *Br J Anaesth.* 2021; 126 (1): 256–264. DOI: 10.1016/j.bja.2020.08.027. PMID: 32977957
9. *Zhang M., Cui Y., Cheng Y., Wang Q., Sun H.* The neuroprotective effect and possible therapeutic application of xenon in neurological diseases. *J Neurosci Res.* 2021; 99 (12): 3274–3283. DOI: 10.1002/ jnr.24958. PMID: 34716615
10. *Maze M., Laitio T.* Neuroprotective properties of xenon. *Mol Neurobiol.* 2020; 57 (1): 118–124. DOI: 10.1007/s12035-019-01761-z. PMID: 31758401
11. *Wang J., Li R., Peng Z., Hu B., Rao X., Li J.* HMGB1 participates in LPS-induced acute lung injury by activating the AIM2 inflammasome in macrophages and inducing polarization of M1 macrophages via TLR2, TLR4, and RAGE/NF-kB signaling pathways. *Int J Mol Med.* 2020; 45 (1): 61–80. DOI: 10.3892/ijmm.2019.4402. PMID: 31746367.
12. *Zewinger S., Reiser J., Jankowski V., Alansary D., Hahm E., Triem S., Klug M. et al.* Apolipoprotein C3 induces inflammation and organ damage by alternative inflammasome activation. *Nat Immunol.* 2020; 21 (1): 30–41. DOI: 10.1038/s41590-019-0548-1. PMID: 31819254
13. *Mitsui Y., Hou L., Huang X., Odegard K.C., Pereira L.M., Yuki K.* Volatile anesthetic sevoflurane attenuates toll-like receptor 1/2 activation. *Anesth Analg.* 2020; 131 (2): 631–639. DOI: 10.1213/ANE. 0000000000004741. PMID: 32149756
14. *Brücken A., Kurnaz P., Bleilevens C., Derwall M., Weis J., Nolte K., Rossaint R. et al.* Dose dependent neuroprotection of the noble gas argon after cardiac arrest in rats is not mediated by K (ATP)-channel opening. *Resuscitation.* 2014; 85 (6): 826–32. DOI: 10.1016/j.resuscitation.2014.02.014. PMID: 24582739.
15. *Lemoine S., Blanchart K., Souplis M., Lemaitre A., Legallois D., Coulbault L., Simard C. et al.* Argon exposure induces postconditioning in myocardial ischemia-reperfusion. *J Cardiovasc Pharmacol Ther.* 2017; 22 (6): 564–573. DOI: 10.1177/107424 8417702891. PMID: 28381122.
16. *Mayer B., Soppert J., Kraemer S., Schemmel S., Beckers C., Bleilevens C., Rossaint R. et al.* Argon induces protective effects in cardiomyocytes during the second window of preconditioning. *Int J Mol Sci.* 2016; 17 (7): 1159. DOI: 10.3390/ijms17071159. PMID: 27447611.
17. *Ulbrich F., Kaufmann K., Roesslein M., Wellner F., Auwärter V., Kempf J., Loop T. et al.* Argon mediates anti-apoptotic signaling and neuroprotection via inhibition of toll-Like receptor 2 and 4. *PLoS One.* 2015; 10 (12): e0143887. DOI: 10.1371/journal.pone. 0143887. PMID: 26624894.
18. *Ulbrich F., Lerach T., Biermann J., Kaufmann K.B., Lagreze W.A., Buerkle H., Loop T. et al.* Argon mediates protection by interleukin-8 suppression via a TLR2/TLR4/STAT3/NF-kB pathway in a model of apoptosis in neuroblastoma cells *in vitro* and following ischemia-reperfusion injury in rat retina *in vivo*. *J Neurochem.* 2016; 138 (6): 859–73. DOI: 10.1111/jnc.13662. PMID: 27167824
19. *Spaggiari S., Kepp O., Rello-Varona S., Chaba K., Adjemian S., Pype J., Galluzzi L. et al.* Antiapoptotic activity of argon and xenon. *Cell Cycle.* 2013; 12 (16): 2636–42. DOI: 10.4161/cc.25650. PMID: 23907115
20. *Fahlenkamp A.V., Rossaint R., Coburn M.* Neuroprotektion durch edelgase: neue entwicklungen und erkenntnisse. [Neuroprotection by noble gases: new developments and insights]. *Anaesthesist.* 2015; 64 (11): 855-858. (in German). DOI: 10.1007/s00101-015-0079-6. PMID: 26329914
21. *Fahlenkamp A.V., Rossaint R., Haase H., Al Kassam H., Ryang Y.M., Beyer C., Coburn M.* The noble gas argon modifies extracellular signal-regulated kinase 1/2 signaling in neurons and glial cells. *Eur J Pharmacol*. 2012; 674 (2-3): 104–111. DOI: 10.1016/j.ejphar.2011. 10.045. PMID: 22094065.
22. *Zhao H., Mitchell S., Ciechanowicz S., Savage S., Wang T., Ji X., Ma D.* Argon protects against hypoxic-ischemic brain injury in neonatal rats through activation of nuclear factor (erythroid-derived 2)-like 2. *Oncotarget.* 2016; 7 (18): 25640–51. DOI: 10.18632/oncotarget.8241. PMID: 27016422

23. *Zhao H., Mitchell S., Koumpa S., Cui Y.T., Lian Q., Hagberg H., Johnson M.R. et al.* Heme oxygenase-1 mediates neuroprotection conferred by argon in combination with hypothermia in neonatal hypoxia-ischemia brain injury. *Anesthesiology.* 2016; 125 (1): 180–92. DOI: 10.1097/ALN.0000000000001128. PMID: 27065095.
24. *Harris K., Armstrong S.P., Campos-Pires R., Kiru L., Franks N.P., Dickinson R.* Neuroprotection against traumatic brain injury by xenon, but not argon, is mediated by inhibition at the N-methyl-D-aspartate receptor glycine site. *Anesthesiology.* 2013; 119 (5): 1137–48. DOI: 10.1097/ALN.0b013e3182a2a265. PMID: 23867231
25. *David H.N., Haelewyn B., Risso J.-J., Abraini J.H.* Modulation by the noble gas argon of the catalytic and thrombolytic efficiency of tissue plasminogen activator. *Naunyn Schmiedebergs Arch Pharmacol* 2013; 386 (1): 91-5. DOI: 10.1007/s00210-012-0809-0. PMID: 23142817
26. *Höllig A., Weinandy A., Liu J., Clusmann H., Rossaint R., Coburn M.* Beneficial properties of argon after experimental subarachnoid hemorrhage: early treatment reduces mortality and influences hippocampal protein expression. *Crit Care Med.* 2016; 44 (7): e520-9. DOI: 10.1097/CCM.0000000000001561. PMID: 26751611
27. *Zhuang L., Yang T., Zhao H., Fidalgo A.R., Vizcaychipi M.P., Sanders R.D., Yu B. et al.* The protective profile of argon, helium, and xenon in a model of neonatal asphyxia in rats. *Crit Care Med.* 2012; 40 (6): 1724–1730. DOI: 10.1097/CCM.0b013e3182452164. PMID: 22610177
28. *Fahlenkamp A.V., Coburn M., de Prada A., Gereitzig N., Beyer C., Haase H., Rossaint R. et al.* Expression analysis following argon treatment in an *in vivo* model of transient middle cerebral artery occlusion in rats. *Med Gas Res.* 2014; 4: 11. DOI: 10.1186/2045-9912-4-11. PMID: 25671080
29. *Ulbrich F., Schallner N., Coburn M., Loop T., Lagrèze W.A., Biermann J., Goebel U.* Argon inhalation attenuates retinal apoptosis after ischemia/reperfusion injury in a time- and dose-dependent manner in rats. *PLoS One*. 2014; 9 (12): e115984. DOI: 10.1371/journal.pone. 0115984. PMID: 25535961
30. *Ulbrich F., Kaufmann K.B., Coburn M., Lagrèze W.A., Roesslein M., Biermann J., Buerkle H. et al.* Neuroprotective effects of argon are mediated via an ERK-1/2 dependent regulation of heme-oxygenase-1 in retinal ganglion cells. *J Neurochem.* 2015; 134 (4): 717–727. DOI: 10.1111/jnc.13115. Epub 2015. PMID: 25876941
31. *Abraini J.H., Kriem B., Balon N., Rostain J.-C., Risso J.J.* Gamma-aminobutyric acid neuropharmacological investigations on narcosis produced by nitrogen, argon, or nitrous oxide. *Anesth Analg.* 2003; 96 (3): 746–749. DOI: 10.1213/01.ANE.0000050282.14291.38. PMID: 12598256
32. *Faure A., Bruzzese L., Steinberg J.-G., Jammes Y., Torrents J., Berdah S.V., Garnier E. et al.* Effectiveness of pure argon for renal transplant preservation in a preclinical pig model of heterotopic autotransplantation. *J Transl Med.* 2016; 14: 40. DOI: 10.1186/s12967-016-0795-y. PMID: 26847569
33. *Liu J., Nolte K., Brook G., Liebenstund L., Weinandy A., Höllig A., Veldeman M. et al.* Post-stroke treatment with argon attenuated brain injury, reduced brain inflammation and enhanced M2 microglia/macrophage polarization: a randomized controlled animal study. *Crit Care.* 2019; 23 (1): 198. DOI: 10.1186/s13054-019-2493-7. PMID: 31159847
34. *De Roux Q., Lidouren F., Kudela A., Slassi L., Kohlhauer M., Boissady E., Chalopin M. et al.* Argon attenuates multiorgan failure in relation with HMGB1 inhibition. *Int J Mol Sci*. 2021; 22 (6): 3257. DOI: 10.3390/ijms22063257. PMID: 33806919
35. *Qi H., Soto-Gonzalez L., Krychtiuk K.A., Ruhittel S., Kaun C., Speidl W.S., Kiss A. et al.* Pretreatment with argon protects human cardiac myocyte-like progenitor cells from oxygen glucose deprivation-induced cell death by activation of AKT and differential regulation of mapkinases. *Shock.* 2018; 49 (5): 556–563. DOI: 10.1097/SHK.00000 00000000998. PMID: 29658909
36. *Grüßer L., Blaumeiser-Debarry R., Krings M., Kremer B., Höllig A., Rossaint R., Coburn M.* Argon attenuates the emergence of secondary injury after traumatic brain injury within a 2-hour incubation period compared to desflurane: an *in vitro* study. *Med Gas Res.* 2017; 7 (2): 93–100. DOI: 10.4103/2045-9912.208512. PMID: 28744361
37. *Creed J., Cantillana-Riquelme V., Yan B.H., Ma S., Chu D., Wang H., Turner D.A. et al.* Argon inhalation for 24 h after closed-head injury does not improve recovery, neuroinflammation, or neurologic outcome in mice. *Neurocrit Care.* 2021; 34 (3): 833–843. DOI: 10.1007/s12028-020-01104-0. PMID: 32959200
38. *David H.N., Dhilly M., Degoulet M., Poisnel G., Meckler C., Vallée N., Blatteau J.É. et al.* Argon blocks the expression of locomotor sensitization to amphetamine through antagonism at the vesicular monoamine transporter-2 and mu-opioid receptor in the nucleus accumbens. *Transl Psychiatry.* 2015; 5 (7): e594. DOI: 10.1038/tp. 2015.27. PMID: 26151922
39. *Zhuang L., Yang T., Zhao H., Fidalgo A.R., Vizcaychipi M.P., Sanders R.D., Yu B. et al.* The protective profile of argon, helium, and xenon in a model of neonatal asphyxia in rats. *Crit Care Med.* 2012; 40 (6): 1724–1730. DOI: 10.1097/CCM.0b013e3182452164. PMID: 22610177
40. *Koziakova M., Harris K., Edge C.J., Franks N.P., White I.L., Dickinson R.* Noble gas neuroprotection: xenon and argon protect against hypoxic-ischaemic injury in rat hippocampus in vitro via distinct mechanisms. *Br J Anaesth*. 2019; 123 (5): 601–609. DOI: 10.1016/j.bja.2019.07.010. PMID: 31470983
41. *Shakova F.M.; Kirova Y.I.; Silachev D.N.; Romanova G.A.; Morozov S.G.* Protective effects of PGC-1α activators on ischemic stroke in a rat model of photochemically induced thrombosis. *Brain Sci.* 2021; 11 (3): 325. DOI: 10.3390/brainsci11030325. PMID: 33806692
42. *De Ryck M., Van Reempts J., Borgers M., Wauquier A., Janssen P.A.* Photochemical stroke model: flunarizine prevents sensorimotor deficits after neocortical infarcts in rats. *Stroke.* 1989; 20 (10): 1383–1390. DOI: 10.1161/01.str.20.10.1383. PMID: 2799870
43. *Jolkkonen J., Puurunen K., Rantakömi S., Härkönen A., Haapalinna A., Sivenius J.* Behavioral effects of

the alpha (2)-adrenoceptor antagonist, atipamezole, after focal cerebral ischemia in rats. *Eur J Pharmacol.* 2000; 400 (2–3): 211–219. DOI: 10.1016/s0014-2999(00)00409-x. PMID: 10988336

44. *Silachev D.N., Uchevatkin A.A., Pirogov Yu.A., Zorov D.B., Isaev N.K.* Comparative evaluation of two methods for studies of experimental focal ischemia: magnetic resonance tomography and triphenyltetrazoleum detection of brain injuries. *Bull Exp Biol Med.* 2009; 147 (2): 269–272. DOI: 10.1007/s10517-009-0489-z. PMID: 19513437
45. *Isaev N.K., Novikova S.V., Stelmashook E.V., Barskov I.V., Silachev D.N., Khaspekov L.G., Skulachev V.P. et al.* Mitochondria-targeted plastoquinone antioxidant SkQR1 decreases trauma-induced neurological deficit in rat. *Biochemistry (Mosc).* 2012; 77 (9): 996–999. DOI: 10.1134/S0006297912090052. PMID: 23157258
46. *Голубев А. М.* Модели ишемического инсульта (обзор). *Общая реаниматология.* 2020; 16 (1): 59–72. [*Golubev A.M.* Models of ischemic stroke (Review). *General Reanimatology/ Obshchaya Reanimatologya.* 2020; 16 (1): 59–72. (in Russ.)]. DOI: 10.15360/1813-9779-2020-1-59-72
47. *Ma S., Chu D., Li L., Creed J.A., Ryang Y.-M., Sheng H., Yang W. et al.* Argon inhalation for 24 hours after onset of permanent focal cerebral ischemia in rats provides neuroprotection and improves neurologic outcome. *Crit Care Med.* 2019; 47 (8): e693–e699. DOI: 10.1097/CCM.0000000000003809. PMID: 31094741
48. *Zhang L., Chopp M., Zhang Y., Xiong Y., Li C., Sadry N., Rhaleb I. et al.* Diabetes mellitus impairs cognitive function in middle-aged rats and neurological recovery in middle-aged rats after stroke. *Stroke.* 2016; 47 (8): 2112–2118. DOI: 10.1161/STROKEAHA.115.012578. PMID: 27387991
49. *Shin S.S., Hwang M., Diaz-Arrastia R., Kilbaugh T.J.* Inhalational gases for neuroprotection in traumatic brain injury. *J Neurotrauma.* 2021; 38 (19): 2634–2651. DOI: 10.1089/neu.2021.0053. PMID: 33940933
50. *Заржецкий Ю.В., Борисов К.Ю., Гребенчиков О.А., Шайбакова В.Л., Левиков Д.И., Лихванцев В.В.* Влияние севофлурана на функциональное восстановление животных, перенесших системную остановку кровообращения. *Общая реаниматология.* 2012; 8 (2): 15. [*Zarzhetsky Yu.V., Borisov K.Yu., Grebenchikov O.A., Shaibakova V.L., Levikov D.I., Likhvantsev V.V.* Effect of sevoflurane on functional recovery in animals sustaining systemic circulatory arrest. *General Reanimatology/ Obshchaya Reanimatologya.* 2012; 8 (2): 15. (In Russ.)]. DOI: 10.15360/1813-9779-2012-2-15
51. *Гребенчиков О.А., Аврущенко М.Ш., Борисов К.Ю., Ильин Ю.В., Лихванцев В.В.* Нейропротекторные эффекты севофлурана на модели тотальной ишемии-реперфузии. *Клиническая Патофизиология.* 2014; 2; 57–65. [*Grebenshchikov O.A., Avrushchenko M.Sh., Borisov K.Yu., Ilyin Yu.V., Likhvantsev V.V.* Neuroprotective effects of sevoflurane on the model of total ischemia-reperfusion. *Clinical Pathophysiology/ Klinicheskaya Patofysiologiya.* 2014; 2; 57–65. (in Russ.)]. eLIBRARY ID: 26292775
52. *Likhvantsev V.V., Landoni G., Levikov D.I., Grebenchikov O.A., Skripkin Y.V., Cherpakov R. A.* Sevoflurane versus total intravenous anesthesia for isolated coronary artery bypass surgery with cardiopulmonary bypass: a randomized trial. *J Cardiothorac Vasc Anesth.* 2016; 30 (5): 1221–1227. DOI: 10.1053/j.jvca.2016.02.030. PMID: 27431595
53. *Silachev D.N., Usatikova E.A., Pevzner I.B., Zorova L.D., Babenko V.A., Gulyaev M.V., Pirogov Y.A. et al.* Effect of anesthetics on efficiency of remote ischemic preconditioning. *Biochemistry (Mosc).* 2017; 82 (9): 1006–1016. DOI: 10.1134/S0006297917090036. PMID: 28988529.
54. *Боева Е.А., Гребенчиков О.А.* Органопротективные свойств аргона (обзор). *Общая реаниматология.* 2022; 18 (5): 44–59. [*Boeva E.A., Grebenchikov O.A.* Organoprotective Properties of Argon (Review). *General Reanimatology/ Obshchaya Reanimatologya.* 2022; 18 (5): 44–59. (in Russ.)]. DOI: 10.15360/1813-9779-2022-5-44-59.
55. *David H.N., Haelewyn B., Degoulet M., Colomb D.G. Jr, Risso J.J., Abraini J.H. Ex vivo* and *in vivo* neuroprotection induced by argon when given after an excitotoxic or ischemic insult. *PLoS One.* 2012; 7 (2): e30934. DOI: 10.1371/journal.pone.0030934. PMID: 22383981

Received 25.01.2023
Accepted 01.06.2023

https://doi.org/10.15360/1813-9779-2023-3-54-65

Photochemicallly Induced Thrombosis as a Model of Ischemic Stroke

Irina V. Ostrova*, Anastasia S. Babkina, Maxim A. Lyubomudrov, Andrey V. Grechko, Arkady M. Golubev

Federal Research and Clinical Center of Intensive Care Medicine and Rehabilitology, 25 Petrovka Str., Bldg. 2, 107031 Moscow, Russia

For citation: *Irina V. Ostrova, Anastasia S. Babkina, Maxim A. Lyubomudrov, Andrey V. Grechko, Arkady M. Golubev.* Photochemicallly Induced Thrombosis as a Model of Ischemic Stroke. *Obshchaya Reanimatologiya = General Reanimatology.* 2023; 19 (3): 54–65. https://doi.org/10.15360/1813-9779-2023-3-54-65 [In Russ. and Engl.]

***Correspondence to:** Irina V. Ostrova, irinaostrova@mail.ru

Summary

Better understanding of ischemic brain injury mechanisms is important for the development and improvement of diagnostic and therapeutic modalities for management of ischemic stroke. As experimental studies are on demand, there's a need for relevant models of focal brain lesions. Photochemically induced thrombosis remains one of the most popular models of ischemic stroke.

The purpose of the review is to consider the pathogenesis and applicational relevance of the photochemical thrombosis in ischemic stroke modeling.

Material and methods. The information was searched using PubMed and Google Scholar databases and keywords «photothrombotic stroke» without language restrictions. 74 papers out of more than 600 sources were found the most relevant for the purpose of this review and selected for the analysis. Of these, more than 50% have been published in the last five years. The criterion for excluding a source was an inconsistency with the objectives of the review and low information content.

Results. We outlined a variety of features in modeling photothrombotic stroke, analyzed the advantages and disadvantages of the model, presented data on current method's modifications, as well as approaches to evaluation of brain lesions in ischemic stroke induced by photothrombosis, and summarized information about the mechanisms of brain damage induced in this model.

Conclusion. Several advantages of the photothrombotic stroke model, such as low invasiveness, high reproducibility, inherent control of brain infarction volume and low mortality, determine its active use in experimental studies of ischemic stroke. Pathological processes in the brain modeled by photochemical thrombosis are similar to the processes occurring in acute ischemic cerebral circulation events. Therefore, this model provides insights into cellular and molecular mechanisms of ischemic brain damage, and can be used for developing novel therapeutic approaches for management of ischemic stroke.

Keywords: focal ischemia; photothrombosis; photothrombotic stroke; mechanisms; brain damage

Conflict of interest. The authors declare no conflict of interest.

Introduction

Stroke is a leading cause of death and disability worldwide [1]. Despite an enormous number of studies, the therapeutic options for stroke patients remain very limited. This prompts further research into the intricate pathophysiological mechanisms of stroke development in order to develop new effective ways to prevent and treat stroke.

The pathogenesis of acute ischemic stroke is best mimicked by models of focal brain lesions, most commonly caused by occlusion of the middle cerebral artery (MCA) [2]. Arterial occlusion is usually achieved by the use of small-diameter synthetic filaments, blood clots, or prothrombotic drugs [3]. One such experimental model is the photochemical thrombosis model. This model allows the simulation of the events triggered by the occlusion of cerebral arteries in human stroke as closely as possible to natural conditions [4].

Most studies simulate neocortical stroke by photothrombotic occlusion of microvessels. Although this method induces a thrombotic stroke, it does not have a direct clinical analogy because it mainly involves occlusion of small cortical vessels (less than 40 μm) rather than a large artery or its branches [3, 5]. Nevertheless, it is a relatively simple, noninvasive way to induce a local infarct in any preselected region of the neocortex in the rat or mouse, and is therefore actively used in experiments on modeling, diagnosis, and therapy of ischemic stroke [6].

The aim of this review is to consider the pathogenesis and practical significance of photochemical thrombosis in ischemic stroke modeling.

Materials and Methods

Information was searched in PubMed and Google Scholar databases using the keywords «photothrombotic stroke» without language restrictions. From more than 600 sources for analysis, 74 were selected as most relevant to the objective of the review. Of these, more than 50% were published within the last five years. Criteria for the exclusion

of sources were their inappropriateness to the aim of the review and their low informative value.

Modeling photothrombotic stroke (PTS). To induce photothrombosis, a solution of a photosensitive dye (most commonly rose Bengal dye) is injected into the circulatory system (intravenously in rats or intraperitoneally in mice) [7]. It does not penetrate cells and remains in the cerebral vasculature. The animal's head is fixed in a stereotactic unit, a longitudinal skin incision is made, and the periosteum is removed. In rats, it may be necessary to perform a craniotomy at the desired site using a special drill [8, 9]. The skull is irradiated with light from a laser placed at a certain distance with a wavelength of 520–560 nm for 10–30 min, after which the surgical wound is sutured. The photosensitizer, when exposed to intense light, produces reactive oxygen species that damage the membranes of vascular endothelial cells, causing platelet adhesion and aggregation and ultimately thrombus formation in the irradiated area (Fig. 1).

Stroke localization is determined by the site of laser irradiation, whereas its severity is related to the dosage of photosensitizer and light [10, 12].

Advantages and limitations of the photothrombosis model. The pathophysiology of the PTS model is based on thrombosis due to disruption of endothelial integrity with rapidly progressing ischemic infarction and cell death in a relatively small cortical volume. In contrast, other stroke models require more invasive surgical techniques, such as middle cerebral artery (MCA) occlusion. In this case, the cortex and subcortical regions are damaged simultaneously, and the area of ischemic penumbra is well defined [5]. The PTS is a well-established model for the study of focal ischemic brain lesions [12]. The pathological processes in the brain simulated by photochemical thrombosis are similar to those occurring in acute cerebrovascular accidents of ischemic type (atherothrombotic or cardioembolic stroke). This model is characterized by high reproducibility, the ability to control cerebral infarct size, and low mortality [10, 13–15]. It has been shown that the infarct volume depends on the intensity of the laser radiation [12, 16], as well as on the duration of light exposure: increasing the exposure time from 15 to 20 minutes leads to an increase in infarct volume without worsening functional deficits [17]. The PTS model allows the study of the changes in sensorimotor pathways without the influence of subcortical areas [18]. The use of this model makes it possible to obtain statistically reliable quantitative data on the degree of brain damage and changes in pathophysiology and regeneration, as well as to assess the neuroprotective effect of pharmacological drugs [13].

Thus, the advantages of this model include minimal invasiveness, good reproducibility of cortical

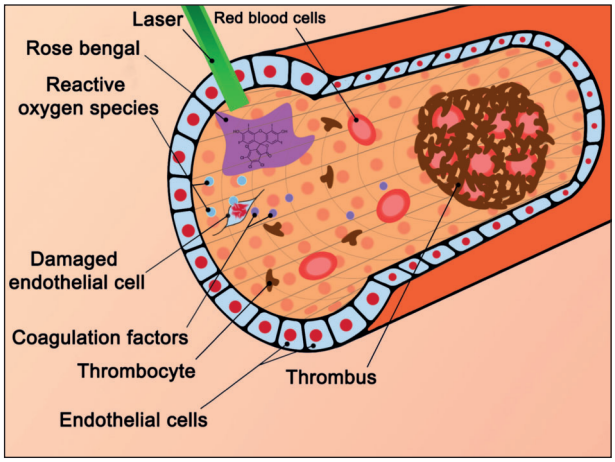

Fig. 1. Schematic illustration of the mechanism of blood vessel occlusion in photo-induced thrombosis.

stroke in both rats and mice, low animal mortality, ability to select the area of exposure, accuracy of localization of ischemic site, and potential control of the size and depth of ischemic damage [15, 19, 20].

The limitations of the model include its permanent occlusive nature, which does not allow using this model to study the mechanisms of ischemia-reperfusion cell damage, as well as reperfusion therapy [10]. Another problem is that photothrombosis causes both vascular and cytotoxic edema equally, whereas human ischemic stroke causes mainly cytotoxic edema, which does not immediately result in blood-brain barrier disruption, a major limitation that hinders extrapolation of data obtained with this model [5, 10, 21]. The rapid and intense development of tissue edema and necrosis results in a relatively small penumbra zone. This is one of the limitations of the photothrombotic model that should be considered when evaluating reperfusion efficacy [5, 22]. The ischemic penumbra was first defined by Astrup and colleagues [23] based on electrophysiological findings as the area where the reduction in cerebral blood flow causes electrical dysfunction but not membrane insufficiency. The penumbra is a spatially dynamic region of the brain with limited viability, characterized by sophisticated pathophysiological changes affecting neuronal and glial functions [24]. Today, the penumbra is defined more broadly as an area of ischemic tissue that is functionally damaged and at risk of infarction, but potentially viable [20].

Another drawback of the photothrombosis model is that experimental animals usually do not have neurological deficits or have deficits that are difficult to diagnose [18].

To address these and other problems, modifications of the PTS model and new modern methods of lesion diagnosis are being developed. In early versions of the model, photothrombosis caused a

severe stroke with a rapidly growing ischemic zone and no penumbra zone, but later modifications of the model using different laser parameters made it possible to obtain a wider penumbra zone [11]. For example, a less intense but longer photodynamic exposure of the rat cerebral cortex (diode laser; 532 nm, 60 mW/cm^2, 30 min) resulted in a 1.5–2 mm wide penumbra around a 3 mm diameter infarct core, which was confirmed by histological and ultrastructural examination [11]. Tuor et al. (2016) showed that irradiation of the rat cerebral cortex with light at 555 nm and an intensity of approximately 40 mW/cm^2 for 5 min after administration of 10 mg/kg rose bengal induced a small infarct with moderate to diffuse penumbra [25]. Clark et al. (2019) proposed a modification of the photothrombosis model in mice using a digital micromirror device [20]. Occlusion of multiple branches of the MCA was performed on the surface of the motor cortex, while limiting collateral cerebral blood flow and blocking the branches of the anterior cerebral artery. This technique made it possible to expand the penumbra zone and delay spontaneous reperfusion of the target arteries, similar to what happens in humans. This was different from the traditional photothrombotic model, which usually results in permanent arterial occlusion and relatively limited collateral blood flow. In this context, the proposed modification may serve as a potential model of cerebral ischemia-reperfusion [20].

The resistance of the PTS model to fibrinolytic therapy is thought to be related to the formation of a platelet-rich but fibrin-poor clot as a result of the photochemical reaction. Recently, a model of murine photothrombosis was proposed in which a combination of rose bengal dye (50 mg/kg) and a subthrombotic dose of thrombin (80 U/kg) was used to induce thrombosis in the proximal branch of the MCA and produce a fibrin-rich and tPA-sensitive clot. Meanwhile, infarct size and localization were constant, and intravenous injection of tPA (Alteplase, 10 mg/kg) for 2 h after photoactivation significantly reduced infarct size. Thus, the thrombin-enhanced PTS model may be useful for testing thrombolytic therapies [26].

Kim et al. (2021) developed a system of photochemical induction of thrombosis that can reproduce the damage of a specific brain region in the rabbit. The main advantage of this system is the ability to locally induce ischemic stroke in the brain region responsible for specific functions [27]. This model has shown that the volume of damage increases 24–48 hours after induction of photothrombosis and tends to decrease 72 hours after induction.

Qian et al. (2016) developed a modification of the murine PTS model in which both the cortex and basal ganglia were damaged [9]. The model is based on occlusion of the proximal MCA using a convenient laser system with an optical fiber. Other advantages of this technique include high reproducibility of results, significant penumbra, and low animal mortality. In another study, optical fibers stereotactically implanted into the surgically isolated proximal MCA were used to create infarcts in subcortical regions of the brain in rats [28]. In this model, magnetic resonance imaging (MRI) demonstrated signs of penumbra as well as the feasibility of thrombolysis with tissue plasminogen activator rt-PA [28].

More recently, Hosseinic et al. (2018) proposed a method to induce selective unilateral hippocampal ischemia in rats using a modified photothrombotic model [29]. Twenty-four hours after exposure, histological examination of the hippocampus revealed shrunken nuclei and pyknotic neurons in the ischemic zone. The average infarct volume was 6.5%, and its size did not differ significantly between experimental animals.

A disadvantage of the photothrombosis model is that a procedure of skull thinning with a special drill is used to gain access to the cortical vessels of the rat. This procedure may cause changes in intracranial pressure and may also result in bleeding during surgery or inflammation postoperatively. The use of optical tissue imaging techniques can help to avoid these problems [12]. One such technique is optical tissue clearing. Optical clearing refers to the temporary reduction of light scattering in biological tissues, and is one of the simplest and most effective methods for increasing the depth and quality of images of deep tissue structures, as well as improving the accuracy of spectroscopic information from deep layers of tissue and blood. Optical immersion clearing is based on the impregnation (immersion) of tissue with a biocompatible chemical agent (an optical clearing agent) that has a sufficiently high refractive index so that it can match the refractive indices of the scatterers and their surroundings by penetrating into the tissue fluid. In particular, glycerol, propylene glycol, ethanol, thiazone, etc. are used as tissue permeability enhancers for optical clearing of skull bone [30].

Recently, a technique of optical skull clearing in mice without craniotomy has been proposed, in which an «optical window» is created through which a light beam can pass [31]. Based on this technique, a controlled model of ischemic stroke was created by combining an in vivo optical skull clearing technique with a photothrombosis procedure. In this case, the degree of thrombotic occlusion and infarction severity can be effectively controlled by changing the light dose. The optical window can also be used for continuous blood analysis and flow mapping. This model represents a valuable asset for ischemic stroke studies [12].

Methods of Brain Research in Stroke Modeling with Photothrombosis

Imaging techniques to determine the size and volume of the lesion. Various MRI techniques are currently used to determine the volume of ischemic injury and to identify the penumbra area in both clinical and experimental settings [9, 21, 27, 32, 33]. The volume of the lesion is most commonly determined using T2-weighted MRI images [9, 18]. It is an effective non-invasive method to assess infarct size during the first 2 weeks after the onset of ischemia. Whole-brain volumetric microscopy techniques, such as serial two-photon tomography (STPT), can provide detailed information about damage and regeneration in the brain after stroke [34]. Automated mapping, connectivity, and histologic analysis using atlases are also used to compare the size and location of the lesion area [35, 36]. In contrast to other stroke models, in PTS the vasogenic edema, which corresponds to a strong hyperintense signal on T2WI, resolves within the first 2 weeks after stroke and transforms into a hypointense cavity [37].

Remodeling of the vessels surrounding the infarcted area of the brain is known to occur after stroke. A method was developed to monitor changes in vascular structure and blood flow with high spatiotemporal accuracy after photothrombotic infarction in the murine motor cortex using longitudinal two-photon and multi-exposure speckle imaging. Vascular remodeling in the peri-infarct cortex developed during the first 2 weeks after stroke, with old vessels being replaced by new ones and selectively stabilized. This vascular structural plasticity coincided with temporal activation of transcriptional programs relevant to vascular remodeling, restoration of peri-infarct blood flow, and significant improvements in motor activity. The results confirmed that vascular remodeling contributes to behavioral recovery after stroke by restoring blood flow to the peri-infarct cortex [39].

Electrophysiological methods to detect ischemic damage. Other methods for quantitative assessment of structural brain damage in the rat PTS model are being developed, particularly based on electroencephalography (EEG). Spectral analysis revealed a significant correlation of the relative power of alpha, theta, delta, delta/alpha ratio, (delta + theta) / (alpha + beta) ratio with stroke size. Analysis of auditory evoked potentials revealed a significant relationship of amplitude and latency with stroke size. These results demonstrate the usefulness of EEG in monitoring brain damage after stroke [16].

Histochemical and immunohistochemical techniques to assess brain damage in photothrombotic stroke.

Serial brain sections stained with triphenyltetrazolium chloride (TTC) solution are also used to determine the volume of damage [7–9, 27, 39].

To analyze and confirm brain damage at the cellular level, classical histological methods, such as morphometry of fixed brain sections stained with toluidine blue or Nissl cresyl violet or hematoxylin and eosin, are used [8, 26, 40–42]. A correlation has been demonstrated between the volume of the lesion detected by MRI and by histological methods [9, 18, 27].

For more detailed analysis, immunohistochemical staining techniques can be used to identify neurons and glial cells and their death or proliferation.

For example, NeuN protein is a marker of mature neurons and is used to visualize and analyze the infarct zone and assess neuronal death [7, 17, 40, 42]. Markers such as c-fos and heart shock protein 90 are used to detect the penumbra zone [9]. The astroglial marker, glial fibrillary acidic protein (GFAP), reveals the interface between ischemic and intact areas and is used to visualize activated astrocytes surrounding the stroke core as a glial scar [18, 37, 41].

Impairment of blood-brain barrier (BBB) permeability is assessed using histochemical dyes, particularly Evans Blue [17, 40]. It is known that dyes bound to serum albumin can cross the BBB after ischemia. Evans Blue dye is commonly used to assess BBB damage due to its rapid binding to serum albumin. Indocyanine green (ICG), a clinically available dye that binds to serum proteins, can also be used. More recently, a new dye, the zwitterionic NIR fluorophore (ZW800-1), has been proposed. Its advantage is that it does not bind to serum, has an extremely low nonspecific tissue uptake and is rapidly eliminated from the body by renal filtration, while allowing successful visualization of ischemic lesions in brain tissue, as demonstrated in the PTS model [43].

The response of microglia in PTS-induced brain injury can be assessed by immunohistochemical staining. In particular, antibodies against CD68 and Iba1, which are markers of macrophages and microglial cells, are used to assess the activation of microglia, which are resident macrophages of the brain [7, 17, 41, 44, 45].

Molecular methods of investigation. After ischemic stroke, cellular damage extends from the infarct site to the surrounding tissue (penumbra). To identify the proteins involved in the mechanisms of neuronal alteration and neuroprotection in the penumbra, changes in protein expression are studied using antibody microarrays [46], NanoString technologies [44], etc. For example, changes in the expression of more than 200 neuronal proteins in the penumbra 4 or 24 hours after focal photothrombotic infarction were studied using antibody microarrays. The largest changes

were detected 4 hours after injury [46] and were recorded in proteins of signal transduction pathways, proteins responsible for axonal growth and direction, vesicular transport, neurotransmitter biosynthesis, intercellular interactions, cytoskeletal proteins, and others. These proteins are known to be involved in both neuronal injury and neuroprotection.

Choi et al. (2019) examined changes in the expression of specific genes during the period from the acute to the chronic phase (up to 8 weeks) of stroke in a rat photothrombosis model. One week after stroke, there was a significant decrease in the expression of genes for neurotransmitter synaptic and signaling pathways, as well as genes for neurotrophic factors, while an activation of apoptosis-associated molecules was observed. In the first 4 and 8 weeks after stroke, proliferation of cellular adhesion and inflammatory cells increased [47].

A study of protein expression 3 days after photothrombotic MCA occlusion in mice using NanoString technologies revealed distinct regulatory proteomic profiles in the damaged hemisphere according to regions of interest, including the ischemic core, peri-infarct tissue, and peri-infarct normal tissue. The core border profile showed apoptosis, autophagy, neuronal death and immunoreactivity for early degenerative proteins. Specifically, the core border showed decreased neuronal proteins Map2 and NeuN; increased autophagy proteins BAG3 and CTSD; increased microglial and peripheral immune invasion proteins Iba1, CD45, CD11b, and CD39; and increased neurodegenerative proteins BACE1, APP, amyloid β 1-42, ApoE, and tau protein S-199. Increased apoptotic and altered proteomic profiles with increases in BAG3, GFAP, and hyperphosphorylated tau protein S-199 were detected in the peri-infarct area [44].

X-ray fluorescence analysis allows the identification of metabolically distinct areas of neuronal tissue, such as the infarct core and the intermediate area surrounding the infarct core, the so-called metabolic penumbra in the early period or the peri-infarct zone in the later post-stroke period. Studies have shown that as early as 1 hour after PTS in mice, the levels of phosphorus, sulfur, and potassium were significantly reduced in the infarct focus, with the level of potassium remaining below normal for 1 month after injury. At the same time, the concentration of chlorine and calcium increases and exceeds the physiological parameters throughout the period studied. Elemental concentrations in the penumbra or peri-infarct zone appear to be intermediate between those in the infarct core and in normal tissue. Responding glial cells alter the average elemental composition of the stroke focus, so that elemental levels 1 week after stroke and beyond are a combination of elemental levels in these cells and in the surrounding tissue. The results of the study showed that the therapeutic window for survival of a significant portion of the penumbra is within the first 24 hours, after which the penumbra expands to include previously unaffected tissue. The change in K^+ and Ca^{2+} levels is an early sign of significant neuronal tissue dysfunction and irreversible damage. It has been found that the total area of tissue affected in the acute phase (including infarct core and penumbra) reaches its maximum by the 2nd day after stroke. The method of tissue metabolic analysis is useful for monitoring stroke severity in the presence of stroke risk factors, as well as for quantifying the efficacy of stroke treatment in animal models [48].

Morphologic Changes in the Brain after PTS

Early morphological changes. Morphological studies of rat cerebral cortex showed that 4 h after PTS, neurons, glial cells, and capillaries in the infarct core were damaged, the neuropil was altered, and significant intracellular and vasogenic edema developed with cyst formation [11, 49]. In mice, one hour after proximal MCA photothrombosis (532 nm, 35 mW, 2 min), karyolysis and pyknosis were observed in the injury zone [9]. In rats with photothrombosis of sensorimotor cortical vessels caused by prolonged laser irradiation (532 nm, 64 mW/cm^2, 30 min), initial necrotic changes within the stroke core were observed, such as an increased proportion of hyperchromic neurons and the appearance of pyknotic neurons at 1 hour. At 24 hours, morphologic changes intensified. Typical ischemic changes such as massive vacuolization of neuropil, edema, and degeneration of neurons, glia, and blood vessels were observed. Microscopically, edema and destruction of mitochondria, endoplasmic reticulum and dictyosomes of the Golgi apparatus, degradation of synapses, disorganization of myelin, swelling of neurons and glial cells, edema and destruction of capillary components were evident. The morphological changes in the penumbra region were similar to those in the necrotic core, but gradually decreased toward the penumbra border [11].

While necrosis is the underlying mechanism of cell damage in the stroke core, apoptosis plays a more important role in the penumbra [11]. In the areas of the penumbra adjacent to the infarct zone, the highest percentage of apoptotic cells was observed 24 hours after PTS, and necrotic cells predominated 48 hours later [50]. Repair of damaged brain tissue begins at 72 hours and ends approximately 28 days after PTS [51].

The decrease in neuronal density at the infarct border is accompanied by an early response of glial cells. Generalized microglial activation in the ipsilateral cortex can be detected as early as 3 hours after occlusion. Astrocyte activation is observed in intact parts of the ischemic hemisphere 6 hours after occlusion [24].

Activation of microglial cells is associated with changes in their morphology and number. Signs of microglial activation include an increase in cell number and soma area, a decrease in cell area and diameter, a reduction in primary processes and their length, and an increase in cell density [41]. Thus, the immunohistochemistry studies in a rat photothrombosis model revealed an increase in the circularity index of Iba1+ cells. This index peaked at 24 hours in peri-infarct tissue and remained elevated for 3 days [42]. The proportion of Iba1-positive material in the peri-infarct zone increased significantly by day 3 and remained elevated until day 7, mainly due to an increase in the number of microglial cells [37, 42]. In a study of the PTS model in mice, microglial activation persisted up to 84 days after stroke [41].

Secondary damage. Local brain damage causes distant structural and functional abnormalities that contribute to behavioral deficits and impair functional recovery of the brain. Secondary brain cell damage is one of the major mechanisms that initiates additional selective cell death in non-ischemic brain regions with synaptic connections to the site of primary damage and correlates with functional deficit and outcome [52–54]. Thus, a murine model of photothrombosis showed secondary neurodegeneration in ipsilateral brain regions, particularly in the sensorimotor area of the thalamus [187, 54].

Focal ischemic cortical lesions can also cause distant white matter damage, but this is limited to fibers associated with the area of the primary lesion. Thus, in a model of focal unilateral PTS of the rat sensorimotor cortex, severe axonal changes were observed in the ipsilateral external capsule as well as in remote regions, including the contralateral external capsule and the corpus callosum. Further analysis of fiber tractography showed that only fibers with direct axonal connections to the primary lesion area were significantly damaged. These fibers mostly represented perilesional, interhemispheric and subcortical axonal connections. The size of the primary lesion was found to be a determinant of motor deficit [32].

In mice with photothrombotic cortical stroke, damage to hippocampal CA1 field neurons was also observed 28 days after exposure compared to sham-operated animals [40].

In addition, secondary death of midbrain dopaminergic neurons has been reported in a rat primary motor cortex model of PTS [55]. Secondary dopaminergic degeneration after stroke is associated with adverse outcomes such as a post-stroke depression or parkinsonism [45].

Mechanisms of Photothrombotic Brain Injury

The neural tissue damage in the PTS core is similar to that in other stroke models and in human stroke. However, there are some differences (Fig. 2).

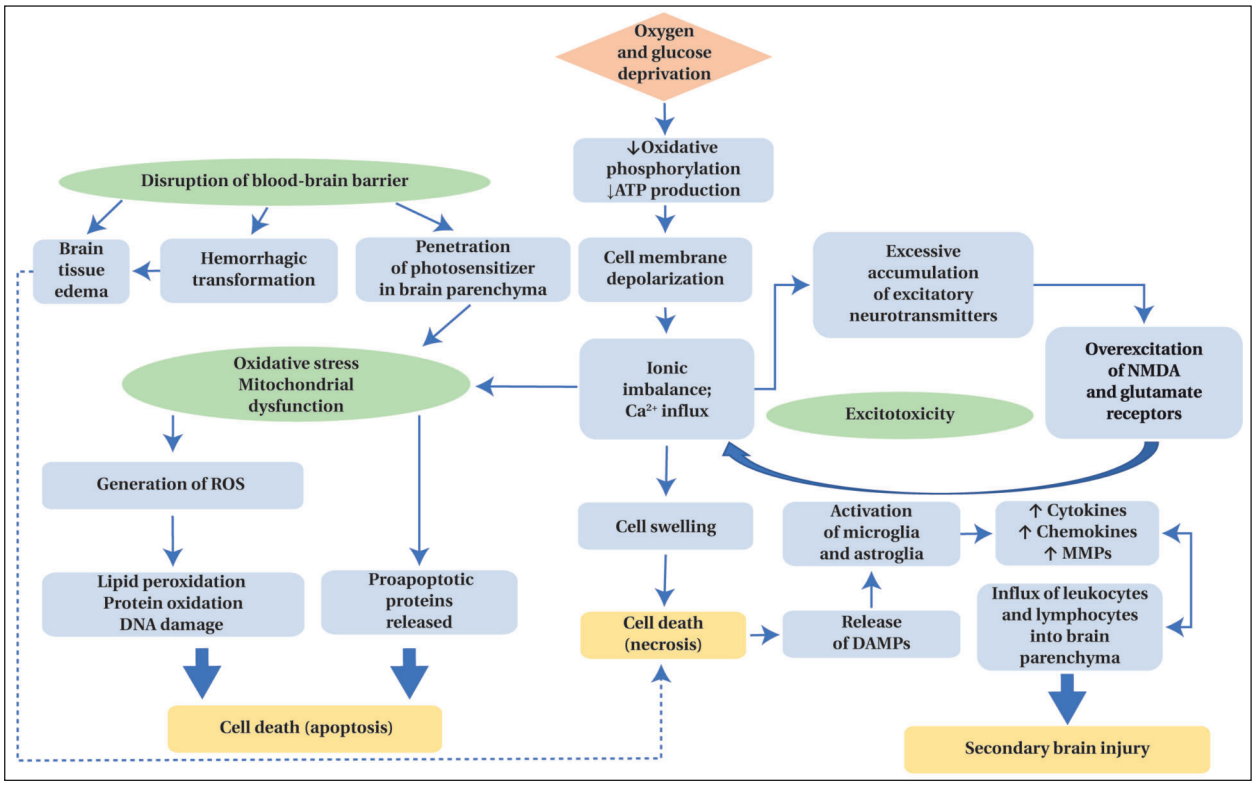

Fig. 2. Signal pathways of cell damage in photothrombotic stroke.
Note. DAMPs — damage-associated molecular patterns; NMDA — N-methyl-D-aspartate; MMPs — matrix metalloproteinases; DNA — deoxyribonucleic acid.

The PTS model is characterized by rapidly developing ischemic brain cell damage. However, in contrast to the MCA occlusion model, where platelet aggregation and coagulation abnormalities are the main pathogenic factors, neuronal damage in photothrombosis may have other causes [11]. Alterations in the PTS core include several interrelated events, such as direct photodynamic damage to cells, signaling and metabolic pathways leading to cell death, similar to other types of ischemic stroke, and the sequelae of tissue edema. As in other types of stroke, vascular occlusion and decreased blood flow result in reduced and interrupted delivery of oxygen and glucose to the infarct core, inhibition of oxidative phosphorylation, and cessation of ATP production [56]. ATP deficiency leads to rapid failure of energy-dependent ion pumps and channels, loss of membrane potential and depolarization of neurons and glia, and Ca^{2+} influx into cells [57]. As a result, the concentration of potentially toxic excitatory neurotransmitters in brain tissue increases. Massive release of glutamate and aspartate from damaged neurons causes overexcitation of cell receptors, leading to opening of calcium channels and influx of calcium and sodium ions into neurons. This causes passive water entry into the cells and their edema. Cell lysis occurs, especially in the ischemic core [5]. In addition, large amounts of Ca^{2+} ions activate hydrolytic enzymes such as nucleases, lipases, and proteinases, promoting cell destruction in the stroke core [1]. This is known as excitotoxicity.

The integrity of the BBB is very rapidly compromised in stroke due to oxidative stress, increased levels of matrix metalloproteinases, cytokines, disruption of dense contacts and proteins of integrins (transmembrane glycoprotein receptors). This leads to vasogenic edema and hemorrhagic transformation [58]. In the experiments of Kuroiwa et al. (2013), BBB disruption was observed in rat brain 4 h after basal ganglia PTS. It peaked on day 1 and completely disappeared 6 days after PTS [28]. Four to six hours after stroke, there is an influx of serum proteins, which also leads to vasogenic edema [21]. It has been shown that in PTS, during the first hour after exposure to light, there is a massive leakage of blood plasma through the vascular walls into the brain tissue. This process almost stops after 4 hours, but persists in the penumbra up to 24 hours after photothrombosis. Thus, both clot formation and blood plasma leakage through the damaged vascular walls play an important role in the pathogenesis of PTS [11, 59].

Due to the disrupted BBB, photosensitizer molecules penetrate into glia and neurons, contributing to direct photodynamic damage to brain cells [60].

Increased intracellular calcium leads to enhanced production of free oxygen radicals, causing lipid peroxidation, protein oxidation, and nucleic acid damage [61]. Calcium ions cause mitochondrial pore opening and release of pro-apoptotic proteins into the cytosol. Disruption of mitochondrial membrane integrity and mitochondrial dysfunction leads to the production of reactive oxygen species and nitrogen [11]. Mitochondria play a central role in the development of oxidative stress, which leads to cellular and structural brain damage [62]. In general, intense oxidative stress in the infarct core leads to cell necrosis, whereas moderate stress in the penumbra mainly results in apoptosis [63].

Neuronal death triggers several cascades of responses, including the release of damage-associated molecular patterns (DAMPs), which initiate the activation of microglial and astroglial cells and the production of bioactive substances, cytokines, chemokines and other factors that can affect surrounding tissues [64, 65]. In the site of injury, cytokines and chemokines cause recruitment of leukocytes and lymphocytes, which permeate brain tissue through the disrupted BBB [66].

Microglial cells can become activated within minutes of ischemia and produce biologically active substances such as interleukin-1β (IL-1β) and tumor necrosis factor-alpha (TNF-α). In the murine PTS model, neurons at the core of the injury have been shown to die as early as 2 hours, accompanied by activation of microglia and astrocytes [67]. Peak microglial activity is observed two to three days after injury and persists for several weeks [21, 40].

Ischemia also causes activation of astrocytes. After PTS in rats, the astroglial response is initiated 4 h to 1 day later, peaks at 4 days, and persists for up to 28 days [15, 40, 68]. Cytokines released by neurons and glial cells after ischemia induce reactive hyperplasia of astrocytes. Activated astrocytes begin to produce monocytic chemotoxic protein-1, IL-1β, GFAP, vimentin, and nestin, resulting in reactive gliosis and glial scarring [69, 70]. In addition, astrocytes produce metalloproteinases (MMPs) that degrade basement membrane proteins and tight junctions of the BBB, increasing its permeability and leukocyte penetration into brain tissue [66]. However, astrocytosis may play a positive role in healing. Recently, in a murine PTS model, reactive astrocytes were shown to be critical mediators of vascular remodeling, which is important for functional repair [48].

Leukocytes and lymphocytes produce neurotoxic proteins such as inducible nitric oxide synthase (iNOS) and MMPs, reactive oxygen species, and proinflammatory factors [71, 72], which causes secondary brain damage [66].

The role of lymphocytes, as well as microglia and astroglia, in post-ischemic brain injury is far from clear and requires further study, which is important for the development of future immunomodulatory therapeutic strategies [8, 72–74].

The progression of secondary brain damage is believed to be associated with the activation of glial cells, the production of biologically active substances, while the severity and outcome of stroke depend on its severity [75, 76]. A difference has been found in the nature of the changes that occur in the regions adjacent to the area of necrosis (cortex) and in the subcortical structures of the brain (hippocampus) [40]. Neuronal damage in the peri-infarct area develops earlier and subsides with time, which explains the recovery of motor functions. In the hippocampus, these processes last for a very long time (3 months), which explains the persistence of cognitive dysfunction [40].

Conclusion

The advantages of the photothrombotic stroke model, such as low invasiveness, high reproducibility, ability to control the infarct volume, and low mortality, allow its active use in experimental studies of ischemic stroke. Brain abnormalities simulated by photochemical thrombosis are similar to those seen in acute cerebrovascular disorders of ischemic type (atherothrombotic or cardioembolic stroke). Consequently, this model helps to study the cellular and molecular mechanisms of ischemic brain injury and may be useful in the search for therapeutic options for stroke.

References

1. *Paul S., Candelario-Jalil E.* Emerging neuroprotective strategies for the treatment of ischemic stroke: an overview of clinical and preclinical studies. *Exp Neurol.* 2021; 335: 113518. DOI: 10.1016/j.expneurol.2020.113518. PMID: 33144066
2. *Golubev A.M.* Models of ischemic stroke (Review). *General Reanimatology.* 2020; 16 (1): 59–72. DOI: 10.15360/1813-9779-2020-1-59-72
3. *Тюренков И. Н., Куркин Д. В., Литвинов А. А., Логвинова Е. А., Морковин Е. И., Бакулин Д. А., Волотова Е. В.* Методы моделирования острых нарушений мозгового кровообращения, применяемые при проведении доклинических исследований церебропротекторов. *Разработка и регистрация лекарственных средств.* 2018; 1: 186–197. [*Tyurenkov I.N., Kurkin D.V., Litvinov A.A., Logvinova E.A., Morkovin E.I., Bakulin D.A., Volotova E.V.* Acute stroke models used in preclinical reserch. *Drug Development & Registration//Razrabotka i Registraciya Lekarstvennykh Sredstv*. 2018; (1): 186–197. (In Russ.)]
4. *Weber R.Z., Grönnert L., Mulders G., Maurer M.A., Tackenberg C., Schwab M.E., Rust R.* Characterization of the blood brain barrier disruption in the photothrombotic stroke model. *Front Physiol.* 2020; 11: 586226. DOI: 10.3389/fphys.2020.586226. PMID: 33262704.
5. *Carmichael S.T.* Rodent models of focal stroke: size, mechanism, and purpose. *NeuroRx.* 2005; 2 (3): 396–409. DOI: 10. 1602/neurorx.2.3.396.
6. *Llovera G., Pinkham K., Liesz A.* Modeling stroke in mice: focal cortical lesions by photothrombosis. *J Vis Exp.* 2021; (171). DOI: 10.3791/ 62536. PMID: 34028443
7. *Eid M., Dzreyan V., Demyanenko S.* Sirtuins 1 and 2 in the acute period after photothrombotic stroke: expression, localization and involvement in apoptosis. *Front. Physiol.* 2022; 13: 782684. DOI: 10.3389/fphys.2022.782684. PMID: 35574497
8. *Nucci M.P., Oliveira F.A., Ferreira J.M., Pinto Y.O., Alves A.H., Mamani J.B., Nucci L.P. et al.* Effect of cell therapy and exercise training in a stroke model, considering the cell track by molecular image and behavioral analysis. *Cells.* 2022; 11 (3): 485. DOI: 10.3390/ cells11030485. PMID: 35159294
9. *Qian C., Li P.C., Jiao Y., Yao H.H., Chen Y.C., Yang J., Ding J. et al.* Precise characterization of the penumbra revealed by MRI: a modified photothrombotic stroke model study. *PLoS One.* 2016; 11 (4): e0153756. DOI: 10.1371/journal.pone.0153756. PMID: 27093556
10. *Macrae I.M.* Preclinical stroke research--advantages and disadvantages of the most common rodent models of focal ischemia. *Br J Pharmacol.* 2011; 164 (4): 1062–1078. DOI: 10.1111/j.1476-5381.2011.01398.x. PMID: 21457227
11. *Узденский А. Б., Демьяненко С. В.* Фототромботический инсульт. Биохимия пенумбры. 2016. Издательство: Южный федеральный университет [*Uzdensky A. B., Demyanenko S. V.* Photothrombotic stroke. Biochemistry of penumbra. 2016. Publisher: Southern Federal University]. eLibrary: 29456163; EDN: YUPIBL
12. *Hu Sh., Wu G., Wu B., Du Zh., Zhang Yi.* Rehabilitative training paired with peripheral stimulation promotes motor recovery after ischemic cerebral stroke. *Exp Neurol.* 2021; 349: 113960. DOI: 10.1016/j.expneurol.2021.113960. PMID: 34953896
13. *Барсков И.В., Тактаров В.Г., Иванова М.В., Сергеев В.А., Павлова Е. А.* Морфологическое исследование очага фокального ишемического повреждения коры головного мозга крыс на модели лазерного фотоиндуцированного тромбоза. *Вестник медицинского института «Реавиз»: реабилитация, врач и здоровье.* 2016. 3 (23): 39–43. [*Barskov I.V., Taktarov V.G., Ivanova M.V., Sergeev V.A., Pavlova E. A.* Morphological studies of focus of focal cerebral cortex ischemic injury of rats on the laser photoinduced thrombosis model. *Bulletin of the Medical Institute «Reaviz»: Rehabilitation, Doctor and Health/Vestnik Meditsinskogo Instituta «Reaviz»: Reabilitatsiya, Vrach i Zdorovie.* 2016. 3 (23): 39–43. (in Russ.)]. eLIBRARY ID: 27631994. EDN: XGRLHZ
14. *Yao Z., Yazdan-Shahmorad A.A.* Quantitative model for estimating the scale of photochemically induced ischemic stroke. *Annu Int Conf IEEE Eng Med Biol Soc.* 2018; 2018: 2744–2747. DOI: 10.1109/EMBC.2018.8512880. PMID: 30440969
15. *Ota Y., Kubota Y., Hotta Y., Matsumoto M., Matsuyama N., Kato T., Hamakawa T. et al.* Change in the central control of the bladder function of rats with focal cerebral infarction induced by photochemically-induced thrombosis. *PLoS One.* 2021; 16 (11): e0255200. DOI: 10.1371/journal.pone.0255200. PMID: 34752461
16. *Yoo H.J., Ham J., Duc N.T., Lee B.* Quantification of stroke lesion volume using epidural EEG in a cerebral ischeamic rat model. *Sci Rep.* 2021; 11 (1): 2308. DOI: 10.1038/s41598-021-81912-2. PMID: 33504903
17. *Knezic A., Broughton B.R.S., Widdop R.E., McCarthy C.A.* Optimising the photothrombotic model of stroke in the C57BI/6 and FVB/N strains of mouse. *Sci Rep.* 2022; 12 (1): 7598. DOI: 10.1038/s41598-022-11793-6. PMID: 35534531.
18. *Aswendt M., Pallast N., Wieters F., Baues M., Hoehn M., Fink G.R.* Lesion size- and location-dependent recruitment of contralesional thalamus and motor cortex facilitates recovery after stroke in mice. *Transl Stroke Res.* 2021; 12 (1): 87–97. DOI: 10.1007/s129. PMID: 32166716
19. *Sommer C.J.* Ischemic stroke: experimental models and reality. *Acta Neuropathol.* 2017; 133 (2): 245–261. DOI: 10.1007/s00401-017-1667-0. 2017. PMID: 28064357.
20. *Clark T.A., Sullender C., Kazmi S.M., Speetles B.L., Williamson M.R., Palmberg D.M., Dunn A.K. et al.* Artery targeted photothrombosis widens the vascular penumbra, instigates peri-infarct neovascularization and models forelimb impairments. *Sci Rep.* 2019; 9 (1): 2323. DOI: 10.1038/s41598-019-39092-7.PMID: 30787398.
21. *Barthels D., Das H.* Current advances in ischemic stroke research and therapies. *Biochim Biophys Acta Mol Basis Dis.* 2020; 1866 (4): 165260. DOI: 10.1016/j.bbadis.2018.09.012. PMID: 31699365.
22. *Uzdensky A.B.* Photothrombotic stroke as a model of ischemic stroke. *Transl Stroke Res.* 2018; 9 (5): 437–451. DOI: 10.1007/s12975-017-0593-8. 2017. PMID: 29188434.
23. *Astrup J., Siesjö B.K., Symon L.* Thresholds in cerebral ischemia — the ischemic penumbra. *Stroke.* 1981; 12 (6): 723–725. DOI: 10.1161/01.str.12.6.723. PMID: 6272455

24. *Back T.* Pathophysiology of the ischemic penumbra--revision of a concept. *Cell Mol Neurobiol.* 1998; 18 (6): 621–638. DOI: 10.1023/a: 1020629818207. PMID: 9876870
25. *Tuor U.I., Deng Q., Rushforth D., Foniok T., Qiao M.* Model of minor stroke with mild peri-infarct ischemic injury. *J. Neurosci Methods.* 2016; 268: 56–65. DOI: 10.1016/j.jneumeth.2016.04.025. PMID: 27139736
26. *Kuo Y.M., Sun Y.Y., Kuan C.Y.* A Fibrin-enriched and tPA-sensitive photothrombotic stroke model. *J Vis Exp.* 2021; (172). DOI: 10.3791/61740. PMID: 34152310.
27. *Kim Y., Lee Y.B., Bae S.K., Oh S.S., Choi J.R.* Development of a photochemical thrombosis investigation system to obtain a rabbit ischemic stroke model. *Sci Rep.* 2021; 11 (1): 5787. DOI: 10.1038/s41598-021-85348-6. PMID: 33707580.
28. *Kuroiwa T., Xi G., Hua Y., Nagaraja T.N., Fenstermacher J.D., Keep R.F.* Development of a rat model of photothrombotic ischemia and infarction within the caudoputamen. *Stroke.* 2009; 40 (1): 248–253. DOI: 10.1161/STROKEAHA.108.527853. PMID: 19038913.
29. *Hosseini S.M., Pourbadie H.G., Naderi N., Sayyah M., Zibaii M.I.* Photothrombotically induced unilateral selective hippocampal ischemia in rat. *J Pharmacol Toxicol Methods.* 2018; 94 (Pt 1): 77–86. DOI: 10.1016/j.vascn.2018.06.003. 2018 PM. PMID: 29906509
30. *Генина Э.А., Башкатов А.Н., Семячкина-Глушковская О.В., Тучин В.В.* Оптическое просветление черепной кости многокомпонентными иммерсионными растворами и визулизация церебрального венозного кровотока. *Известия Саратовского университета. Новая серия. Серия Физика.* 2017; 17 (2): 98–110. [*Genina E.A., Bashkatov A.N., Semyachkina-Glushkovskaya O.V., Tuchin V.V.* Optical illumination of the cranial bone with multicomponent immersion solutions and visualization of cerebral venous blood flow. *News of Saratov University. A New Series. Physics Series//Izvestiya Saratovskogo Universiteta. Novaya Seriya. Seriya Fizika.* 2017; 17 (2): 98–110. (in Russ.)]. DOI: 10.18500/1817-3020-2017-17-2-98-110
31. *Zhang C., Feng W., Zhao Y., Yu T., Li P., Xu T., Luo Q. et al.* A large, switchable optical clearing skull window for cerebrovascular imaging. *Theranostics.* 2018; 8 (10): 2696–2708. DOI: 10.7150/thno. 23686. PMID: 29774069.
32. *Li Z., Gao H., Zeng P., Jia Y., Kong X., Xu K., Bai R.* Secondary degeneration of white matter after focal sensorimotor cortical ischemic stroke in rats. *Front Neurosci.* 2021; 14: 611696. DOI: 10.3389/fnins. 2020.611696. PMID: 33536869
33. *Wahl A.S., Correa D., Imobersteg S., Maurer M.A., Kaiser J., Augath M.A., Schwab M.E.* Targeting therapeutic antibodies to the CNS: a comparative study of intrathecal, intravenous, and subcutaneous anti-Nogo A antibody treatment after stroke in rats. *Neurotherapeutics.* 2020; 17 (3): 1153–1159. DOI: 10.1007/s13311-020-00864-z. PMID: 32378027.
34. *Poinsatte K., Betz D., Torres V.O., Ajay A.D., Mirza S., Selvaraj U.M., Plautz E.J. et al.* Visualization and quantification of post-stroke neural connectivity and neuroinflammation using serial two-photon tomography in the whole mouse brain. *Front Neurosci.* 2019; 13: 1055. DOI: 10.3389/fnins.2019.01055. PMID: 31636534.
35. *Pallast N., Diedenhofen M., Blaschke S., Wieters F., Wiedermann D., Hoehn M., Fink R.G. et al.* Processing pipeline for atlas-based imaging data analysis of structural and functional mouse brain MRI (AIDAmri). *Front Neuroinform.* 2019; 13: 42. DOI: 10.3389/fninf. PMID: 31231202
36. *Pallast N., Wieters F., Fink G.R., Aswendt M.* Atlas-based imaging data analysis tool for quantitative mouse brain histology (AIDAhisto). *J Neurosci Methods.* 2019; 326: 108394. DOI: 10.1016/j.jneumeth. 2019.108394. PMID: 31415844
37. *Li H., Zhang N., Lin H.Y., Yu Y., Cai Q.Y., Ma L., Ding S.* Histological, cellular and behavioral assessments of stroke outcomes after photothrombosis-induced ischemia in adult mice. *BMC Neurosci.* 2014; 15: 58. DOI: 10.1186/1471-2202-15-58. PMID: 24886391
38. *Williamson M.R., Franzen R.L., Fuertes C.J.A., Dunn A.K., Drew M.R., Jones T.A.* A window of vascular plasticity coupled to behavioral recovery after stroke. *J Neurosci.* 2020; 40 (40): 7651–7667. DOI: 10.1523/JNEUROSCI.1464-20.2020. PMID: 32873722
39. *Aamir R., Fyffe C., Korin N., Lawrence D.A., Su E.J., Kanapathipillai M.* Heparin and arginine based plasmin nanoformulation for ischemic stroke therapy. *International Journal of Molecular Sciences.* 2021; 22 (21): 11477. DOI: 10.3390/ijms222111477.
40. *Zhou M.Y., Zhang Y.J., Ding H.M., Wu W.F., Cai W.W., Wang Y.Q., Geng D.Q.* Diprotin A TFA exerts neurovascular protection in ischemic cerebral stroke. *Front Neurosci.* 2022; 16: 861059. DOI: 10.3389/fnins.2022.861059. PMID: 35615279.
41. *Sanchez-Bezanilla S., Hood R.J., Collins-Praino L.E., Turner R.J., Walker F.R., Nilsson M., Ong L.K.* More than motor impairment: a spatiotemporal analysis of cognitive impairment and associated neuropathological changes following cortical photothrombotic stroke. *J Cereb Blood Flow Metab.* 2021; 41 (9): 2439–2455. DOI: 10.1177/0271678X211005877 2021. PMID: 33779358.
42. *Yew W.P., Djukic N.D., Jayaseelan J.S.P., Woodman R.J., Muyderman H., Sims N.R.* Differential effects of the cell cycle inhibitor, olomoucine, on functional recovery and on responses of peri-infarct microglia and astrocytes following photothrombotic stroke in rats. *J Neuroinflammation.* 2021; 18 (1): 168. DOI: 10.1186/s12974-021-02208-w. PMID: 34332596.
43. *Lee S., Lim W., Ryu HW., Jo D., Min JJ., Kim HS., Hyun H.* ZW800-1 for assessment of blood-brain barrier disruption in a photothrombotic stroke model. *Int J Med Sci.* 2017; 14 (13): 1430–1435. DOI: 10.7150/ijms.22294. PMID: 29200957
44. *Noll J.M., Augello C.J., Kürüm E., Pan L., Pavenko A., Nam A., Ford B.D.* Spatial analysis of neural cell proteomic profiles following ischemic stroke in mice using high-plex digital spatial profiling. *Mol Neurobiol.* 2022; 59 (12): 7236–7252. DOI: 10.1007/s12035-022-03031-x. PMID: 36151369
45. *Frase S., Löffler F., Hosp J.A.* Enhancing post-stroke rehabilitation and preventing exo-focal dopaminergic degeneration in rats-a role for substance P. *Int J Mol Sci.* 2022; 23 (7): 3848. DOI: 10.3390/ ijms23073848. PMID: 35409207.
46. *Uzdensky A., Demyanenko S., Fedorenko G., Lapteva T., Fedorenko A.* Protein profile and morphological alterations in penumbra after focal photothrombotic infarction in the rat cerebral cortex. *Mol Neurobiol.*

2017; 54 (6): 4172–4188. DOI: 10.1007/s12035-016-9964-5. PMID: 27324898.
47. *Choi I.A., Yun J.H., Kim J.H., Kim H.Y., Choi D.H., Lee J.* Sequential transcriptome changes in the penumbra after ischemic stroke. *Int J Mol Sci.* 2019; 20 (24): 6349. DOI: 10.3390/ijms20246349. PMID: 31888302
48. *Pushie M.J., Sylvain N.J., Hou H., Caine S., Hackett M.J., Kelly M.E.* Tracking elemental changes in an ischemic stroke model with X-ray fluorescence imaging. *Sci Rep.* 2020; 10 (1): 17868. DOI: 10.1038/ s41598-020-74698-2. PMID: 33082455
49. *Gu W.G., Brännström T., Jiang W., Wester P.* A photothrombotic ring stroke model in rats with remarkable morphological tissue recovery in the region at risk. *Exp Brain Res.* 1999; 125 (2): 171–183. DOI: 10.1007/s002210050672. PMID: 10204770.
50. *Hu X., Johansson I.M., Brännström T., Olsson T., Wester P.* Long-lasting neuronal apoptotic cell death in regions with severe ischemia after photothrombotic ring stroke in rats. *Acta Neuropathol.* 2002; 104 (5): 462–470. DOI: 10.1007/s00401-002-0579-8. PMID: 12410394
51. *Gu W., Brännström T., Wester P.* Cortical neurogenesis in adult rats after reversible photothrombotic stroke. *J Cereb Blood Flow Metab.* 2000; 20 (8): 1166–1173. DOI: 10.1097/00004647-200008000-00002. PMID: 10950377.
52. *Zhang J., Zhang Y., Xing S., Liang Z., Zeng J.* Secondary neurodegeneration in remote regions after focal cerebral infarction: a new target for stroke management? *Stroke.* 2012; 43 (6): 1700–1705. DOI: 10.1161/STROKEAHA.111.632448. PMID: 22492515
53. *Pietrogrande G., Zalewska K., Zhao Z., Abdolhoseini M., Chow W.Z., Sanchez-Bezanilla S., Ong L.K. et al.* Low oxygen post conditioning prevents thalamic secondary neuronal loss caused by excitotoxicity after cortical stroke. *Sci Rep.* 2019; 9 (1): 4841. DOI: 10.1038/s41598-019-39493-8. PMID: 30890719.
54. *Necula D., Cho F.S., He A., Paz J.T.* Secondary thalamic neuroinflammation after focal cortical stroke and traumatic injury mirrors corticothalamic functional connectivity. *J Comp Neurol.* 2022; 530 (7): 998–1019. DOI: 10.1002/cne.25259. PMID: 34633669.
55. *Hosp J.A., Greiner K.L., Arellano L.M., Roth F., Löfflfler F., Reis J., Fritsch B.* Progressive secondary exo-focal dopaminergic neurodegeneration occurs in not directly connected midbrain nuclei after pure motor-cortical stroke. *Exp. Neurol.* 2020; 327: 113211. DOI: 10.1016/j.expneurol.2020.113211. PMID: 31987834
56. *Hertz L.* Bioenergetics of cerebral ischemia: a cellular perspective. *Neuropharmacology.* 2008; 55 (3): 289–309. DOI: 10.1016/j.neuropharm.2008.05.023. PMID: 18639906
57. *Leichsenring A., Riedel T., Qin Y., Rubini P., Illes P.* Anoxic depolarization of hippocampal astrocytes: possible modulation of P2X7 receptors. *Neurochem Int.* 2013; 62 (1): 15–22. DOI: 10.1016/j.neuint.2012.11.002. PMID: 23147683
58. *Abdullahi W., Tripathi D., Ronaldson P.T.* Blood-brain barrier dysfunction in ischemic stroke: targeting tight junctions and transporters for vascular protection. *Am J Physiol Cell Physiol.* 2018; 315 (3): C343–C356. DOI: 10.1152/ajpcell.00095.2018. PMID: 29949404
59. *Hoff E.I., oude Egbrink M.G., Heijnen V.V., Steinbusch H.W., van Oostenbrugge R.J. In vivo* visualization of vascular leakage in photochemically induced cortical infarction. *J Neurosci Methods.* 2005; 141 (1): 135–141. DOI: 10.1016/j.jneumeth.2004.06.004. PMID: 15585297.
60. *Hirschberg H., Uzal F.A., Chighvinadze D., Zhang M.J., Peng Q., Madsen S. J.* Disruption of the blood-brain barrier following ALA-mediated photodynamic therapy. *Lasers Surg Med.* 2008; 40 (8): 535–542. DOI: 10.1002/lsm.20670. PMID: 18798293
61. *Sun L., Strelow H., Mies G., Veltkamp R.* Oxygen therapy improves energy metabolism in focal cerebral ischemia. *Brain Res.* 2011; 1415: 103–108. DOI: 10.1016/j.brainres.2011.07.064. PMID: 21872850
62. *Qin C., Yang S., Chu Y.H., Zhang H., Pang X.W., Chen L., Zhou L.Q. et al.* Signaling pathways involved in ischemic stroke: molecular mechanisms and therapeutic interventions. *Signal Transduct Target Ther.* 2022; 7 (1): 215. DOI: 10.1038/s41392-022-01064-1. PMID: 35794095.
63. *Chen H., Yoshioka H., Kim G.S., Jung J.E., Okami N., Sakata H., Maier C.M. et al.* Oxidative stress in ischemic brain damage: mechanisms of cell death and potential molecular targets for neuroprotection. *Antioxid Redox Signal.* 2011; 14 (8): 1505–1517. DOI: 10.1089/ars.2010.3576. PMID: 20812869
64. *Banjara M., Ghosh C.* Sterile neuroinflammation and strategies for therapeutic intervention. *Int J Inflam.* 2017; 2017: 8385961. DOI: 10.1155/2017/8385961. PMID: 28127491.
65. *Gülke E., Gelderblom M., Magnus T.* Danger signals in stroke and their role on microglia activation after ischemia. *Ther Adv Neurol Disord.* 2018; 11: 1756286418774254. DOI: 10.1177/175628641 8774254. PMID: 29854002.
66. *Jayaraj R.L., Azimullah S., Beiram R., Jalal F.Y., Rosenberg G.A.* Neuroinflammation: friend and foe for ischemic stroke. *J Neuroinflammation.* 2019; 16 (1): 142. DOI: 10.1186/s12974-019-1516-2. PMID: 31291966
67. *Gorlamandala N., Parmar J., Craig A.J., Power J.M., Moorhouse A.J., Krishnan A.V., Housley G.D.* Focal ischaemic infarcts expand faster in cerebellar cortex than cerebral cortex in a mouse photothrombotic stroke model. *Transl Stroke Res.* 2018; 9 (6): 643–653. DOI: 10.1007/ s12975-018-0615-1. PMID: 29455391
68. *Nowicka D., Rogozinska K., Aleksy M., Witte O.W., Skangiel-Kramska J.* Spatiotemporal dynamics of astroglial and microglial responses after photothrombotic stroke in the rat brain. *Acta Neurobiol Exp (Wars).* 2008; 68 (2): 155–168. PMID: 18511952.
69. *Hennessy E., Griffin É.W., Cunningham C.* Astrocytes are primed by chronic neurodegeneration to produce exaggerated chemokine and cell infiltration responses to acute stimulation with the cytokines IL-1β and TNF-α. *J Neurosci.* 2015; 35 (22): 8411–8422. DOI: 10.1523/JNEUROSCI.2745-14.2015. PMID: 26041910
70. *Wang H., Song G., Chuang H., Chiu C., Abdelmaksoud A., Ye Y., Zhao L.* Portrait of glial scar in neurological diseases. *Int J Immunopathol Pharmacol.* 2018; 31: 2058738418801406. DOI: 10.1177/2058738418801406. PMID: 30309271
71. *Clausen B.H., Lambertsen K.L., Babcock A.A., Holm T.H., Dagnaes-Hansen F., Finsen B.* Interleukin-1beta and tumor necrosis factor-alpha are expressed by different subsets of microglia and macrophages after

ischemic stroke in mice. *J Neuroinflammation*. 2008; 5: 46. DOI: 10.1186/1742-2094-5-46. PMID: 18947400
72. *Jin R., Liu L., Zhang S., Nanda A., Li G.* Role of inflammation and its mediators in acute ischemic stroke. *J Cardiovasc Transl Res*. 2013; 6 (5): 834–851. DOI: 10.1007/s12265-013-9508-6. PMID: 24006091
73. *Xie L., Yang S.H.* Interaction of astrocytes and T cells in physiological and pathological conditions. *Brain Res*. 2015; 1623: 63–73. DOI: 10.1016/j.brainres.2015.03.026. PMID: 25813828
74. *Qiu Y.M., Zhang C.L., Chen A.Q., Wang H.L., Zhou Y.F., Li Y.N., Hu B.* Immune cells in the BBB disruption after acute ischemic stroke: targets for immune therapy? *Front Immunol*. 2021; 12: 678744. DOI: 10.3389/fimmu.2021.678744. PMID: 34248961
75. *Chamorro Á., Meisel A., Planas A.M., Urra X., van de Beek D., Veltkamp R.* The immunology of acute stroke. *Nat Rev Neurol*. 2012; 8 (7): 401–410. DOI: 10.1038/nrneurol.2012.98. PMID: 22664787.
76. *Veltkamp R., Gill D.* Clinical trials of immunomodulation in ischemic stroke. *Neurotherapeutics*. 2016; 13 (4): 791–800. DOI: 10.1007/s13311-016-0458-y. PMID: 27412685

Received 25.01.2023
Accepted 25.04.2023

Светлой памяти Анатолия Петровича Зильбера (13.02.1931–25.04.2023)

Двадцать пятое апреля 2023 г. — черный день отечественной анестезиологии-реаниматологии. Умер последний из основателей этой специальности в нашей стране Анатолий Петрович Зильбер. Писать об этом событии чрезвычайно тяжело, поскольку вся его жизнь была посвящена жизни, здоровью и трудам людей, посвятивших себя новому разделу медицины. Называя себя одним из российских динозавров анестезиологии-реаниматологии, он был вместе с тем основоположником медицины критических состояний, считая ее краеугольным камнем науки о здоровье и жизни человека. Именно этому посвящены 627 его печатных трудов, перечисленных в библиографическом указателе, опубликованном менее года назад научной библиотекой Петрозаводского государственного университета.

Эти труды отражены в его титулах и званиях, которые он не любил выставлять напоказ: доктор медицинских наук (1971), профессор (1973), Заслуженный врач РСФСР, Заслуженный деятель науки РФ (1989), академик Российской Академии медико-технических наук (1997) и Академии проблем безопасности, обороны и правопорядка РФ (2007), Почетный работник высшего профессионального образования РФ (2000), Народный врач Республики Карелия (2001), Почетный гражданин города Петрозаводска и Карелии (2003), визитирующий профессор Гарвардского и Южно-Калифорнийского университетов (США), почетный профессор Хорезмского университета (Узбекистан). Почетный член Правления Федерации анестезиологов и реаниматологов РФ (2000), член Правления Ассоциации анестезиологов и реаниматологов Республики Карелия (2003), Почетный член Федерации анестезиологов и реаниматологов РФ (2014).

Все награды, которых он удостоен — и государственные, и негосударственные — им заслужены. А это Ордена Дружбы (1998) и Почета (2006), орден Пирогова (2022), высшая награда Республики Карелия орден «Сампо» (2019), орден Гиппократа, медали «За выдающиеся достижения в реаниматологии» (2004), «За укрепление авторитета Российской науки» (2007), «Золотая медаль А. Л. Чижевского за профессионализм и деловую репутацию» (2008), медаль Ломоносова (2012), золотой знак «Ibi Victoria ubi Concordia» («Там победа, где согласие») (2012), Памятная медаль им. академика РАМН В. А. Неговского (2013).

Весь жизненный путь профессора А. П. Зильбера изложен в многочисленных статьях, посвященных его юбилеям, а также во вступительной статье к упомянутому библиографическому указателю.

Все, за что брался Анатолий Петрович, было помечено знаком «первый». Первое в СССР отделение интенсивной терапии, анестезии и реанимации — знаменитое ИТАР (1959), первый курс преподавания анестезиологии и реаниматологии студентам-медикам (1966), Первый Пленум Правления Всесоюзного научного общества анестезиологов-реаниматологов (1967)

как акт признания роли карельской школы анестезиологии-реаниматологии, первое руководство по клинической физиологии для анестезиологов (1977), первое четырехтомное собрание «Этюдов критической медицины»... Каждый труд проходил тщательную доводку и буквально ювелирную отделку, чтобы не было повода для критики, для недопонимания проблемы. Первый в Европе ежегодный семинар анестезиологов-реаниматологов, ставший впоследствии международной Школой Зильбера, состоялся в Петрозаводске в 1964 г. по инициативе Анатолия Петровича и проходил в последние годы в формате международных конференций, проводимых совместно с Комитетом по европейскому анестезиологическому образованию (CEEA) Европейского общества анестезиологии и интенсивной терапии (ESAIC). Международный день анестезиолога-реаниматолога 16 октября — это тоже результат работы А. П. Зильбера. Первый за последние 250 лет истории Европы кводлибет состоялся в Петрозаводском университете 23 апреля 2015 г. В нем участвовали более 600 человек, велась Интернет-трансляция. Выступали студенты, практические врачи Карелии, США, Австралии, преподаватели Петрозаводского университета и медицинских вузов Санкт-Петербурга и Армении. Кводлибетарием (т. е. ведущим) выступал, разумеется, профессор А. П. Зильбер. Эту форму образования подхватили и в других университетах. В Ереване, например, кводлибет был проведен дважды.

Занявшись изучением проблем дыхательной недостаточности, А. П. Зильбер выдвинул концепцию респираторной медицины в качестве еще одного междисциплинарного раздела здравоохранения. В 1985 г. по инициативе профессора А. П. Зильбера в Петрозаводске прошел объединенный пленум Правлений Всесоюзных обществ анестезиологов-реаниматологов и пульмонологов. В 1989 г. в Республиканской больнице Карелии создано отделение респираторной терапии, превратившееся затем (2001) в Республиканский респираторный центр. На базе этого Центра и курса респираторной медицины Петрозаводского университета в 2006 г. был открыт Петрозаводский филиал Института пульмонологии РАМН — Федерального центра респираторной медицины и пульмонологии России.

Еще один враг человечества, которому давно объявил войну профессор, это Боль. Боль с большой буквы. Боль не как следствие каких-то действий человека или развивающейся болезни, а как причина критического состояния, от которого человек может страдать годами, теряя работоспособность, возможность жить по-человечески. Фотография одной из скульптур Родена с названием «Боль» долгое время висела в кабинете Анатолия Петровича, напоминая о необходимости бороться с этим злом. Эта борьба привела к организации при кафедре курса алгологии, признанного Всемирной федерацией обществ анестезиологов (WFSA).

Основными направлениями научной работы профессора были не только создание клинико-физиологического направления в медицине критических состояний, но и разработка концепции гуманитарных основ образования и практики врачей, этических и юридических основ МКС.

Будучи разносторонне образованным человеком, Анатолий Петрович не ограничивался только трудами по медицине. Его работы о врачах-труэнтах, то есть специалистах, оставивших заметный след не только в медицине, но и в других разделах науки и практики человечества, считаются самыми полными и достоверными в современной литературе.

Особое место в работе профессора занимали книги об образовании, поскольку идею непрерывного медицинского образования он считал главным условием профессионального роста врачей любой специальности. Научно-техническая революция со сверхзвуковым ростом массива новой информации вообще и медицинской в частности требует соответствующего, креативного подхода к методике образования. Трудность же современного образования заключается в том, что масса новой информации базируется на фундаменте уже имеющихся знаний. Старые методики образования приведут к тому, что специалист получит высшее образование без среднего. Решению этой непростой задачи были посвящены работы профессора в последние годы его неспокойной жизни.

С лекциями и выступлениями профессор объехал не только всю Россию — он побывал во многих странах ближнего и дальнего зарубежья, странах Старого и Нового Света, и везде его сообщения с восторгом воспринимались слушателями. В последние годы профессор использовал для своих выступлений современные технологии (Skype, V-Point). Лекции А. П. Зильбера для студентов и врачей — прекрасно организованные и интересные по форме — содержали новейшие данные по специальности и с удовольствием посещались студентами старших курсов и врачами разных специальностей. А. П. Зильбер — один из профессоров университета, которые целенаправленно занимались гуманитарным воспитанием студентов и врачей.

Главное достижение профессора — созданная им Петрозаводская школа критической и респираторной медицины — живет и работает. Подготовленные ею специалисты

высоко ценятся не только в России, но и за ее пределами.

Прощаясь с Анатолием Петровичем, сотни его учеников и последователей, работающих в России, в странах ближнего и дальнего зарубежья, могут сказать: «Дорогой Учитель, мы всегда будем помнить Вас, Ваши труды и лекции и осуществлять Ваши идеи».

Ректор Петрозаводского государственного университета,
д. т. н., профессор А. В. Воронин

Директор Медицинского института Петрозаводского государственного университета,
д. м. н., профессор А. Т. Балашов

Главный врач Республиканской больницы им. В. А. Баранова Т. Д. Карапетян

Доцент Медицинского института Петрозаводского государственного университета,
д. м. н., А. П. Спасова

Доцент Медицинского института Петрозаводского государственного университета,
к. м. н., В. В. Мальцев

Правление и Президиум Общероссийской общественной организации «Федерация анестезиологов и реаниматологов», многочисленные коллеги в разных концах нашей страны и за рубежом глубоко скорбят о кончине Анатолия Петровича Зильбера вместе с его учениками и друзьями, и от всей души присоединяются к словам Президента Союза медицинского сообщества «Национальная медицинская палата» профессора Леонида Михайловича Рошаля:

«Я считал, что Анатолий Петрович Зильбер будет жить вечно. Потрясающий человечище. Это глыба и законодатель, которыми Бог послал быть немногих. Мои соболезнования семье, сослуживцам, ученикам и пациентам. Соболезнования всем нам…»

Коллектив редакции журнала «Общая реаниматология» и Федерального научно-клинического центра реаниматологии и реабилитологии выражают соболезнования родным, близким и коллегам Анатолия Петровича и скорбят вместе с ними.

ФЕДЕРАЛЬНОЕ ГОСУДАРСТВЕННОЕ БЮДЖЕТНОЕ НАУЧНОЕ УЧРЕЖДЕНИЕ
"Федеральный научно-клинический центр реаниматологии и реабилитологии"
ФНКЦ РР

Федеральное государственное бюджетное научное учреждение **«Федеральный научно-клинический центр реаниматологии и реабилитологии» (ФНКЦ РР)**

Симуляционный центр ФНКЦ РР

Лаборатория перспективных симуляционных технологий

СИМУЛЯЦИОННЫЕ ОБРАЗОВАТЕЛЬНЫЕ ПРОГРАММЫ:

/ Первая помощь
/ Подготовка инструкторов первой помощи
/ Базовая сердечно-легочная реанимация
/ Расширенная сердечно-легочная реанимация
/ Ультразвуковой мониторинг и навигация в анестезиологии-реаниматологии
/ Трудный дыхательный путь
/ Респираторная поддержка
/ Критические состояния в анестезиологии-реаниматологии
/ Подготовка к первичной специализированной аккредитации
/ Обучение преподавателей симуляционных центров

Все образовательные программы обеспечены баллами НМО
Возможно формирование образовательных циклов по требованию

Тел.: 8(495)650-96-77
www.fnkcrr.ru/edu
edu@fnkcrr.ru

Реамберин®

НАВСТРЕЧУ ЖИЗНИ

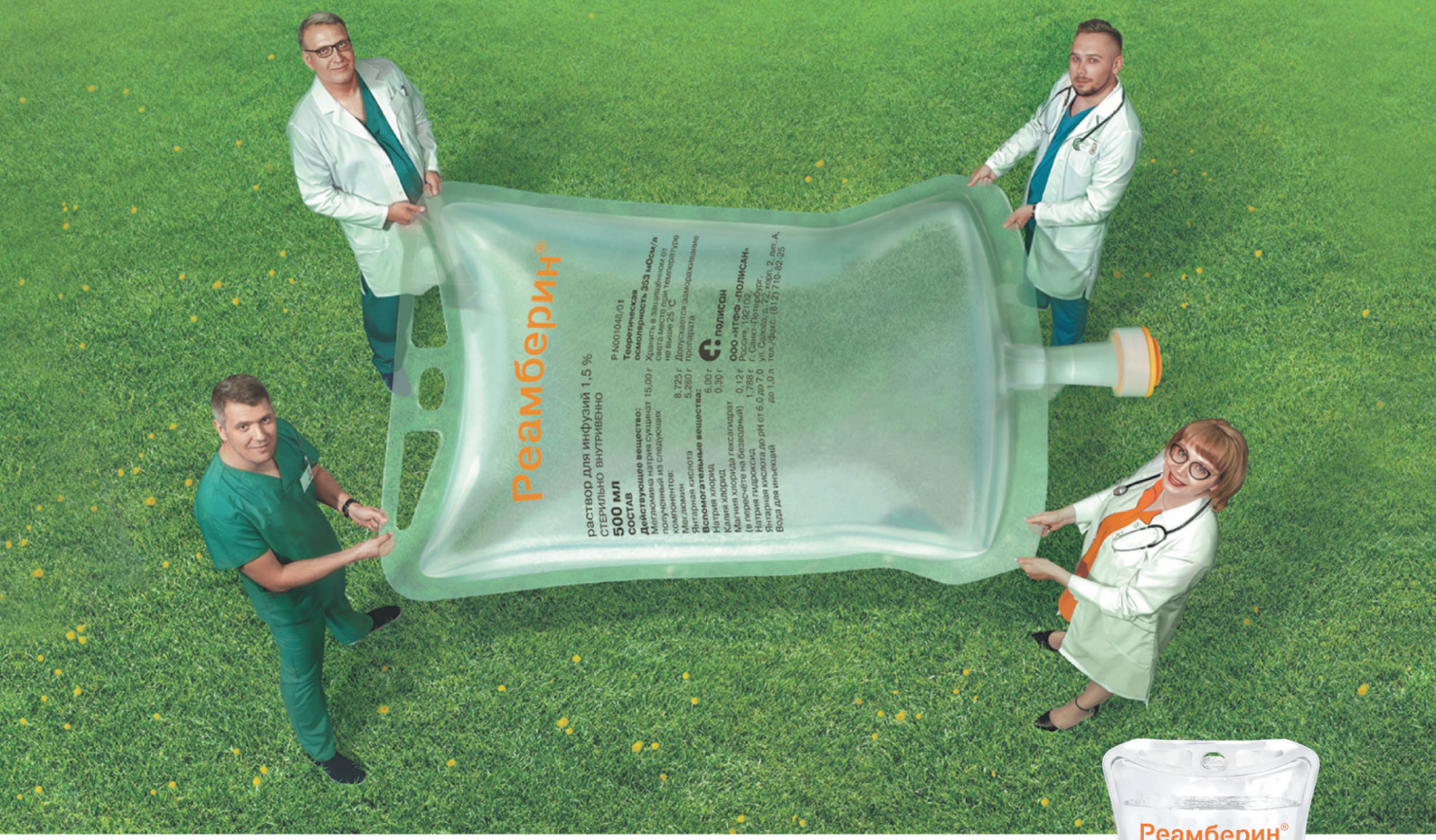

- Сбалансированный сукцинатсодержащий кристаллоидный раствор
- Оказывает дезинтоксикационное, антиоксидантное и антигипоксическое действия[1]
- Сокращает сроки госпитализации и летальность[2]
- Нормализует кислотно-основное состояние[1,3]

Инфузионная терапия

Реклама. Форма выпуска: раствор для инфузий 1,5 %, в бутылках стеклянных 400 мл, в контейнерах из многослойной полиолефиновой пленки по 250 или 500 мл.
Рег. номер №ЛП(000801)-(РГ-RU) от 19.05.22.

1 Инструкция по применению лекарственного препарата РЕАМБЕРИН® раствор для инфузий 1,5% МЗ РФ
2 Шахмарданова С.А., Гулевская О.Н., соавт., «Препараты янтарной и фумаровой кислот как средства профилактики и терапии различных заболеваний», «Журнал фундаментальной медицины и биологии», 2016, №3
3 Герасимов Л.В., Марченков Ю.В., соавт. «Возможности коррекции метаболических нарушений с использованием реамберина в остром периоде травмы», Анестезиология и реаниматология № 6, 2015

Polysan